Master's Theses   Master's Theses and Graduate Research

1997

Characterization of derivatized silica surfaces by ¹H-NMR spectroscopy and ESCA

Paul Jeffrey Christensen
San Jose State University

Follow this and additional works at: https://scholarworks.sjsu.edu/etd_theses

INFORMATION TO USERS

This manuscript has been reproduced from the microfilm master. UMI films the text directly from the original or copy submitted. Thus, some thesis and dissertation copies are in typewriter face, while others may be from any type of computer printer.

The quality of this reproduction is dependent upon the quality of the copy submitted. Broken or indistinct print, colored or poor quality illustrations and photographs, print bleedthrough, substandard margins, and improper alignment can adversely affect reproduction.

In the unlikely event that the author did not send UMI a complete manuscript and there are missing pages, these will be noted. Also, if unauthorized copyright material had to be removed, a note will indicate the deletion.

Oversize materials (e.g., maps, drawings, charts) are reproduced by sectioning the original, beginning at the upper left-hand corner and continuing from left to right in equal sections with small overlaps. Each original is also photographed in one exposure and is included in reduced form at the back of the book.

Photographs included in the original manuscript have been reproduced xerographically in this copy. Higher quality 6" x 9" black and white photographic prints are available for any photographs or illustrations appearing in this copy for an additional charge. Contact UMI directly to order.

UMI

CHARACTERIZATION OF DERIVATIZED SILICA SURFACES BY ^{1}H-NMR SPECTROSCOPY AND ESCA

A Thesis

Presented to

The Faculty of the Department of Chemistry

San Jose State University

In Partial Fulfillment

of the Requirements for the Degree

Master of Science

by

Paul Jeffrey Christensen

May 1997

UMI Number: 1384677

Copyright 1997 by
Christensen, Paul Jeffrey
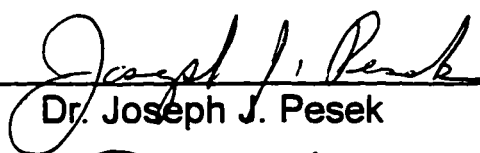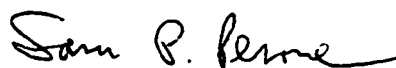

UMI
300 North Zeeb Road
Ann Arbor, MI 48103

APPROVED FOR THE DEPARTMENT OF CHEMISTRY

Dr. Joseph J. Pesek

Dr. Sam Perone

Dr. Bradley M. Stone

APPROVED FOR THE UNIVERSITY

M. Lou Lewandowski

ABSTRACT

CHARACTERIZATION OF DERIVATIZED SILICA SURFACES BY ^{1}H-NMR SPECTROSCOPY AND ESCA

by Paul J. Christensen

Metal-oxide surfaces are commonly used in chromatographic applications such as High Pressure Liquid Chromatography (HPLC); the most commonly used metal-oxide substrate is silica (SiO_2). Because silica surfaces generally contain hydroxyl groups that can lead to poor chromatographic separations, the surfaces are derivatized by adding organic linkages. A new method under investigation, "Silanization," involves adding organic linkages via a two-step process: (1) converting the surface-hydroxyl groups (Si-OH) to surface-hydride groups (Si-H), and (2) reacting the surface-hydride groups with an olefinic compound ($CH_2=CH-R$) with the aid of a platinum-based catalyst. This study shows that the hydride intermediates can be evaluated with solid-state ^{1}H-NMR using the Combined Rotation and Multiple Pulse Spectroscopy (CRAMPS) technique. The NMR data provide quantitative information pertaining to hydroxyl groups and newly formed hydride groups on reaction intermediates. Electron Spectroscopy for Chemical Analysis (ESCA), a surface analytical technique that provides elemental composition, shows that some of the derivatized products contain platinum from catalyst deposition.

ACKNOWLEDGMENTS

TABLE OF CONTENTS

LIST OF TABLES

LIST OF FIGURES

INTRODUCTION

Background Information on HPLC

Since the 1960's, High Performance Liquid Chromatography (HPLC) has gained widespread acceptance as a versatile chromatographic technique. In general, HPLC uses a stationary phase in a column to separate the components that are dissolved in a mobile phase (i.e., a solvent). Two of the most common HPLC techniques include size-exclusion chromatography (SEC) and adsorption chromatography. As the name implies, SEC separates molecules based on size; larger molecules elute first because they are retained less by the pores of the stationary phase. With adsorption chromatography, however, the various-dissolved components interact dynamically with the stationary phase by undergoing repeated adsorption-desorption processes. These processes are strongly influenced by the polarity of the stationary phase with respect to the mobile phase.

Adsorption chromatography can be further subdivided into two main types: normal-phase chromatography and reversed-phase chromatography. In normal-phase chromatography, the stationary phase is polar and the mobile phase is nonpolar; thus nonpolar molecules elute first from the column. Just the inverse occurs with reversed-phase chromatography; the stationary phase is nonpolar and the mobile phase is polar. Thus the more polar molecules elute first.

Stationary Phase In HPLC:

Silica gel, generally expressed as $SiO_2 \cdot xH_2O$, is the most commonly used stationary phase in liquid chromatography. The silica particles are porous and the sizes typically range from 3 to 12 μm in diameter. Therefore, silica particles exhibit a very large surface-to-volume ratio and a corresponding large specific-surface area, attractive properties for chromatographic adsorbents. The surfaces of bare silica contain two main types of chemical groups: siloxane (Si-O-Si) and silanol (Si-OH). The surface chemistry of the silica dictates the type of HPLC separation. Because hydroxyl groups are polar, bare silica can be used for normal-phase chromatography. In order to use silica for reversed-phase chromatography, the hydroxyl groups are typically derivatized by adding organic linkages, thereby making the stationary phase nonpolar.

Silica-Surface Derivatization:

Various reaction pathways have been exploited to add organic moieties to silica surfaces. Desirable properties for modified surfaces include a high degree of surface coverage and chemical stability. Depending on the chemical reactions employed, three common types of organic linkages can be obtained: ∥Si-O-R, ∥Si-O-Si-R, or ∥Si-R (where R is an alkyl or substituted-alkyl group).

∥Si-O-R Linkages:

The ∥Si-O-R type of bonding was studied early-on. The mechanistic pathway involves the esterification reaction between surface-hydroxyl groups and primary-organic alcohols.

$$∥Si\text{-}OH + HO(CH_2)_nCH_3 \rightarrow ∥Si\text{-}O\text{-}(CH_2)_nCH_3 + H_2O$$
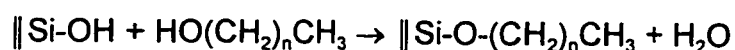
This particular type of bonding configuration, however, exhibits undesirable properties by hydrolyzing under aqueous conditions. Therefore, the surface-adsorption characteristics of the stationary phase can readily degrade with time and usage.

∥Si-O-Si-R Linkages:

The most commonly used reaction pathway for commercially-available-modified silica gives a siloxane linkage, ∥Si-O-Si-R. The reaction scheme is known as "organosilanization" (*1*). The process involves first preparing an organosilane reagent, which is then attached to the silica surface.

$$X_3SiH + CH_2=CHR \rightarrow X_3SiCH_2CH_2R$$

$$∥Si\text{-}OH + X_3SiCH_2CH_2R \rightarrow ∥Si\text{-}O\text{-}Si\text{-}CH_2CH_2R$$
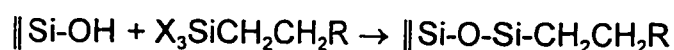
The X components can be a combination of alkyl group(s) and/or groups that easily hydrolyze, such as halides or alkoxys. Depending on the number of X groups that are used, the organosilane attachments can be bonded to the silica surface in two different fashions: monomeric or polymeric.

For monomeric attachments, monofunctionalized silanes are reacted with the silica surface. Chlorodimethylalkylsilanes are the most commonly used reagents to produce monomeric-bonded phases.

$$\| Si\text{-}OH + ClSi(CH_3)_2\text{-}R \rightarrow \| Si\text{-}O\text{-}Si(CH_3)_2\text{-}R + HCl$$
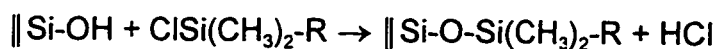
The siloxane linkage of the monomeric-bonded phase, however, is particularly prone to hydrolysis, especially under moderately acidic or slightly alkaline conditions. Also, the degree of surface coverage tends to be less than ideal, thereby leaving unreacted hydroxyl groups exposed on the surface. In reversed-phase chromatography, the hydroxyl groups are undesirable because they can lead to poor separations.

To overcome the hydrolytic instability of the monomeric-bonded phases prepared via the organosilation-reaction pathway, the attachments have been "polymerized" onto silica surfaces. For polymeric attachments, di- or tri-functionalized silanes are used. The additional functional groups can undergo condensation reactions with neighboring attachments and therefore crosslink as shown.

$$\|Si\text{-}OH + ClSi(OH)_2\text{-}CH_2CH_2R \rightarrow \begin{array}{l} \|Si\text{-}O\text{-}Si\text{-}CH_2CH_2R \\ \quad\quad\quad \diagdown O \\ \|Si\text{-}O\text{-}Si\text{-}CH_2CH_2R \\ \quad\quad\quad \diagup O \\ \|Si\text{-}O\text{-}Si\text{-}CH_2CH_2R \end{array}$$
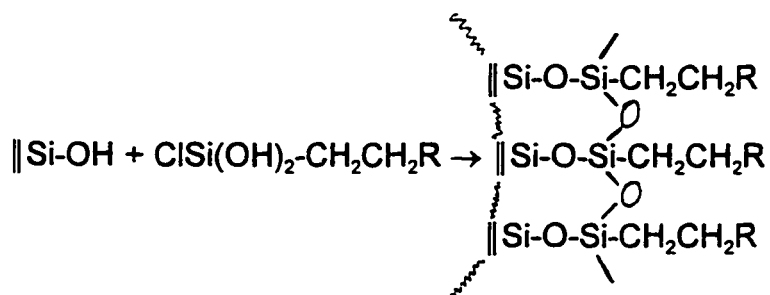
The polymeric-bonded phases, however, are reported to be less reproducible

from batch-to-batch compared to the monomeric-bonded phases (2). Also, not

all of the hydroxyl groups on the bonded silane are eliminated through

condensation, thereby contributing to the number of unreacted-undesirable

silanols on the stationary phase.

‖Si-R Linkages:

Compared to the ‖Si-O-R and ‖Si-O-Si-R types of bonds that have been

discussed, recent studies show that direct Si-C bonds are significantly more

hydrolytically stable than the Si-O bonds (3). Three general synthetic schemes

have been developed to produce silica-modified surfaces with Si-C bonds: (1)

chlorination/alkylation, (2) chlorination/reduction, and (3) silanization.

1) Chlorination/Alkylation: The chlorination/alkylation scheme involves

replacing the surface-hydroxyl groups with chloro groups. An alkylating reagent,

such as a Grignard or organolithium compound, can then be added to the silica

surface.

$$\| Si\text{-}OH + SOCl_2 \rightarrow \| Si\text{-}Cl + SO_2 + HCl$$

Grignard Reaction: $\quad\quad \| Si\text{-}Cl + RMgBr \rightarrow \| Si\text{-}R + MgClBr$

or

Organolithium Reaction: $\quad \| Si\text{-}Cl + Li\text{-}R \rightarrow \| Si\text{-}R + LiCl$
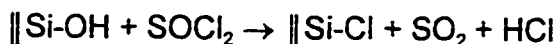
Several factors, however, impede the application of the chlorination/alkylation scheme for commercial use: (1) the two-step reaction is more difficult than the one-step organosilanization reaction, (2) only a limited number of alkylating reagents can be adequately prepared, and (3) the by-product salts (i.e., MgClBr and LiCl) are difficult to separate and remove from the alkylated products (*1*).

2) Chlorination/Reduction: This synthetic method also begins by chlorinating the silica surface. The second step, however, is to replace the chloro groups with hydride groups.

$$\| Si\text{-}OH + SOCl_2 \rightarrow \| Si\text{-}Cl + SO_2 + HCl$$
$$\| Si\text{-}Cl + LiAlH_4 \rightarrow \| Si\text{-}H$$
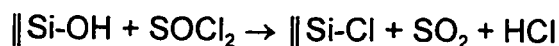
The hydride-coated surface can then react with terminal carbon-carbon double bonds with the aid of a catalyst, a reaction step known as "hydrosilation."

$$\| Si\text{-}H + H_2C\text{=}CHR \rightarrow \| Si\text{-}CH_2CH_2R$$

In addition to enhanced hydrolytic stability, the reaction products of hydrosilation show a more complete surface coverage than the other surface-modification methods. Also, this procedure offers the ability to attach a wide variety of organic-functional groups (e.g., ion-exchange, alkyl groups, liquid crystals, etc.), depending on the particular type of chromatographic-separation desired.

The preparation of the hydride intermediate, however, posses difficulties in the reaction scheme. The conditions must be meticulously free of moisture and the evolving volatile by-products must be collected with a condenser.

3) Silanization: In an effort to overcome the complexities and time-consuming steps encountered with the chlorination/reduction method, the "silanization" procedure was developed to more conveniently prepare the hydride intermediate. The first step in this method is to hydrolyze triethoxysilane (TES) to give silanetriol.

$$H\text{-}Si\text{-}(CH_3CH_2\text{-}O)_3 + 3OH^- \rightarrow H\text{-}Si\text{-}(OH)_3 + 3(CH3CH2\text{-}O)^-$$
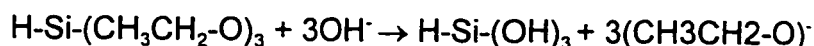
The silanetriol is then bonded to the silica surface through a condensation reaction.

$$\|Si\text{-}OH + H\text{-}Si\text{-}(OH)_3 \rightarrow \|Si\text{-}O\text{-}Si(OH)_2\text{-}H + H_2O$$
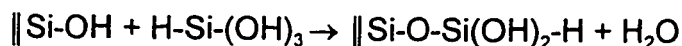
The silanol groups are next crosslinked to produce a hydride intermediate.

$$\| Si\text{-}O\text{-}Si(OH)_2\text{-}H \rightarrow \begin{array}{c} \| Si\text{-}O\text{-}Si\text{-}H \\ O \\ \| Si\text{-}O\text{-}Si\text{-}H \\ O \\ \| Si\text{-}O\text{-}Si\text{-}H \end{array}$$
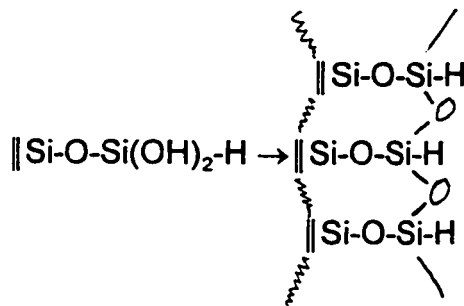
Just as in the hydrosilation step of the "chlorination/reduction" sequence discussed previously, a wide variety of organic-functional groups with terminal olefins can be added to the hydride intermediate with the aid of a catalyst. Most of the reactions studied thus far have involved hexachloroplatinic acid (H_2PtCl_6) as the catalyst.

$$\begin{array}{c} \| Si\text{-}O\text{-}Si\text{-}H \\ O \\ \| Si\text{-}O\text{-}Si\text{-}H + H_2C=CHR \rightarrow \\ O \\ \| Si\text{-}O\text{-}Si\text{-}H \end{array} \qquad \begin{array}{c} \| Si\text{-}O\text{-}Si\text{-}CH_2CH_2R \\ O \\ \| Si\text{-}O\text{-}Si\text{-}CH_2CH_2R \\ O \\ \| Si\text{-}O\text{-}Si\text{-}CH_2CH_2R \end{array}$$

Research Objectives

The chemical nature of the silica surface is extremely important as the stationary phase in HPLC. To help assess the surface-modification techniques, newly derivatized silica was chemically characterized by two analytical techniques: [1]H Nuclear Magnetic Resonance (^{1}H-NMR) Spectroscopy and Electron Spectroscopy for Chemical Analysis (ESCA).

A solid-state ^{1}H-NMR spectroscopy technique known as Combined

Rotation and Multiple-Pulse Spectroscopy (CRAMPS) was evaluated as an

analytical method to directly measure the different types of protons on the silica

surfaces. In particular, we measured the amounts of Si-OH protons on the bare-

silica starting compounds and the amounts of Si-OH and Si-H protons on the

silica-hydride intermediates. Because silica-based compounds are highly

hydrophilic, special precautions were taken to thoroughly dry the samples prior to

the quantitative NMR analyses to remove water protons that have a spectral-

masking effect. Thermogravimetric Analysis (TGA) was used to help identify the

appropriate drying conditions.

ESCA, also commonly known as X-ray Photoelectron Spectroscopy

(XPS), is a surface-analytical technique. The ESCA data quantitatively identify

the various elements present in the outermost ~70 Å (with the exception of H and

He that ESCA does not directly detect). Because some of the silica samples

were discolored, special attention was given for the presence of metal-catalyst

deposition (i.e., platinum from hexachloroplatinic acid, H_2PtCl_6) on the silica

surfaces.

Overview of NMR Spectroscopy

In the mid-1920's, the Austrian physicist Wolfgang Pauli suggested that

certain atomic nuclei should exhibit properties of both spin and magnetic moment

and that their energy levels would be split upon exposure to a magnetic field (4).

These postulates were verified by the mid-1930's. In 1946, two independent

research teams headed by Professors Felix Bloch at Stanford and E. M. Purcell

at Harvard demonstrated that once nuclei are oriented in an external-magnetic

field, transitions between energy levels can be induced by irradiation with radio

waves of the proper frequency. As a result of the energy-absorption process,

the nuclei are considered to be in resonance and "spin-flip" to a higher-energy

state with respect to the external-magnetic field. The 1952 Nobel Prize in

Physics was awarded to Bloch and Purcell for their work in the development of

Nuclear Magnetic Resonance (NMR) spectroscopy (5).

A few years after the physicists discovered NMR spectroscopy, chemists

learned that nuclei in different molecular environments resonate at slightly

different radio-wave frequencies. The frequency of a particular resonance is

commonly known as the "chemical shift." Chemical shifts are influenced by

nearby circulating-electron clouds that act as secondary-magnetic fields that

oppose the main field, thereby shielding the nuclei from the full effect of the

external-magnetic field. Since it is very difficult to measure absolute frequencies

to the required precision, a reference compound is used to measure the

frequency difference between the protons of the reference and the protons of the

sample. Tetramethylsilane (TMS), $(CH_3)_4Si$, is generally used as the chemical-

shift reference compound for ^1H, ^{13}C, and ^{29}Si-NMR spectroscopy. With ^1H-NMR

spectroscopy, the twelve protons are chemically identical and resonate at a

highly shielded frequency. In fact, very few protons in organic-based compounds

are surrounded with a greater electron density. Therefore, TMS protons are typically designated as resonating at 0.0 ppm. The protons of interest for this research project, Si-H and Si-OH, are less shielded by electrons and resonate between 1 and 8 ppm downfield with respect to TMS. With the ability to measure chemical shifts, chemists can use NMR spectroscopy to obtain structural information, both qualitative and quantitative.

NMR Spectroscopy of Solids verses Liquids:

The ability to collect NMR spectra of solids plays an important role in the characterization of many different classes of compounds, including insoluble materials, crosslinked polymers, inorganic compounds, and the surfaces of solids as reported in this research paper. Under the normal experimental parameters (i.e., single pulse excitation) used to collect ^{1}H-NMR spectra of liquids, solid samples typically give extremely broad-featureless spectra. The basic principles for NMR of liquids and solids are the same, except the rapid-molecular motion in the liquid state produces narrow isotropic chemical-shift values for the various types of protons. With rigid solid materials, this motion is absent. As a result, several interactions broaden the spectral lineshape. In more recent years, however, line-narrowing techniques such as "magic-angle spinning" and "multiple-pulse line-narrowing" have been developed to specifically offset the line-broadening effects encountered with ^{1}H-NMR spectroscopy of solids.

NMR Interactions that Broaden Spectra:

Four primary NMR interactions that are anisotropic in nature lead to spectral broadening in solids: (1) quadrupole coupling, (2) J-coupling (also known as "scalar coupling" and "indirect dipole-dipole coupling"), (3) chemical-shift anisotropy, and (4) direct dipole-dipole coupling (both homonuclear and heteronuclear). Fyfe describes these broadening interactions in quantum mechanical terms with a general Hamiltonian equation (6).

$$H = H_Q + H_J + H_{CSA} + H_D$$

Depending on the nature of the solid material under study, usually one or two of these interactions will dominate as the main mechanism(s) for the peak-shape broadening in solid-state NMR.

If the nuclear spin is greater than $\frac{1}{2}$ (e.g., ^{14}N, ^{27}Al, and ^{35}Cl), then the nucleus possesses a nonspherical nuclear electric charge distribution. As a result, the nucleus has a quadrupole moment and interactions with an electric field gradient typically generate significant broadening with solids. With the fast and isotropic motion of molecules in solution, the value for the quadrupole coupling is zero and is therefore not observed. The nuclei studied in the silica samples of this research project all contain a $\frac{1}{2}$ spin, so quadrupole coupling in this case is not a mechanism for line broadening, $H_Q = 0$.

The J-coupling interactions occur between nearby magnetically nonequivalent nuclei through covalent bonds. Molecular motion does not negate these interactions. Instead, these interactions alter the resonance frequency and lead to the splitting patterns that are normally observed in NMR spectroscopy of liquids. Considering the ~0.5 ppm resolution typically obtainable with organic compounds with solid-state ^{1}H-NMR spectroscopy, J-coupling is not a significant-broadening mechanism, $H_J \cong 0$ (7).

Chemical-shift anisotropy arises when the specific magnetic resonance of a nucleus is dependent upon the orientation of the molecule with respect to the external-magnetic field. For example, the nuclear resonance of the protons in a compound such as benzene in the solid state will give different chemical shifts when the molecule is aligned parallel versus perpendicular to the external-magnetic field. This anisotropy in the chemical shift of a powdered solid can be as wide as 100 ppm, which is about ten times the total range for isotropic-chemical shifts obtained with solutions (8). Chemical-shift anisotropy is actually spectral broadening due to a multitude of superpositioned, inherently-sharp chemical shifts of randomly oriented nuclei. To simulate the rapid tumbling of molecules in solution, a line-narrowing technique known as "magic-angle spinning" has been developed to remove the broadening effects attributed to chemical-shift anisotropy, thereby enabling the measurement of isotropic-chemical shifts, $H_{CSA} \rightarrow H_{isotropic-chemical\ shift}$.

Direct dipole-dipole coupling is the interaction between nearby magnetic nuclei (e.g., ^{1}H-^{1}H, ^{13}C-^{13}C, and ^{1}H-^{13}C). The concentration of magnetic nuclei is an important consideration for the NMR spectroscopy of solids. Because of the low natural abundance of ^{13}C (i.e., ~1.4 %), homonuclear ^{13}C-^{13}C coupling in organic solids is statistically a very weak interaction and does not significantly contribute to the line broadening in ^{13}C-NMR. Protons, however, with a high natural abundance (i.e., 100%) can show strong interactions between nuclei. Therefore, heteronuclear ^{1}H-^{13}C interactions broaden the ^{13}C-NMR spectra and ^{1}H-^{1}H interactions broaden the ^{1}H-NMR spectra. Similar to chemical-shift anisotropy, all orientations of direct dipole-dipole interactions of solids are convoluted, thereby co-adding to give broadened chemical shifts. The technique that is used to remove ^{1}H-^{1}H dipolar interactions in ^{1}H-NMR is known as "multiple-pulse line-narrowing," $H_D \rightarrow 0$.

NMR Relaxation Processes:

In the presence of an external-magnetic field of strength B_0, the spin ½ nuclei will align both with and against the magnetic field. They spin like gyroscopes at a rate known as the Larmor frequency about the field direction. Because of a slightly lower energy state, a small excess (~50 ppm in a 7 tesla field) of nuclei will align with the magnetic field to give a net macroscopic magnetic moment. Vector diagrams, with the coordinate system rotating at the

Larmor frequency, can be used to describe the nuclear assembly as shown in Figure 1 (9).
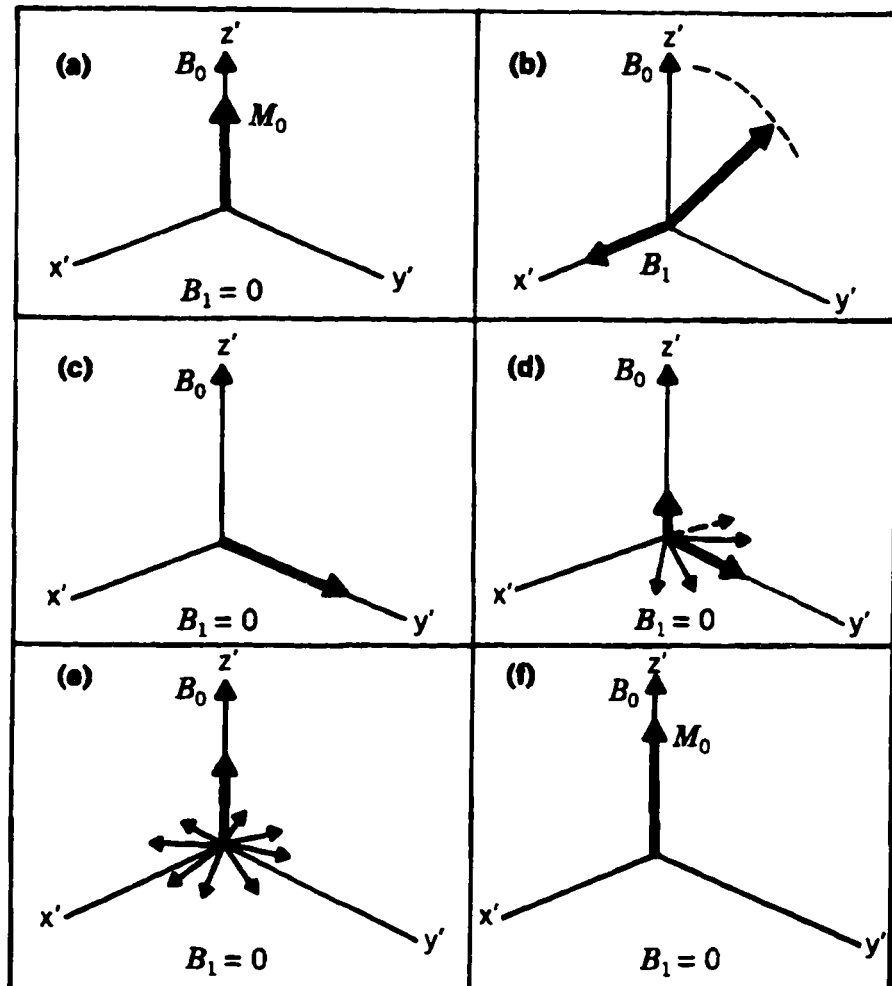
Figure 1: Vector Diagram of Nuclear Assembly

At equilibrium, the net magnetic moment (M_0) is aligned with the z axis, which is parallel to the external-magnetic field (B_0). Upon exposure to a radio-frequency pulse (B_1) at right angles to B_0, M_0 tilts through an angle Θ into the x-y plane,

where NMR signals can be detected. The NMR signal is maximized when Θ is

90°. After the B_1 pulse, the spin system relaxes in the x-y plane by spin-spin

relaxation (T_2). The T_2 process involves energy transfer between two nuclei. A

nucleus in an excited state relaxes and the energy is transferred to a nucleus in

a lower spin state, which then becomes excited. While the overall spin-state

population remains the same, the average lifetime of a particular excited nucleus

is shortened. The result is line broadening. A short T_2 implies a broad peak.

Along with the T_2 process, the excited nuclear spins also relax in the z direction

by a spin-lattice relaxation (T_1). With the T_1 process, thermal energy is

transferred from the excited nucleus to the surrounding lattice through

interactions such as the dipole-dipole coupling previously discussed. Relaxation

parameters such as T_1's have been used to characterize molecular motions of

polymers to relate bulk properties with molecular composition (10). The

magnitude of T_1 can vary significantly. For liquids T_1 values typically fall between

0.01-100 seconds; for solids T_1 values are much longer, sometimes days (11).

For quantitative measurements, the nuclei must be allowed to fully relax.

Therefore, T_1 values become an important property for determining appropriate

repetition rates. As a result of the T_1 and T_2 processes, the M decays back to its

original state along B_0.

High-Resolution Solid-State ^{1}H-NMR Spectroscopy:

As previously mentioned, the rapid molecular motion in liquids leads to narrow isotropic chemical-shift lines. With the restricted motion in the solid state, the lines become excessively broadened. With the silica samples under study, the spectral broadening is attributed to primarily two mechanisms: chemical-shift anisotropy (H_{CSA}) and ^{1}H-^{1}H dipolar coupling (H_D). Two line-narrowing techniques, magic-angle spinning and multiple-pulse line-narrowing, have been developed to minimize the effects of these line-broadening interactions.

The following equation described by Mehring shows the Hamiltonian expression for the chemical-shift anisotropy interaction (12).

$$H_{CSA} = \sigma_i \omega_0 I_z + \tfrac{1}{2}(3\cos^2\theta - 1)(\sigma_{zz} - \sigma_i)\omega_0 I_z$$

The first term on the right-hand side of the equation is an expression that represents the isotropic-chemical shift ($\sigma_{isotropic}$). The second term, however, represents the broadening associated with the orientation dependence of the static nuclei with the external field. By rapidly rotating the sample at $\theta = 54.7°$ with respect to the external-magnetic field, $3\cos^2\theta = 1$ and the broadening term in the equation is reduced to zero. In a rotating-frame diagram, this "magic angle" can be drawn as a vector pointing along the diagonal of a cube as shown in Figure 2.
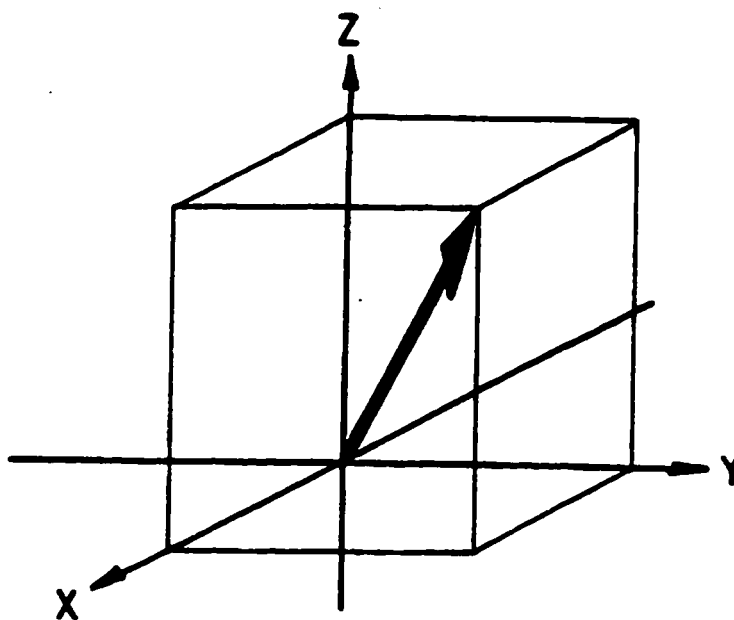
Figure 2: Vector Diagram of Magic Angle

Please note that by rapidly spinning at this angle, the sample does not show a particular bias for any one vector axis, thereby simulating the isotropic molecular motion of liquid materials.

The Hamiltonian expression for a direct dipole-dipole interaction is discussed by Gerstein (*13*).

$$H_D = -g_N^2\beta_N^2 \Sigma 1/r_{ij} \left[(r_i \bullet r_j - 3r_{iz}r_{jz}) \times (I_i \bullet I_j - 3I_{iz}I_{jz})\right]$$

The first term in the brackets is related to the spatial arrangements of the nuclear spins; the second term is related to the actual orientations of the spins.

The dipolar-broadening interaction can be reduced to zero by making one of these terms zero. The influences of the first term, at least in theory, can be reduced to zero by magic-angle spinning. With current technology, the required spinning speeds are too high (8). The second term, however, can be reduced to zero by manipulating the ^1H-^1H nuclear spins via the "multiple-pulse line-narrowing" technique. With this technique a series of radio-frequency pulses, with proper widths and intervals, is applied to the sample. The purpose of the pulse sequence is to give an average-nuclear spin that aligns with the magic-angle axis, thereby nullifying the nuclear dipole-dipole interactions. So while magic-angle spinning uses mechanical motion to mimic molecular motion in "real" space, multiple-pulse line-narrowing uses radio-frequency pulses to mimic molecular motion in "spin" space.

The first true multiple-pulse technique to remove the effects of homonuclear dipole-dipole couplings was introduced in 1968 by Waugh, Huber, and Haeberlen. The line-narrowing technique is commonly known as the WAHUHA sequence. The following diagram by Bovey (Figure 3) illustrates the four-pulse sequence and describes the behavior of the net-magnetization vector (14).
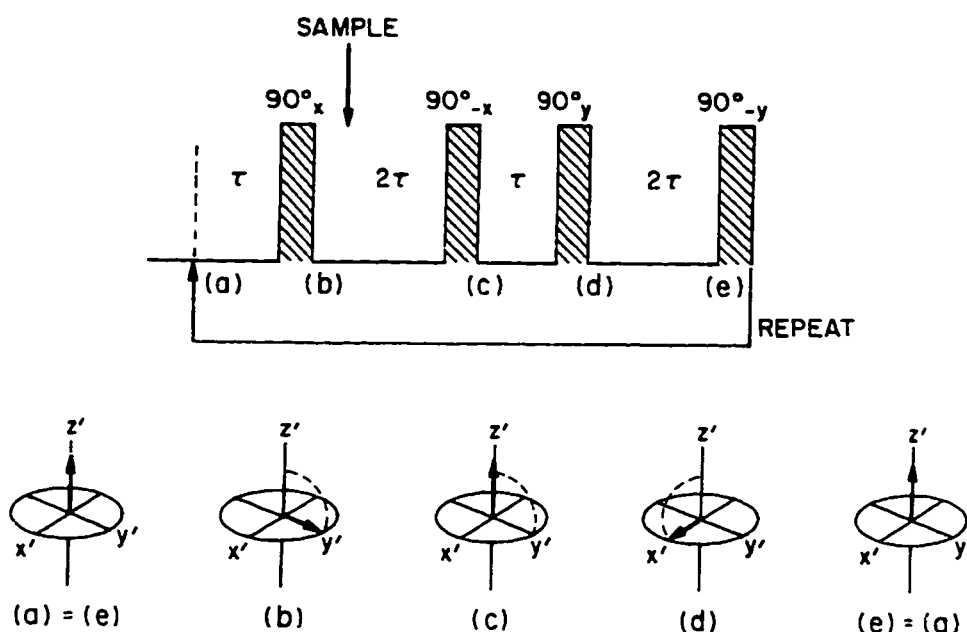
Figure 3: Diagram of WAHUHA Sequence

While the magnetization vector does not actually fall on the cube-diagonal axis, the vector spends an equivalent amount of time along each axis. As a result, the average vector falls along the diagonal. More sophisticated and complex pulse sequences such as MREV-8 and BR-24, which are difficult to describe with vector diagrams, are better at minimizing error by removing higher-order terms and are therefore more commonly used.

Combined Rotation and Multiple-Pulse Spectroscopy (CRAMPS):

The two line-narrowing techniques that have been discussed each have their own limitations. Magic-angle spinning reduces both spectral broadening

interactions under consideration (H_{CSA} and H_D), but it does not completing

remove the strongly coupled proton dipole-dipole interactions (H_D) due to the fast

spinning rates that are required. Multiple-pulse line-narrowing techniques can

achieve these spinning rates, but they do not remove the effects of chemical-

shift anisotropy (H_{CSA}). By simultaneously applying these two techniques during

an analysis, another high-resolution ^{1}H-NMR technique has been developed and

it is known as Combined Rotation and Multiple-Pulse Spectroscopy (CRAMPS).

For strongly coupled proton systems, CRAMPS provides the highest-resolution

^{1}H-NMR spectra of solid materials. Figure 4 illustrates the CRAMPS strategy

(15). The CRAMPS technique, however, is one of the most difficult high-

resolution ^{1}H-NMR methods available for solid-state NMR spectroscopy. Strict

requirements and programmability are necessary for proper pulse widths,

phases, and amplitudes. Extremely stable high power radio-frequency

amplification is also required. Specially designed probes are needed to provide

narrow, intense radio-frequency pulses. Also, the amplifier, probe, and receiver

must ring down quickly to allow collection of the NMR data immediately after the

radio-frequency pulse.

The single ^{1}H resonance of a solid, broadened by ^{1}H-^{1}H dipolar interactions and CSA interactions.

multiple-pulse | line narrowing

$$\left\{ \left(\text{I} \text{I} \quad \text{I} \text{I} \quad \text{I} \text{I} \quad \text{I} \text{I} \quad \text{I} \text{I} \quad \text{I} \text{I} \quad \text{I} \text{I} \middle| \text{I} \text{I} \quad \text{I} \text{I} \quad \text{I} \text{I} \quad \text{I} \text{I} \quad \text{I} \text{I} \right) \tau_{\text{delay}} \right\}_n$$

of the dipolar | interaction

moderate-speed | magic-angle spinning
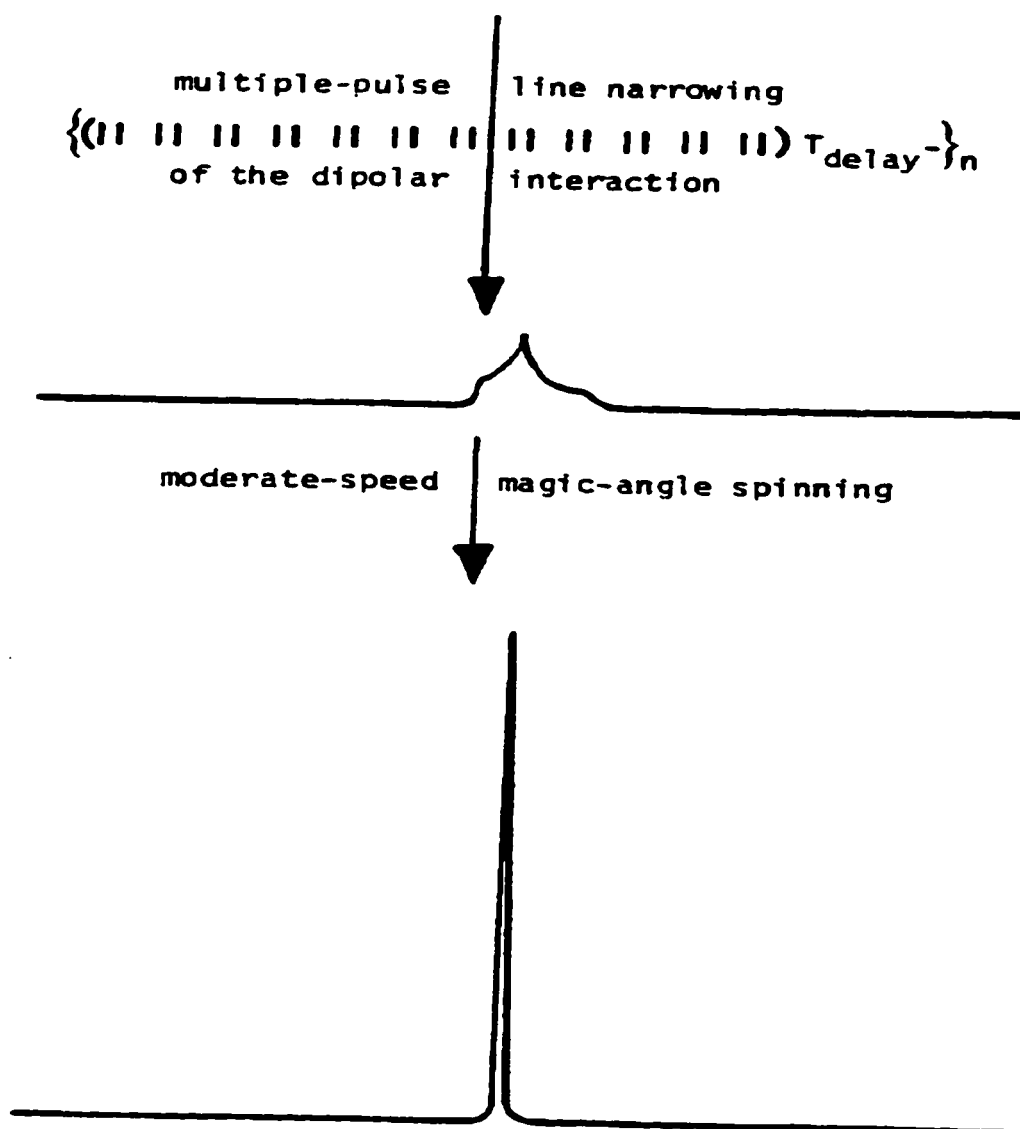
Figure 4: Diagram of CRAMPS Strategy

Quantitative NMR Measurements:

With the ability to collect high-resolution ^{1}H-NMR spectra with the CRAMPS technique, the various types of protons can be measured quantitatively. The fact that peak areas can be directly proportional to proton concentration is an attribute of ^{1}H-NMR spectroscopy. Both internal and external standards can be used to quantitate the various types of protons. To expedite the process of dehydrating the silica samples and collecting the NMR data before water readsorption, an external standard was chosen for this study, thereby eliminating the need to accurately weigh and mix the dehydrated silica and internal-standard compounds. A known amount of polydimethylsiloxane (PDMS) was used as the intensity standard. A recent publication by Maciel and Liu at Colorado State University shows that PDMS makes a good standard for quantitative analysis of solids by the CRAMPS technique (16). In their particular application, they used PDMS as an internal standard. Two types of silica-based compounds were included in their research: fumed silica and silica gel. They were able to quantitatively measure isolated Si-OH protons, hydrogen-bonded Si-OH protons, and physisorbed-water protons.

Overview of ESCA

Kai Siegbahn and his research group at the University of Uppsala, Sweden, developed Electron Spectroscopy for Chemical Analysis (ESCA), also commonly known as X-ray Photoelectron Spectroscopy (XPS), into a viable

analytical technique in the 1960's. Commercial spectrometers became available in the early 1970's. In 1981, Kai Seigbahn was awarded the Nobel Prize in Physics for his research and development of ESCA. ESCA has since become a widely used surface-analytical technique in both industry and academia. The technique is based on the photoelectric effect in which the absorption of X-ray photons causes the emission of photoelectrons. Only electrons from the first 1-10 atomic layers, however, give distinct signals in the ESCA spectra. All of the elements, with the exception of hydrogen and helium that are not directly observed by ESCA, emit photoelectrons with different energy levels. Therefore, ESCA offers the unique ability to quantitatively and qualitatively identify the elemental composition of the outer-atomic layers. In the case of silica-surface modifications, the ESCA data will help us assess catalyst deposition and chemical reactions taking place on the silica-substrate surfaces.

Fundamental Principles of ESCA:

The method is based on the photoelectric effect, originally discovered by Hertz in 1887, that involves the emission of electrons from the surface upon exposure to an X-ray beam (*17*). With modern-day instrumentation, samples are irradiated with soft monochromatic X-rays under ultra-high vacuum conditions, typically 10^{-8} to 10^{-9} torr. The sample surface emits photoelectrons from the atomic core and valence levels. The kinetic energies of the emitted photoelectrons are in turn detected by an electron analyzer. With the

conservation of energy, the binding energy (BE) of an electron is equal to the difference between the monochromatic X-ray photon energy (hv) and the kinetic energy (KE) of the detected photoemitted electron.

$$BE = hv - KE$$

Albert Einstein first described this relationship in 1905 and it is one of the first examples that light, X-rays in this case, behaves like particles rather than waves (*18*).

The ESCA data are presented graphically by plotting KE intensity (counts per second), which is directly related to the number of electrons, as a function of BE. Essentially all elements give unique photoelectron signals with binding energies between 0 and 1100 eV. As a result, all elements (with the exception of hydrogen and helium) provide ESCA spectra that can be used to identify surface compositions. With appropriate atomic-sensitivity factors for the various elements, the BE peak areas can be used to quantitatively identify the elemental composition. In most cases the elements can be detected at concentration levels greater than 0.1 atom percent and in some cases as low as 0.01 atom percent.

Another spectral feature prevalent in ESCA spectra are signals due to Auger electrons. After the emission of a negatively charged photoelectron, an atom resides in an excited state with a positive charge. As part of a relaxation

process to achieve a lower-energy state, an outer-shell electron falls into the inner-orbital vacancy. A concomitant outer-shell electron, known as an Auger electron, is thus emitted that carries off excess energy. The Auger electron is emitted approximately 1×10^{-14} seconds after the photoemitted electron. Therefore, irradiating samples with a monochromatic X-ray normally leads to two different kinds of emitted electrons: photoelectrons and Auger electrons. Figure 5 depicts a graphical representation of the two processes.
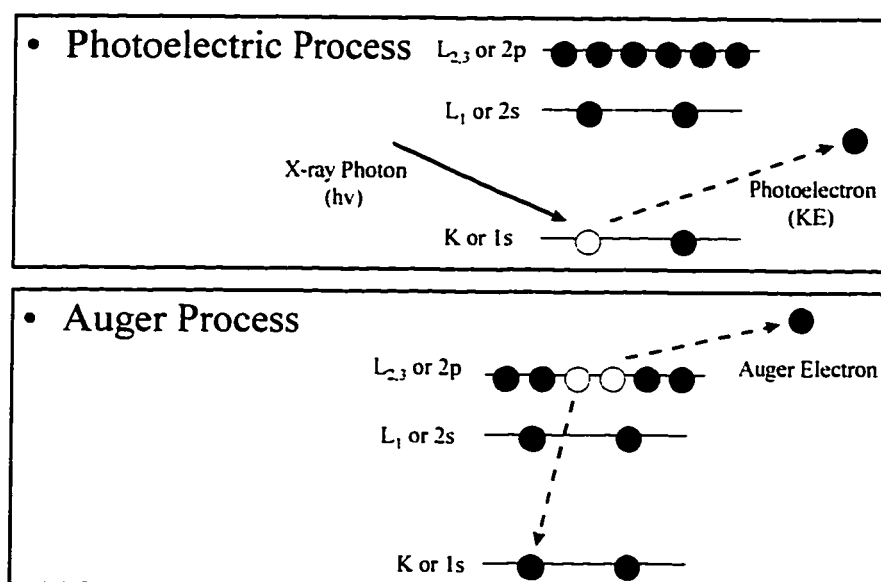
Figure 5: Diagram of ESCA and Auger Electron-Emission Processes

Please note that the nomenclature for describing photoelectrons and Auger electrons differs. The photoelectrons are described with the appropriate quantum numbers (e.g., 1s, 2s, $2p_{1/2}$, and $2p_{3/2}$). The Auger electrons are

identified with X-ray notation that describes the various electronic shells involved in the process (e.g., $K_1L_{2,3}L_{2,3}$, $L_3M_{2,3}M_{2,3}$, and $M_5N_{4,5}N_{4,5}$).

While the incident X-ray photons typically penetrate and ionize the samples to a depth of about 1-10 μm, the photoemitted electrons have a very short mean-free path of only about 100 Å. This is because the size of an electron is much larger than a photon; thus the probability of an electron interacting with other matter is much greater. Only electrons at, or near, the sample surface escape without losing energy by colliding with nearby atoms. Therefore, the photoemitted electrons that leave the surface without losing energy produce sharp peaks in the ESCA spectra. These sharp peaks, however, are superimposed upon a rising background, rather than a flat baseline, due to electrons that undergo inelastic-loss collision processes.

Elemental-Qualitative Analysis by ESCA:

For essentially all samples, a broad-scan survey spectrum from 0 to 1100 eV is first obtained to investigate and identify the various elements present. The primary C(1s) line acts as an internal standard with a generally accepted binding energy of 284.6 eV. The other photoelectron peaks are then evaluated to identify the elemental composition of the sample surface.

An important feature of ESCA is the ability to identify the chemical state of an element based on the "chemical shift" of the binding energy. For many elements, precise measurements of the binding energy can be used to

distinguish between oxidation states and molecular formulations. For example, the binding energies for covalently bound fluorine are about 689 ± 0.5 eV, while the binding energies for ionically bound fluorine are about 685 ± 2 eV. These differences in binding energies for fluorine are considered large and can typically be resolved with survey data. More commonly, however, high-resolution scans in the spectral regions of interest are necessary to make reliable chemical-state identifications for most elements.

Elemental-Quantitative Analysis by ESCA:

The photoelectron-peak areas from the survey data between 0 and 1100 eV are used to determine the relative concentrations of the various elements on the sample surface. The following equation defines the number of photoelectrons/second (I) in a spectral peak (19).

$$I = n(f\sigma\theta y\lambda AT)$$

where n = number of atoms of the element per cm^3 of the sample

 f = x-ray flux in photons/cm^2-sec

 σ = photoelectric cross-section for the atomic orbital of interest in cm^2

 θ = angular efficiency factor for the instrumental arrangement based on the
   angle between the photon path and the detected electron

 y = efficiency in the photoelectric process for the formation of the
   photoelectrons of the normal photoelectron energy

λ = mean free path of the photoelectrons

A = sample area from which the photoelectrons are detected

T = detection efficiency for the emitted photoelectrons

After rearranging the equation,

$$n = I/(f\sigma\theta y\lambda AT)$$

The denominator in this expression can be defined as the atomic-sensitivity factor (S) to give:

$$n = I/S$$

The values of S for the Perkin-Elmer Phi 5600LS Multi-Technique ESCA spectrometer have been determined by the instrument manufacturer for all of the elements. For a chemical system that contains two elements (with the exception of hydrogen and helium), the ratio of the elements can be given as:

$$n_1/n_2 = (I_1/S_1)/(I_2/S_2)$$

For chemical systems containing more than two elements, a more general expression for the atomic percent of a particular element (C_x) can be given as:

$$C_x = n_x/\Sigma n_i = (I_x/S_x)/\Sigma I_i S_i$$

Description of the Perkin-Elmer Phi 5600LS Multi-Technique ESCA

Spectrometer:

Figure 6 shows a schematic diagram of the Phi 5600LS Multi-Technique

ESCA Spectrometer.

Hemispherical-Electrostatic-FieldAnalyzer

Quartz Crystal
Disperser
(monochromator)

e⁻

Sample Stage

X-ray Source (anode)
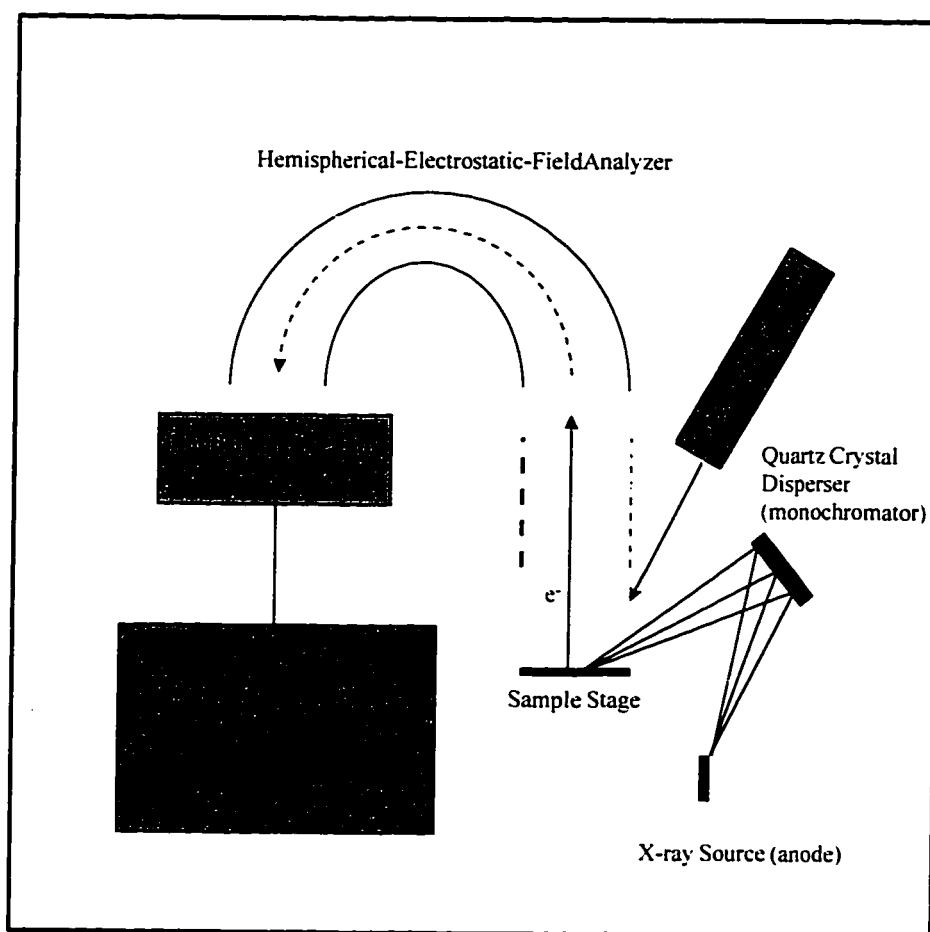
Figure 6: Schematic of Phi 5600LS ESCA Spectrometer

The spectrometer is equipped with an X-ray source (Model 10-610) that emits Al

$K\alpha$ photons of energy 1486.6 eV. To reduce the line width, the X-rays are

dispersed through a toroidal-quartz crystal that serves as a monochromator

(Model 10-420). The monochromatized X-ray radiation is then focused onto the sample surface. As a result, photoelectrons are emitted from the sample surface, passed through an Omni Focus III lens, and detected by a hemispherical-electrostatic-field analyzer (Model 10-360). The analyzer measures electron velocities that differ for the various elements. An Apollo Series 400 serves as the computer-control/data-acquisition system.

The analytical chamber operates under ultra-high vacuum conditions, typically ranging from 10^{-8} to 10^{-9} torr. The reasons for ultra-high vacuum conditions are twofold: (1) minimize the scattering of the emitted electrons due to collisions with gaseous molecules, and (2) minimize the deposition of gaseous components onto the sample surface during data acquisition. Samples are first evacuated in a preparation chamber to about 5×10^{-7} torr before being introduced into the analytical chamber.

While collecting ESCA data, nonconductive samples can develop a positive charge on the outer surface due to the emission of the negatively charged electrons. With conductive samples, the charge is grounded through the sample stage to the spectrometer. For testing nonconductive samples, the spectrometer is equipped with an electron "flood" gun. The flood gun dissipates low-energy electrons onto the sample surface to neutralize the charge.

The Phi 5600LS ESCA spectrometer also contains an argon-ion gun to etch away surfaces for elemental-composition depth profiling. Because the silica samples characterized in this study were porous and irregularly shaped rather

than flat, no surface etching was conducted to characterize the elemental

composition as a function of depth.

EXPERIMENTAL DETAILS

Materials

Samples of bare silicas, silica-hydride intermediates, and organically modified silicas were provided for both ^{1}H-NMR spectroscopy and ESCA characterization. The catalyst, hexacloroplatinic acid (H_2PtCl_6), was also tested as a control sample. For the ESCA analyses, the silica samples were coated and tested on 3M double-sided-sticky tape. Silicone rubber from Scientific Polymer Products, Inc., was used as the external standard for the NMR analyses. The molecular weight of the silicone rubber was 1,010,000 g/mol.

Thermogravimetric Analysis (TGA)

The silica samples were tested on a Thermal Analysis 2950 TGA . The TGA contains a microbalance that monitors the sample-weight change as a function of time and temperature. In the first TGA experiment, the temperature was programmed to ramp from 25 to 900 °C at 20 °C/minute. In other experiments, isothermal hold times of various durations were incorporated into the temperature-ramp profile. Either dry nitrogen or dry helium gas purged the TGA oven at ~50 mL/min throughout each run. The initial sample weights typically ranged from 10 to 15 mg.

Proton Nuclear Magnetic Resonance (NMR) Analysis

The silica samples were first dried in a vacuum oven (~0.1 torr) at 160 °C

for at least one hour. Samples were then transferred to 5-mm alumina NMR

rotors and weighed in a nitrogen-purged glove bag. The proton spectra were

collected on an MSL-200 Bruker spectrometer which operates at a ^{1}H frequency

of 200 MHz. The time lapse between removing a sample from the vacuum oven

and completing the ^{1}H-NMR data acquisition was about ten minutes. A Doty

probe was used to analyze the silica samples with the CRAMPS technique. The

probe spins the rotors at the magic angle (i.e., 54.7° with respect to the external-

magnetic field). The BR-24 sequence was used to remove the homonuclear

dipole-dipole couplings. The radio-frequency pulse widths were 1.5 μs and the

cycle time was 108 μs. The recycle time was set to 8 s. Qualitative

measurements indicated that this delay was sufficient to ensure a complete

return to thermal equilibrium. A 45° "y" pulse was used as a preparation pulse.

Chemical shifts were determined by referencing to tetramethylsilane (TMS) with

δ = 0 ppm. All data were collected at ambient temperature.

Electron Spectroscopy for Chemical Analysis (ESCA)

The ESCA data were obtained with a Perkin-Elmer PHI Model 5600LS

Multi-Technique spectrometer. The silica-powder samples were coated onto 3M

double-sided-sticky tape, mounted on a sample stage, and evacuated to a base

pressure of about 1×10^{-9} torr. To enhance the magnitude of the spectral peaks,

the sample stage was tilted to a take-off angle of 70° with respect to the normal surface plane. A monochromatic Al Kα X-ray source (1486.6 eV) operating at 400 W irradiated the samples with a spot diameter of 800 μm. A hemispherical-electrostatic-field analyzer with a 187.85 eV pass energy and a 0.4 eV resolution detected the kinetic energies of the emitted photoelectrons between 0 and 1100 eV. The binding energies were normalized to the C(1s) line at 284.6 eV. All ESCA data were collected at ambient temperature.

RESULTS AND DISCUSSION

Recent studies show that direct silicon-carbon bonds between silica-based substrates and organic attachments show improved surface coverage and hydrolytic stability (*1, 3, 20*). The reaction sequence first involves converting the surface Si-OH groups into Si-H groups. The Si-H intermediate can then react with a wide variety of terminal olefins to produce organic-derivatized chromatographic-stationary phases. The ability to synthesize a Si-H intermediate with high surface coverage is a critical step in the process. Poor surface coverage of hydride groups leads to poor surface coverage of the organic attachments. In more recent years, the newly developed "silanization" method gives roughly a 4-fold increase in surface Si-H coverage when compared to the older "chlorination/reduction" method (*3*).

Several spectroscopic techniques have been used to characterize the bare silica, the silica-hydride intermediates, and the silica-organic derivatized products. The most important chemically bonded groups to evaluate on the silica surface throughout the reaction sequence include Si-OH, Si-H, and Si-C. Because silica is hydrophilic, physically adsorbed water on the surface is also an important consideration when measuring the -OH and -H contents quantitatively.

In the past, the Si-OH content on bare-silica samples has typically been measured by Thermogravimetric Analysis (TGA). Samples are pretreated at 110 °C to remove adsorbed water. As the temperature is then ramped from 110 to

900 °C, the Si-OH groups condense and liberate water. The amount of weight loss can be used to estimate the original Si-OH content. Caution must be used with this technique, however, because silica has been known to retain water at temperatures up to 180 °C (3). Also, there is the possibility that some of the Si-OH groups are isolated and therefore do not have the ability to condense with neighboring groups at high temperatures

A variety of techniques have also been used in previous studies to evaluate the Si-H content on the intermediate surfaces. Infrared spectroscopy shows a strong absorption band between 2300 and 2100 cm^{-1} that is attributed to Si-H bonds. This particular location in the infrared spectrum is advantageous because very few compounds give absorption bands in this region. Two thermoanalytical techniques, Differential Scanning Calorimetry (DSC) and Thermogravimetric Analysis (TGA), can also be used to characterize the Si-H intermediate under oxidative conditions. DSC shows an exothermic peak due to thermooxidation between 350 and 400 °C; TGA thermograms show a corresponding weight gain.

$$\| Si\text{-}H + \tfrac{1}{2} O_2 \rightarrow \| Si\text{-}OH + heat$$
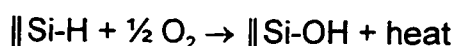
Isolated chemical shifts found with ^{29}Si magic-angle spinning NMR have also been used to characterize the Si-H intermediate. Due to the lack of Si-H standards, the infrared spectroscopy, DSC, TGA, and ^{29}Si-NMR techniques only

provide qualitative analyses and rough semi-quantitative analyses. The best technique currently available to measure the Si-H content is by reacting the substrate under alkaline conditions (KOH in H_2O/ethanol) and measuring the liberated hydrogen gas by gas chromatography. The degree of accuracy for the quantitative aspects of this technique, however, are in still question.

The amount of Si-C on the final product can be determined by elemental analysis. A Perkin-Elmer model 240C elemental analyzer, which uses a combustion technique to determine the carbon content, has been used on derivatized-silica samples in the past.

TGA Analysis to Evaluate Water Content

To better understand the nature of the adsorbed water and to determine how to dehydrate the silica samples for subsequent ^{1}H-NMR tests, the Vydac bare silica was characterized by Therogravimetric Analysis (TGA). Figure 7 shows the weight-loss profile and the corresponding derivative profile as the sample was heated from 25 to 900 °C in a nitrogen-purged environment. The weight loss between 25 and 150 °C is primarily due to the liberation of water. At higher temperatures, the Si-OH groups condense to give off additional water with an associated weight loss. Based on the TGA data, 160 °C was found to be an appropriate temperature to dehydrate the silica samples without condensing the surface Si-OH groups of interest. Figure 8 shows the thermogram of the bare silica heated to 160 °C and held isothermally for two hours. The weight lost was

about 6%. The data indicate that a hold time of at least one hour is sufficient to dehydrate the silica samples for the NMR characterization.

A few interesting observations were noted during the TGA analyses. Silica samples begin loosing weight immediately upon enclosure in the TGA furnace. Figure 9 shows the weight-loss profile for the bare silica that was first held isothermally at 25 °C for one hour before ramping up the temperature. Under the conditions of semi-dry gas purging the silica samples at room temperature, the sample weight decreases about 2%. We also found that after dehydrating the samples at 160 °C, the samples readily regain weight in the TGA furnace upon cooling. Figure 10 shows the temperature profile and corresponding weight-change profile for a sample of bare silica that was heated to 160 °C, held isothermally for one hour, and then rapidly cooled back down to 25 °C. Even though the TGA furnace was purged with dry helium in this case, there was enough moisture in the system for the silica material to rapidly regain ~1.5% of the original weight during the cool-down cycle. Similar observations were made when the TGA furnace was purged with dry nitrogen instead of dry helium.

The rehydration rate under normal open-air laboratory conditions was next determined. The purpose of this test was to measure how much water the silica samples can readsorb in the first ten minutes after the 160 °C dehydration procedure, which is roughly the amount of time required to collect the ^{1}H-NMR CRAMPS data. About 0.1 grams of the TES-hydrosilanized silica was baked at

160 °C for one hour in a vacuum oven (~1.0 x 10^{-2} torr). The sample was removed from the oven at the elevated temperature and placed onto an analytical balance. Under these conditions, the weight gain was hand recorded as a function of time; the data points are plotted in Figure 11. The rehydration rate is rapid. Most of the water is readsorbed within ten minutes. Therefore, special precautions must be taken to effectively dehydrate the silica samples and to minimize the readsorption of water prior to completing the acquisition of the ^{1}H-NMR data.

^{1}H-NMR CRAMPS Analysis

·   To compliment the data that has been previously collected by other spectroscopic techniques (e.g., DSC, TGA, GC, ^{29}Si-NMR, and infrared spectroscopy), ^{1}H-NMR data were collected via the CRAMPS technique on three sets of silica samples: Vydac, Davisil, and Kromasil. With the ability to obtain high-resolution data, the Si-OH and Si-H protons on the silica surfaces can be evaluated. By using an external standard, polydimethylsiloxane (PDMS) in this case, the integrals of the chemical-shift bands provide quantitative information pertaining to the various protons.

A recent study by Maciel and associates at Colorado State University shows that silica-based compounds give an intense chemical-shift band around 4.0 ppm due to physically adsorbed water (21). They also report that the broad band between 2 and 8 ppm can be assigned to Si-OH groups in various

hydrogen-bonded environments. The narrow band around 2.0 ppm can be assigned to isolated Si-OH groups.

Figure 12 shows the overlaid spectra of the "non-dried" Vydac-bare silica, the hydride intermediate, and the octyl-derivatized product. The spectra of the Vydac bare silica and hydride intermediate are essentially identical. The chemical shift for Si-H has not been found in the literature, but it is expected to appear around 4-5 ppm. With the data collected at this point, we suspected that physically adsorbed water masked the chemical-shift band of the Si-H groups. As previously mentioned, the TGA data of the Vydac-bare silica (Figure 8) show that the material is about 6% by weight physically adsorbed water. For the case of the Vydac silica with a surface area of about 106.5 m^2/g as shown in Table i, the proton content on the silica surface due to water is calculated to be about 62,600 $\mu mol/m^2$. The surface density of silanol groups on silica surfaces is generally accepted as about 8 $\mu mol/m^2$ (3). With the abundance of water protons superimposed upon the Si-H chemical-shift band, the need to effectively dehydrate the silica samples prior to collecting the ^{1}H-NMR CRAMPS data is essential.

Based on the TGA data, the silica samples were dehydrated at 160 °C for at least one hour. The samples were then weighed on a balance located in a nitrogen-purged glove bag and immediately analyzed by the ^{1}H-NMR CRAMPS technique. The overlaid spectra for the bare silica and the hydride intermediates for the Vydac, Davisil, and Kromasil samples are shown in Figures 13-15,

respectively. Upon close examination of the bare-silica spectra, the chemical-shift band that was assigned to the adsorbed water around 4-5 ppm has been effectively removed by the dehydration process. As Maciel reported in the literature, a sharp peak for the isolated Si-OH groups is observed at about 2.0 ppm and a broad band for the hydrogen bonded Si-OH groups is observed between 2 and 8 ppm. Also, the chemical-shift band for Si-H was found to be located at about 4.5 ppm.

The total area under the chemical-shift bands can be integrated for a quantitative analysis to determine the total proton content on the various silica samples. The CRAMPS spectrum for 0.00522 grams of PDMS is shown in Figure 16. The chemical shift appears at about 0.2 ppm. By calculating the number of protons in the PDMS standard, the area under this peak can be used to calculate the number of protons on the silica samples. The PDMS standard was tested four times throughout the duration of the NMR tests on the silica samples. The average area for the PDMS protons was found to be 1.28×10^8. The number of protons per PDMS chain and the number of moles of PDMS in the standard were first determined as follows.

No. of $H_{PDMS\,chain}$ = [(MW_{PDMS}, g/mol)/($MW_{repeat\,unit}$, g/mol)](No. of $H_{repeat\,unit}$) = 8.17×10^4

Moles of PDMS standard = (mass PDMS, g)/(MW_{PDMS}, g/mol) = 5.17×10^{-9} moles PDMS

where,

MW_{PDMS} = 1,010,000 g/mol
$MW_{repeat\,unit}$ = 74.16 g/mol {repeat unit $\equiv$ (Si(CH$_3$)$_2$-O)}
No. of $H_{repeat\,unit}$ = 6

Therefore, the total number of protons in the PDMS standard can be determined.

$$\text{Moles } H_{\text{PDMS STD}} = (\text{No. of } H_{\text{PDMS chain}})(\text{Moles PDMS}) = 4.22 \times 10^{-4} \text{ moles H}$$

The peak areas can then be used in the following equation to calculate the total number of hydrogens in the various silica samples.

$$\text{Moles } H_{\text{silica}} = [(\text{Peak Area}_{\text{silica}})/(\text{Peak Area}_{\text{PDMS STD}})](\text{Moles } H_{\text{PDMS STD}})$$

By substituting in the known values shown above,

$$\text{Moles } H_{\text{silica}} = (3.30 \times 10^{-12} \text{ moles H})(\text{Peak Area}_{\text{silica}})$$

Table I lists the weights of the various silica samples, the total areas under the integrated CRAMPS spectra, the surface areas (3, 22), and the total number of moles of hydrogen per sample calculated with the equation shown above. The number of hydrogen atoms were also normalized to the sample weights and corresponding surface areas as shown in Table I.

Table I: Total Proton Content on Silica Samples

Sample ID	Mass, g	Total Peak Area	Surface Area, m^2/g	H Atoms, mmole	H Atoms, mmol/g	H Atoms, $\mu mol/m^2$
Davisil, Bare	0.03935	6.30×10^7	480	0.21	5.3	11
Davisil, Hydride	0.03595	5.50×10^7	480	0.18	5.0	10
Kromasil, Bare	0.02380	5.87×10^7	329.1	0.19	8.0	24
Kromasil, Hydride	0.03770	6.35×10^7	329.1	0.21	5.6	17
Vydac, Bare	0.02643	3.82×10^7	106.5	0.13	4.9	46
Vydac, Hydride	0.03747	5.93×10^7	106.5	0.20	5.3	50

For the bare-silica samples shown above, assuming all of the adsorbed water was effectively removed, the total proton content is attributed to the Si-OH groups. These values are relatively close (i.e., within an order of magnitude) of the generally accepted value of 8 $\mu mol/m^2$. Although the Vydac silica has the smallest surface area, it has the highest Si-OH content; this trend is consistent with data from previous studies (3, 20). Also, the Si-OH content on the Vydac silica has been previously reported to be about 50 $\mu mol/m^2$ based on TGA weight-loss data (3), which agrees very well with the 40-50 $\mu mol/m^2$ values shown in Table I.

To determined the relative populations of the various types of protons on the silica surfaces, the total-peak areas of the CRAMPS spectra (as reported in

Table I) were deconvoluted with curve-fitting software. Table II lists the results of the deconvolution process.

Table II: Relative Populations of Each Proton Species

Sample ID	Relative Proton Populations, %		
	H-Bonded Si-OH	Isolated Si-OH	Si-H
Davisil, Bare	64.8	35.2	-
Davisil, Hydride	30.1	16.3	53.6
Kromasil, Bare	82.1	17.9	-
Kromasil, Hydride	30.7	6.9	62.4
Vydac, Bare	52.8	47.2	-
Vydac, Hydride	34.2	6.8	59.0

The data in Table II show that roughly 55-65% of the original Si-OH groups are converted to Si-H groups. The conversion efficiencies for the three different types of silica samples are fairly similar.

With the total-proton populations in Table I and the relative-proton populations expressed as percentages in Table II, the amounts of the H-bonded Si-OH groups, the isolated Si-OH groups, and the Si-H groups can ultimately be determined as shown in Table III.

Table III: Proton Content for Each Species

Sample ID	H-Bonded Si-OH		Isolated Si-OH		Si-H	
	mmol/g	μmol/m^2	mmol/g	μmol/m^2	mmol/g	μmol/m^2
Davisil, Bare	3.4	7.1	1.9	3.9	-	-
Davisil, Hydride	1.5	3.0	0.8	1.6	2.7	5.4
Kromasil, Bare	6.6	19.7	1.4	4.3	-	-
Kromasil, Hydride	1.8	5.2	0.4	1.2	3.7	10.6
Vydac, Bare	2.6	24.3	2.3	21.7	-	-
Vydac, Hydride	1.8	17.1	0.4	3.4	3.1	29.5

ESCA Analysis

ESCA provides a surface-analytical technique for characterizing materials. ESCA-survey data give the elemental composition of the outermost ~70 Å. With the exception of H and He, all elements can be detected. Because the sensitivity for the various elements differs, the peak areas in the ESCA spectra are not directly proportional to the atomic concentration. With known sensitivity factors for the elements, however, the peak areas can be used to calculate the relative amounts of the elements present. A previous report shows that low levels of Pt on the silica surface can lead to deleterious effects on the

chromatographic properties with some solutes (23). In this study, special

attention is being given for the presence of Pt on the silica surfaces as a result of

catalyst deposition (i.e., H_2PtCl_2).

Because the silica samples are nonconductive, the emission of the

photoelectrons leads to a net positive charge on the sample surface. As a result,

this positive charge alters the kinetic energy of the emitted photoelectrons and

causes the measured binding energies to shift and broaden. To minimize the

influences of sample charging, a flood gun sprays low-energy electrons (usually

10 eV or less) onto the sample surface. Peak shape is the most important

feature to optimize when adjusting the flood gun parameters. The positive

charge on the sample shifts and broadens all the binding energies in the

spectrum to the same degree. For each of the silica samples, the C(1s) band

was used to optimize the flood gun parameters to give sharp-intense signals.

The appropriate flood gun settings varied from sample to sample. After

collecting the data, the spectra were normalized by shifting the entire spectrum

by aligning the C(1s) band with 284.6 eV as suggested by the Perkin-Elmer PHI

5600LS Multi-Technique spectrometer instruction manual. Other instrument

manufactures, however, recommend shifting the C(1s) band to slightly different

values ranging from 284.6 to 285.2 eV, so care must be taken when comparing

data collected on different spectrometers.

After optimizing the flood gun parameters with the C(1s) band, ESCA data

were collected on each sample in the survey mode. The survey mode gives a

broad-scan spectrum for photoelectron binding energies ranging from 0 to 1100

eV. Essentially all detectable elements show major photoelectron peaks in this

region. To collect data in the survey mode, a "pass energy" of 187.85 eV was

used for the electron analyzer. In principle, the pass-energy parameter functions

similarly to the slit-width parameter on a dispersive monochrometer. A higher

pass energy allows more throughput to produce a greater signal intensity, thus

better detection limits. A lower pass energy, however, improves the signal

resolution to give more precise measurements of the binding energies.

Chemical state information on many elements can often be obtained with high-

resolution data. After identifying the various elements present with the survey

scan, lower pass energies of 58 and 5 eV were used in certain cases to collect

high-resolution spectra on certain elements. The time required to collect high-

resolution data is significantly longer. Therefore, only data in narrow spectral

windows (~30 eV wide) around the elements of interest are acquired. High-

resolution data for the C(1s) signal is almost always collected for the

normalization process.

Hexachloroplatinic acid (H_2PtCl_6) was used as the catalyst for most of the

reactions involving the addition of organic linkages to the silica-hydride

intermediates. A Rh-based catalyst and 2,2'-azobisisobutyronitrile (AIBN), a

common radical initiator in polymer chemistry, were also used in a few cases.

Figure 55 shows the ESCA-survey spectrum of a control sample of H_2PtCl_6. The

most intense peaks for Pt fall between 65 and 85 eV and they are attributed to

the emitted photoelectrons from the $Pt(4f_{7/2})$ and $Pt(4f_{5/2})$ orbitals, respectively. Therefore, the regions between 65 and 85 eV of the silica spectra were carefully evaluated for the presence of Pt.

The samples that have been analyzed by ESCA fit into three categories: Davisil silica, Vydac silica, and various miscellaneous samples. Tables IV-VI list the surface-elemental compositions for the three sets of samples. Figures 17-66 show the corresponding spectra. Platinum was detected on several of the silica samples at levels ranging from 0.01 to 0.12 atom percent. With the standard experimental parameters used to collect the ESCA-survey data, the lower detection limit for Pt is estimated to be about 0.01 atom percent.

Table IV: ESCA Data for Atomic % of Detected Elements on Davisil-Silica Samples

Sample Description	Catalyst	C	O	Si	N	F	Pt	Cl	Na	Figure No.
Davisil Diol (Gray) #6	Pt	23.76	53.19	22.55	-	0.24	0.12	-	-	17
Davisil Diol Allyl Glycidyl Ether 6A	Pt	19.23	55.34	22.81	-	2.51	-	-	-	18
Davisil Diol 7-Octene-1,2,-Diol 6B	Pt	22.93	53.65	22.81	-	0.47	0.03	-	-	19
Davisil Diol 7-Octene-1,2-Diol 6C	Pt	25.26	51.47	22.74	-	0.40	-	-	-	20
Davisil Diol Allyl Glycidyl Ether Bonded 0.05M HCl (run 1)	Pt	19.02	55.53	22.78	-	2.60	-	-	-	21
Davisil Diol Allyl Glycidyl Ether Bonded 0.05M HCl (run 2)	Pt	24.40	52.06	20.89	-	2.50	-	-	-	22
Davisil Diol Allyl Glycidyl Ether Bonded 0.05M HCl (run 3)	Pt	19.85	55.22	22.19	-	2.57	-	-	-	23
Davisil + 1H, 1H, 2H- Perfluorooctene	Pt	10.12	60.41	27.99	-	1.42	-	-	-	24
Davisil + 4-Phenyl-1-Butene Run 1	Pt	25.64	48.71	22.48	-	3.09	-	-	-	25
Davisil + 4-Phenyl-1-Butene Run 2	Pt	27.35	48.09	22.12	-	2.35	-	-	-	26
Davisil Bare Silica Run 1	N/A	6.25	65.47	28.03	-	-	-	-	-	27
Davisil Hydride Run 1	N/A	5.45	63.88	30.47	-	-	-	-	-	28
Davisil Diol RD 377 H Run 1	N/A	19.43	56.7	23.6	-	-	-	-	-	29
Davisil Diol Lot# 141614 Run 1	N/A	14.54	59.13	25.02	-	-	-	1.16	-	30
Davisil AGE (set 2)	Pt	21.08	54.23	22.22	-	2.33	-	-	-	31
Davisil MPAB Run 1	Pt	21.53	54.21	23.97	-	0.21	-	-	-	32
Davisil Phenyl Run 1	Pt	32.87	45.20	19.81	-	2.12	-	-	-	33
Davisil C-18	Pt	32.20	46.30	21.00	-	0.60	-	0.01	-	34
Davisil Cholesterol	Pt	27.27	50.47	21.90	-	0.36	-	-	-	35
Davisil -- MPAB, 149300	Rh	36.83	44.09	18.88	-	0.19	-	-	-	36
Davisil MPAB-Silica (13100)	Pt	38.40	43.00	18.60	-	::	-	-	-	37
Davisil MPAB-Silica (15300) (control sample)	Pt	35.90	44.30	18.70	0.80	-	-	-	0.20	38

Table V: ESCA Data for Atomic % of Detected Elements on Vydac-Silica Samples

Sample Description	Catalyst	C	O	Si	N	F	Pt	Cl	Figure No.
Vydac Diol (Gray) #5	Pt	37.64	44.03	18.10	-	-	0.06	-	39
Vydac Diol Allyl Glycidyl Ether #5A	Pt	44.31	40.47	15.00	-	-	-	-	40
Vydac Diol 7-Octene-1,2,-Diol 5B	Pt	34.41	45.82	19.10	0.49	0.17	0.01	-	41
Vydac Diol 7-Octene-1,2-Diol 5C	Pt	39.24	42.75	17.78	-	0.20	-	-	42
Vydac Diol Allyl Glycidyl Ether Bonded 0.05M HCl	Pt	34.63	46.54	18.57	-	-	-	0.22	43
Vydac +1H, 1H, 2H-Perfluorooctene	Pt	20.63	54.34	23.97	-	1.01	-	-	44
Vydac + 4-Phenyl-1-Butene	Pt	39.81	41.65	18.23	-	-	-	-	45
Vydac-Hydride (Run 1)	N/A	21.36	54.06	24.40	-	-	-	-	46
Vydac Bare Silica Run1	N/A	24.21	53.34	22.26	-	-	-	-	47
Vydac Hydride Batch 2 Run 1	N/A	19.77	55.05	25.09	-	-	-	-	48
Vydac Diol from Vydac-H Batch 2 Run 1	Pt	38.67	42.84	18.46	-	-	-	-	49
Vydac + AGE Sample 5D Run 1	Pt	38.35	43.87	17.50	-	0.26	-	-	50
Vydac AGE-Diol (Vydac-H) -- batch# 2 (Run 1)	Pt	31.37	48.17	19.71	0.49	-	0.03	0.23	51
Vydac TP – C18	Pt	42.69	39.20	18.50	0.62	-	-	-	52
Vydac TP – C8	Pt	36.17	44.05	19.28	0.50	-	-	-	53

Table VI: ESCA Data for Atomic % of Detected Elements on Miscellaneous Samples

Sample Description	Catalyst	C	O	Si	N	F	Pt	Cl	Ti	Na	Rh	Figure No.
Double-Sticky Tape Run 1	N/A	83.91	15.81	0.15	-	-	-	-	-	-	-	54
Platinum Catalyst (H_2PtCl_6)	N/A	60.85	12.37	-	-	-	6.11	20.67	-	0.13	-	55
Platinum Catalyst (H_2PtCl_6)	N/A	62.54	6.53	-	2.69	0.30	6.67	21.26	-	-	-	56
S01P31C	Pt	25.7	49.7	23.2	-	-	1.4	-	-	-	-	57
S01P34C	Pt	20.1	52.1	27.1	-	-	0.7	-	-	-	-	58
S01P35C	Pt	23.2	52.1	24	-	-	0.7	-	-	-	-	59
Titania 3 days (batch# 2) dated 7-8-94	N/A	44.5	43.7	-	-	-	-	0.4	11.4	-	-	60
Titania 7 days (batch# 2) dated 7-15-94	N/A	62.3	29.1	0.3	1.6	-	-	-	6.7	-	-	61
C30 Pt ST9031	Pt	37.7	43.2	19.2		-	-	-	-	-	-	62
C30 AIBN STG032	AIBN	26	50.8	23.2	-	-	-	-	-	-	-	63
R(+) NEA	Pt	28.9	48.7	21.5	1.0		-	-	-	-	-	64
S(-) NEA	Pt	16.7	57.5	25.4	-	0.5	-	-	-	-	-	65
BKSI004	Rh	14.7	57.1	25.3	2.5	0.5	-	-	-	-	-	66
2-Methyl-3-Butennitrile	AIBN	26.5	50.0	21.3	1.4	0.8	-	-	-	-	0.02	67
$NC(CH_2)_4CN$	AIBN	36.1	44.3	18.7	-	0.9	-	-	-	-	-	68

52

In an attempt to detect lower levels of Pt on the silica surfaces, a greater

number of scans were collected to enhance the signal-to-noise ratios. The PHI

5600LS spectrometer does not report levels below 0.01 atom percent. To

evaluate a method for detecting lower levels, two samples from the

miscellaneous group [NC(CH2)4CN and 2-methyl-3-butenitrile] were scanned

with narrow analysis windows for just C and Pt. The other instrumental

parameters used to obtain the data in this "high-sensitivity mode," particularly the

pass energy of the electron analyzer, were the same as those used to collect the

ESCA-survey data. By testing in this mode, many more scans can be collected

on specific-spectral regions than in the survey mode (e.g., 4300 vs 32 numbers

of scans) for a given amount of time, thereby increasing the signal-to-noise

ratios. With the areas from these spectral windows and the corresponding

sensitivity factors for each element, the ratio of Pt (if present) with respect to

carbon can be determined. With this ratio and the amount of carbon from the

survey data, lower levels of Pt can be evaluated. The following general equation

can be used to determine the amounts of the elements at lower levels tested in

this manner.

% of element X = [(Area$_x$)/(SF$_x$)]/[(Area$_{carbon}$)/(SF$_{carbon}$)] x (% carbon from survey data)

where SF$_x$ = sensitively factor for specific element

Even after 4300 scans in the Pt(4f) region with these two samples, no spectral bands were detected. This technique, however, can still be used to establish lower-level detection limits for Pt. The C and Pt spectra for the two samples are shown in Figures 69-72. The integrated areas for C and Pt (which is the baseline noise in this case) are listed in Table VII. The sensitively factors for C and Pt, provided by the software of the Perkin-Elmer Phi 5600LS Multi-Technique ESCA spectrometer, and the carbon-content data from the survey spectra are also listed.

Table VII: ESCA Data for High-Sensitivity Analysis of Pt

Sample ID	Element	Area, cts-eV/s	Sensitivity Factor	% C (from survey data)	% Pt (calculated)
NC(CH2)4CN	C Pt	69,319 57	58.185 939.769	36.14 N/A	N/A 0.002
2-methyl-3-butenitrile	C Pt	57,001 69	58.185 939.769	26.53 N/A	N/A 0.002

As shown in Table VII, the integrated area of the flat baseline in the Pt(4f) region gives a value for Pt at 0.002 atom percent for both samples. By assuming that a signal-to-noise ratio of at least 3 is needed to assign a peak to Pt, then the

lower detection limit for Pt by testing in this manner is about 0.006 atom percent.

Compared to the lower detection limit of about 0.01 atom percent obtainable with

the survey mode, this high-sensitivity technique for acquiring data was not found

to significantly enhance the detection limits for Pt.

The ESCA data collected thus far also revealed the presence of some

unexpected elements on the surfaces of several silica samples. Chlorine,

presumably from the H_2PtCl_6 catalyst, was detected on a variety of samples at

concentrations ranging from 0.22 to 1.16 atom percent. Although no F was

found on the bare silica samples and the hydride intermediates, levels between

0.17 and 3.09 atom percent were observed on many of the organic-derivatized

samples, especially the derivatives of the Davisil silica. Based on the ESCA-

survey data, the binding energy for F was about 689 eV in all cases, which is

consistent with F in the covalent state rather than the ionic state. For a more

thorough analysis to accurately characterize the molecular environment of F,

high-resolution spectra were collected on F and C of two samples: Davisil Diol

Allyl Glycidyl Ether and Davisil 4-Phenyl-1-Butene. The ESCA spectra for F are

shown in Figures 73 and 74, respectively. As with the ESCA-survey data, the F

was found to be covalent with a binding energy of about 689 eV.

The only apparent source of covalently bound F on the silica surfaces was

from Teflon-coated stirring bars used during the derivatization process. To test

this hypothesis, a sample of bare silica (Vydac TPB5, E950505-31) was stirred

with three Teflon-coated stirring bars for five days. ESCA-survey data were then

collected on the "stirred" silica and compared to a "control" sample. Table VIII

lists the surface-elemental compositions; the corresponding spectra are shown in

Figures 75 and 76.

Table VIII: ESCA Data of Silica Stirred with Teflon-Coated Bars

Sample ID	C	O	Si	F
Stirred Sample	17.1	55.7	25.0	2.2
Control Sample	17.4	57.6	25.0	-

Based on the data shown in Table VIII, the F detected on most samples

described in this report comes from the Teflon coating on the stir bars,

presumably through an abrasion-type process.

CONCLUSION

CRAMPS, which is a solid-state ^{1}H-NMR technique that combines "magic-angle spinning" with "multiple-pulse line-narrowing," was used to acquire high-resolution spectra on the silica-based compounds. The ^{1}H-NMR spectra were deconvoluted and integrated with curve-fitting software. With the use of an external standard (i.e., PDMS in this case), the data provide a way to quantitatively measure the Si-OH protons on the bare silica and both the Si-OH and Si-H protons on the silica-hydride intermediates.

ESCA, which is a surface-analytical technique that gives the elemental composition of the outermost ~70 Å, showed that Pt from the catalyst deposited on some of the organically derivatized-silica products. Covalent F was also detected on most of the derivatized-silica samples. A series of controlled experiments showed that the F comes from Teflon-coated stir bars that are used while bonding the organic groups to the silica surface with the "silanization" technique.

REFERENCES

1. Sandoval, J. E.; Pesek, J. J. *Anal. Chem.* **1991**, *63*, 2634-2641.

2. Wirth, M. J.; Fatunmbi, H. O. *Anal. Chem.* **1993**, *65*, 822-826.

3. Chu. C.; Jonsson, E.; Auvinen, M.; Pesek, J. J.; Sandoval, J. E. *Anal. Chem.* **1993**, *65*, 808-816.

4. Pauli, W. *Naturwiss* **1924**, *12*, 741.

5. Skoog, D. A. *Principles of Instrumental Analysis,* 3rd ed.; CBS College: Philadelphia, 1985; pp 407-450.

6. Fyfe, C. A. *Solid State NMR for Chemists*; C.F.C.: Guelph, Ontario, Canada, 1983.

7. Maciel, G.; Frye, J. S. Notes from the Solid State NMR Course given by NMR Concepts, Fort Collins, Colorado, December 1989.

8. Gerstein, B. C. *Anal. Chem.* **1983**, *55*, 781A-790A.

9. Bovey, F. A.; Jelinski, L. W. In *Concise Encyclopedia of Polymer Science and Engineering*, Kroschwitz, J. I., Ed.; John Wiley and Sons: New York, 1990; pp 660-668.

10. Gerstein, B. C. *Anal. Chem.* **1983**, *55*, 899A-907A.

11. Paudler, W. W. *Nuclear Magnetic Resonance, General Concepts and Applications*; John Wiley and Sons: New York, 1987.

12. Mehring, M. *High Resolution NMR in Solids*; Springer-Verlag, Berlin Heidelberg: New York, 1983.

13. Gerstein, B. C. *Phil. Trans. R. Soc. Lond.* **1981**, *299*, 521-546.

14. Bovey, F. A. *Nuclear Magnetic Resonance Spectroscopy,* 2nd ed.; Acedemic: San Diego, CA, 1988.

15. Bronnimann, C. E.; Hawkins, B. L.; Zhang, M.; Maciel, G. E. *Anal. Chem.* **1988**, *60*, 1743-1750.

16. Liu, C. C.; Maciel, G. E. *Anal. Chem.* **1996**, *68*, 1401-1407.

17. Briggs, D.; Seah, M. P. *Practical Surface Analysis*; John Wiley and Sons: New York, 1983.

18. Garrett, J. W. "Materials Outgassing Effects, Detection, and Standards." Lecture presented at the Institute of Environmental Sciences Technical Meeting, 1995.

19. Moulder, J. F.; Stickle, W. F.; Sobol, P. E.; Domben, K. D. *Handbook of X-ray Photoelectron Spectroscopy*; Chastain, J. Ed.; Perkin-Elmer Corporation: Eden Prairie, Minnesota, 1992.

20. Pesek, J. J.; Sandoval, J. E.; Chu, C. H.; Jonsson, E. *Chemically Modified Surfaces*, **1992**, 57-72.

21. Chuang, I.; Kinney, D. R.; Maciel, G. E. *J. Am. Chem. Soc.* **1993**, *115*, 8695-8705.

22. Pesek, J. J.; Matyska, M. T.; Soczewinski, E.; Christensen, P. J. *Chromatographia* **1994**, 39, 520-528.

23. Pesek, J. J.; Matyska, M. T.; Hemphala, H.; Christensen, P. J. *J. Liq. Chromatogr.* **1995**, 18, 2507-2526.

Sample: VYDAC BARE SILICA (LT# 900806-4) TGA
Size: 28.8710 mg
Method: RT TO 900 °C @ 10 °C/min
Comment: L/R XXXXXX, N2 @ 30mL/20mL/min

File: A:7SILICA.193
Operator: P. J. CHRISTENSEN
Run Date: 18-Apr-95 19:01

Weight-loss Curve

Derivative Curve

Deriv. Weight (%/°C)

Weight (%)

Temperature (°C)

General V4.1C DuPont 2100
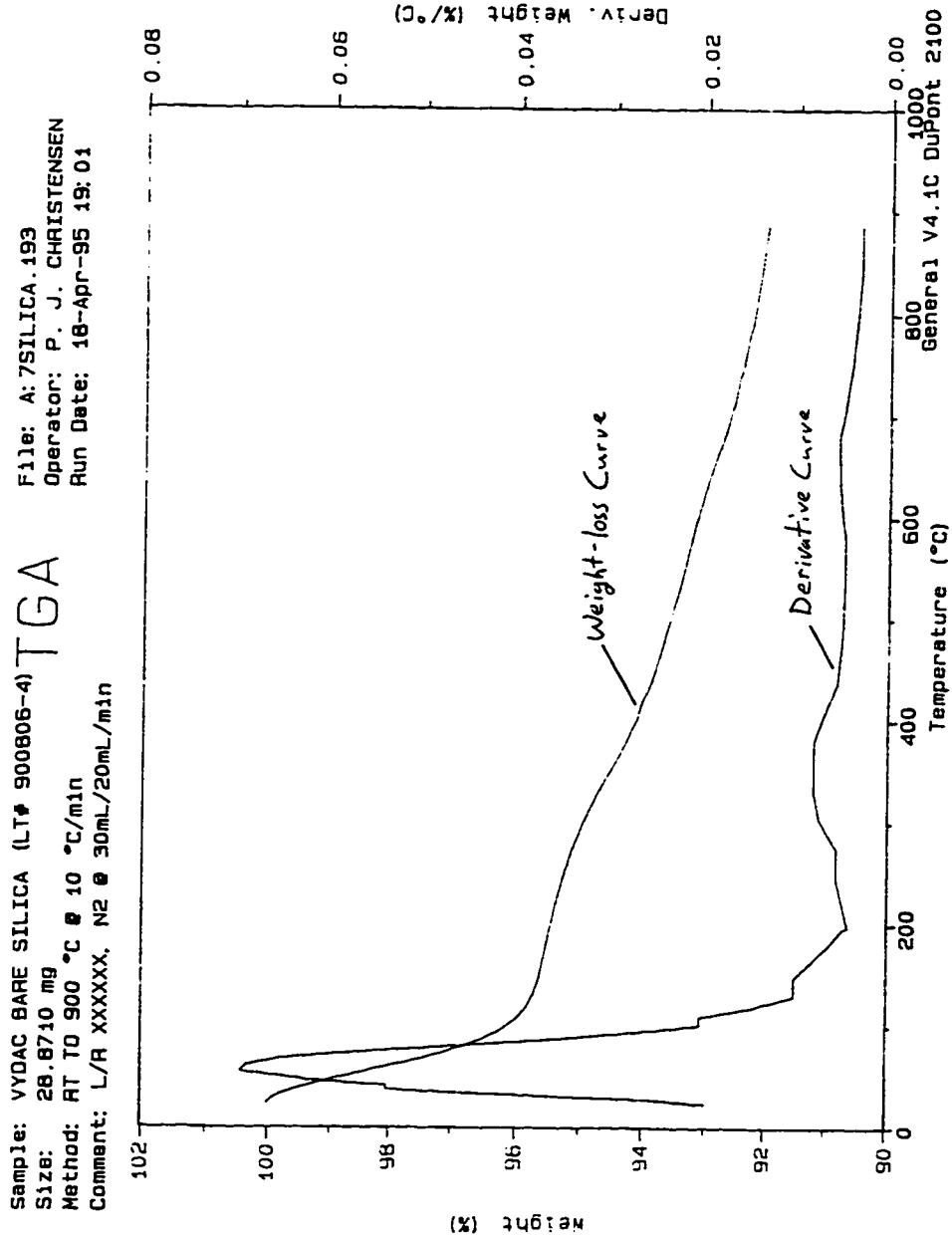
Figure 7: TGA Data of Vydac-Bare Silica (25-900 °C)

TGA

Sample: VYDAC BARE SILICA
Size: 25.3630 mg
Method: RT TO 160 °C and hold
Comment: XXXXXX Nitrogen Flowing @ 50mL/30mL/min

File: C:7VYDAC.318
Operator: P. J. CHRISTENSE
Run Date: 9-Sep-96   12:15

120 min. at 160 °C

10 %/min.

General V4.1C DuPont 2100

Temperature (°C)

Weight (%)

Time (min)
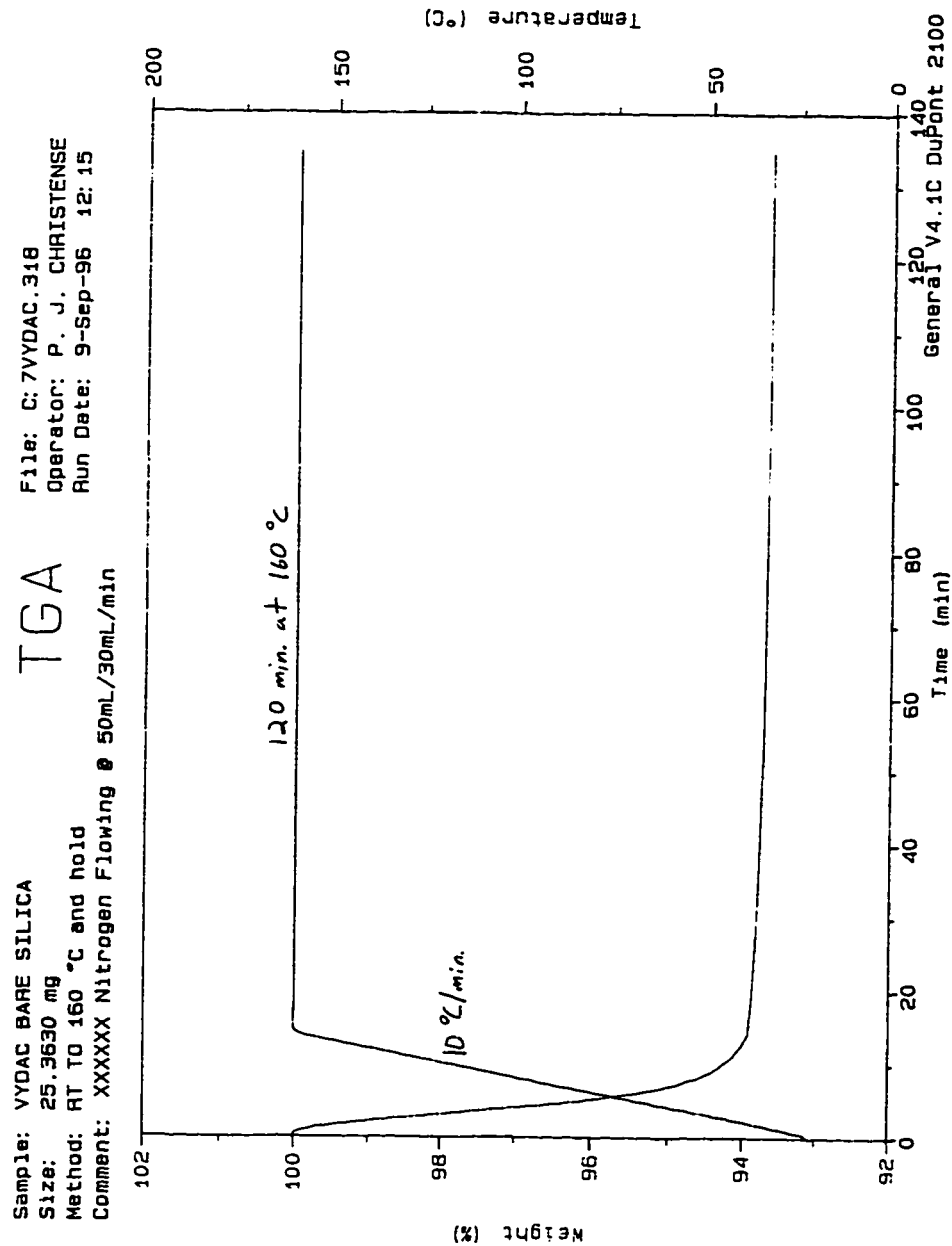
Figure 8: TGA Data of Vydac-Bare Silica (25-160 °C and Held Isothermally for Two Hours)
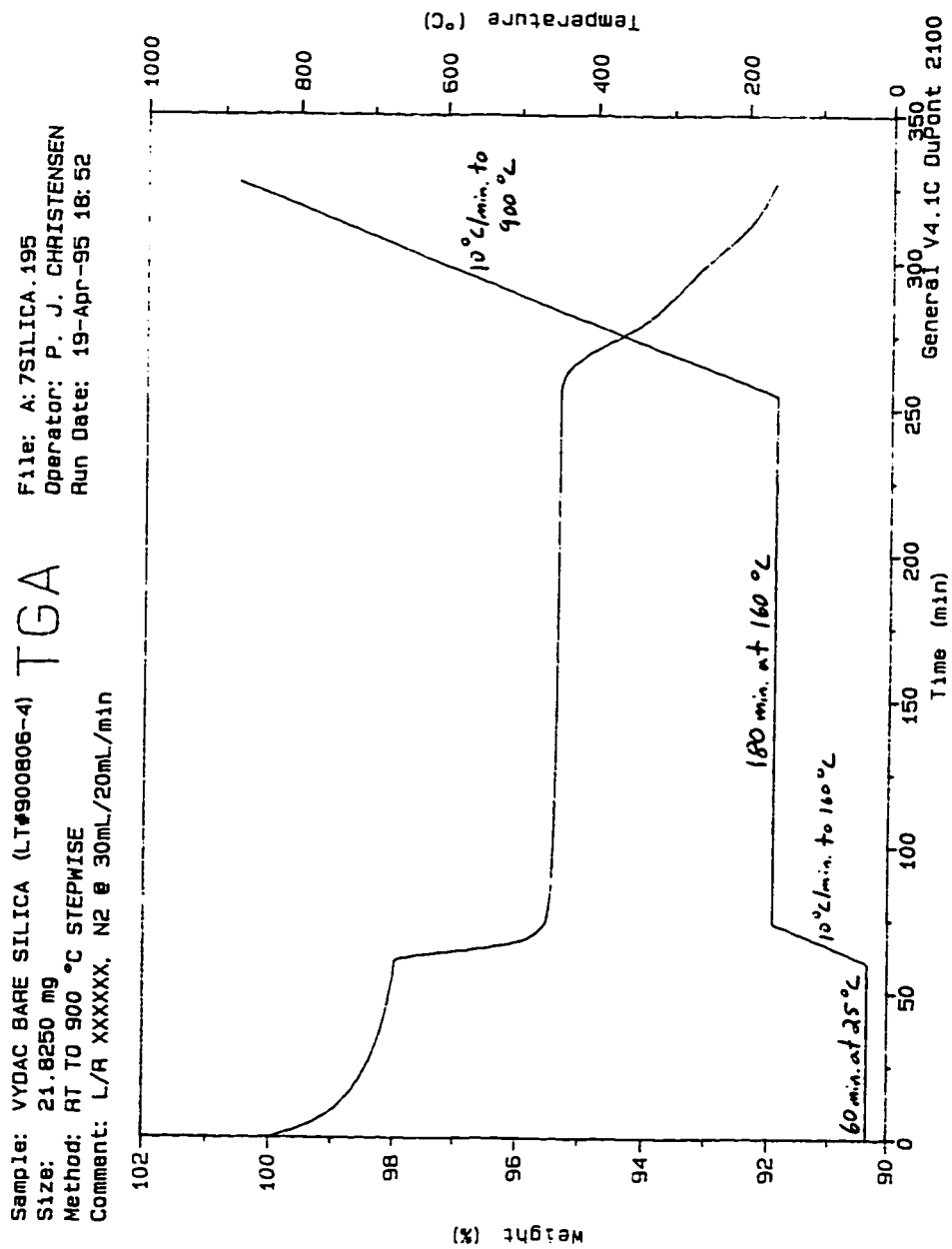
Figure 9: TGA Data of Vydac-Bare Silica (25-900 °C Stepwise)
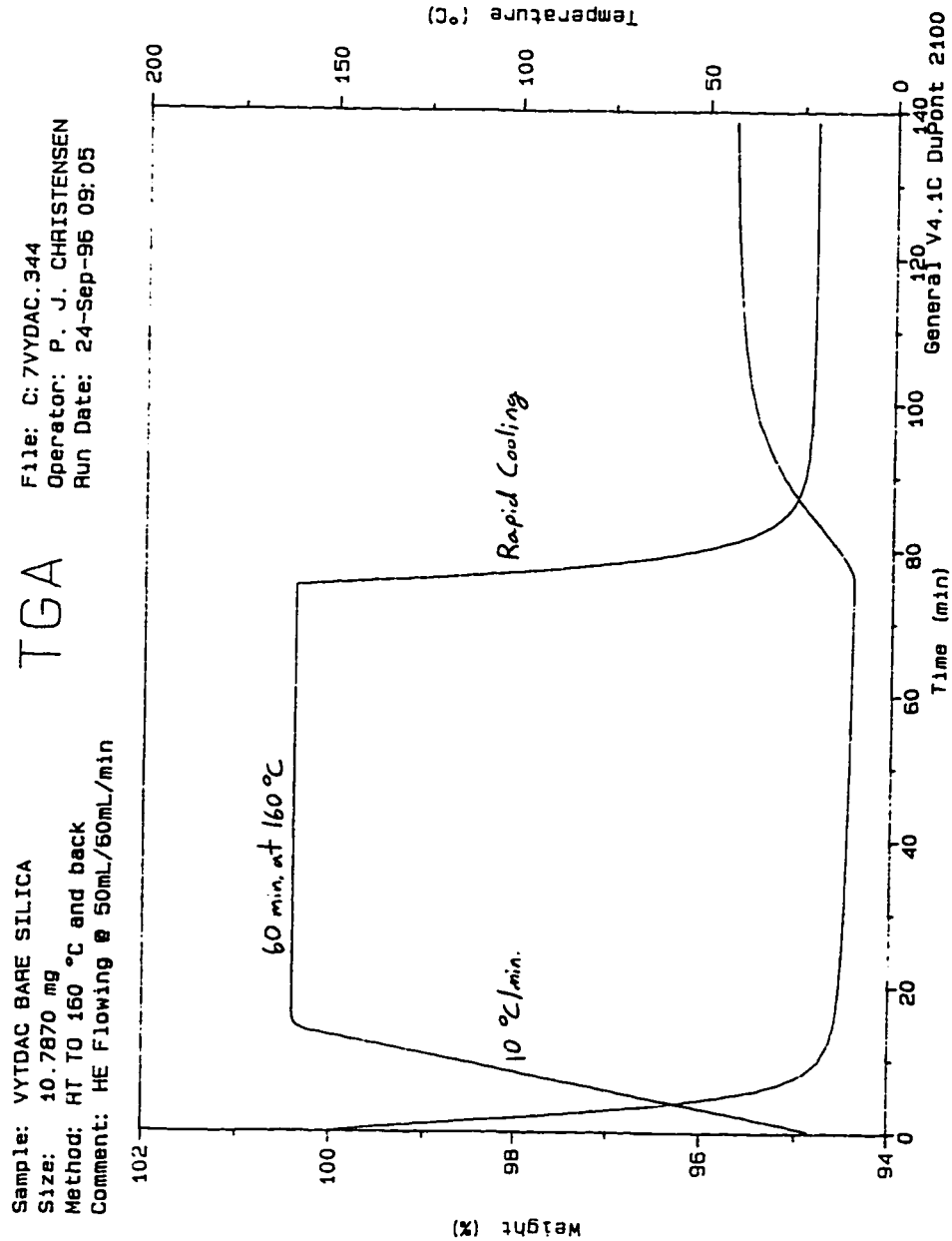
Figure 10: TGA Data of Vydac-Bare Silica (25-160 °C, Held for One Hour, and Rapidly Cooled to 25 °C)

64
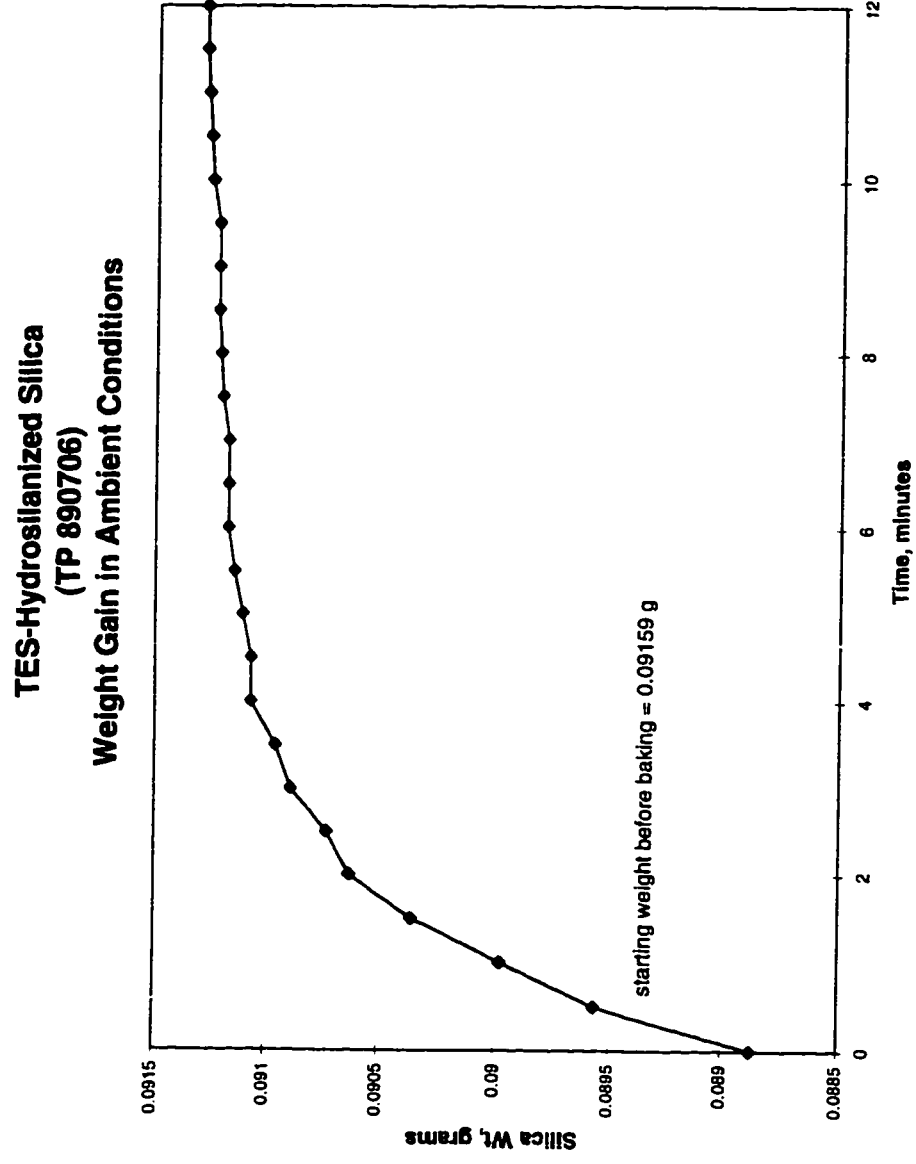
Figure 11: Silica Weight Gain in Ambient Conditions

VYDAC SILICA GEL. WET

VYDAC SILICA GEL. HYDRIDE. WET

WET VYDAC SILICA GEL. DERIVATIZED MATERIAL

```
  10.0        5.0        0.0
              PPM
```
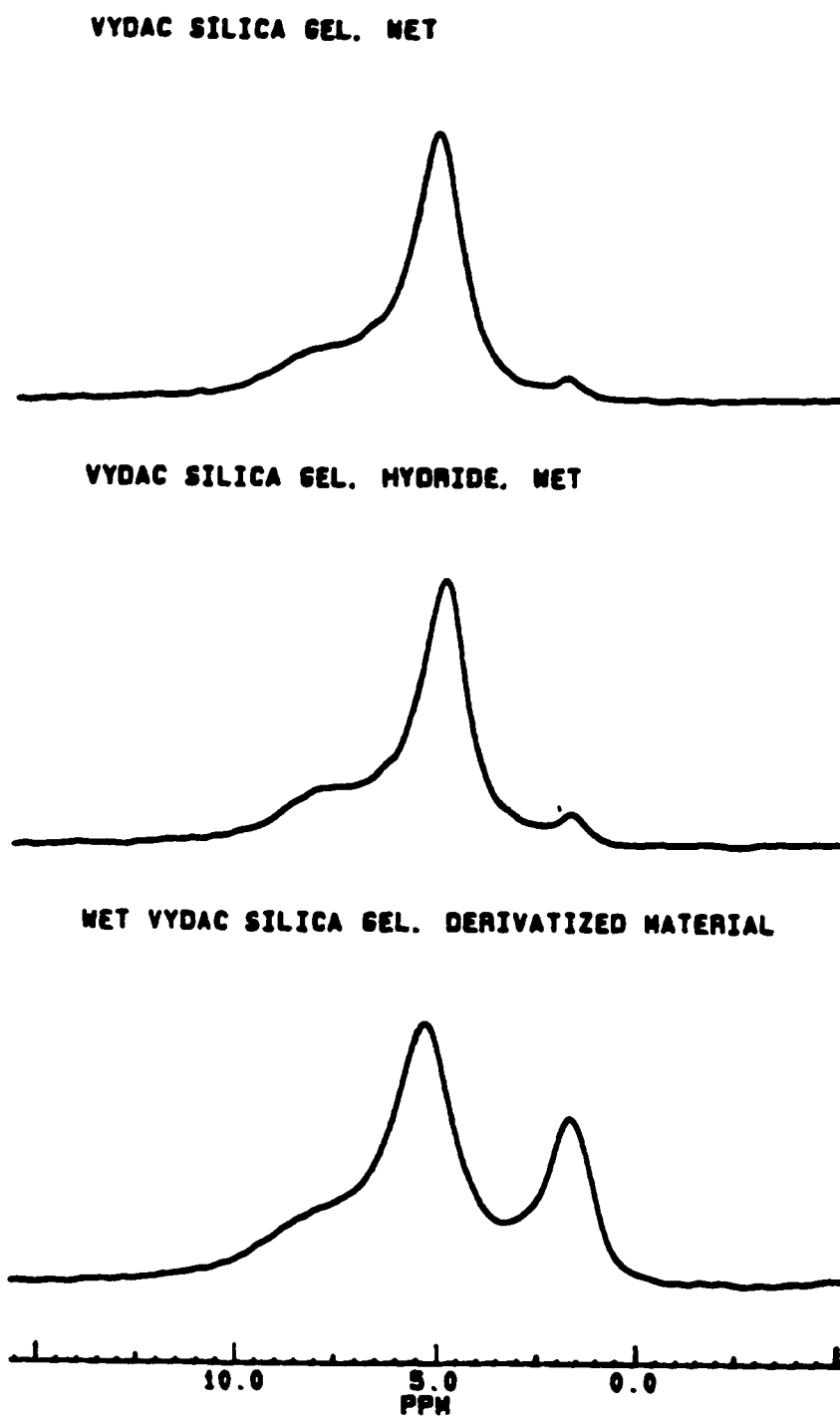
Figure 12: CRAMPS Spectra of Non-Dried Vydac Samples

VYDAC SILICA GEL

VYDAC SILICA GEL, HYDRIDE

10.0   5.0   0.0
PPM
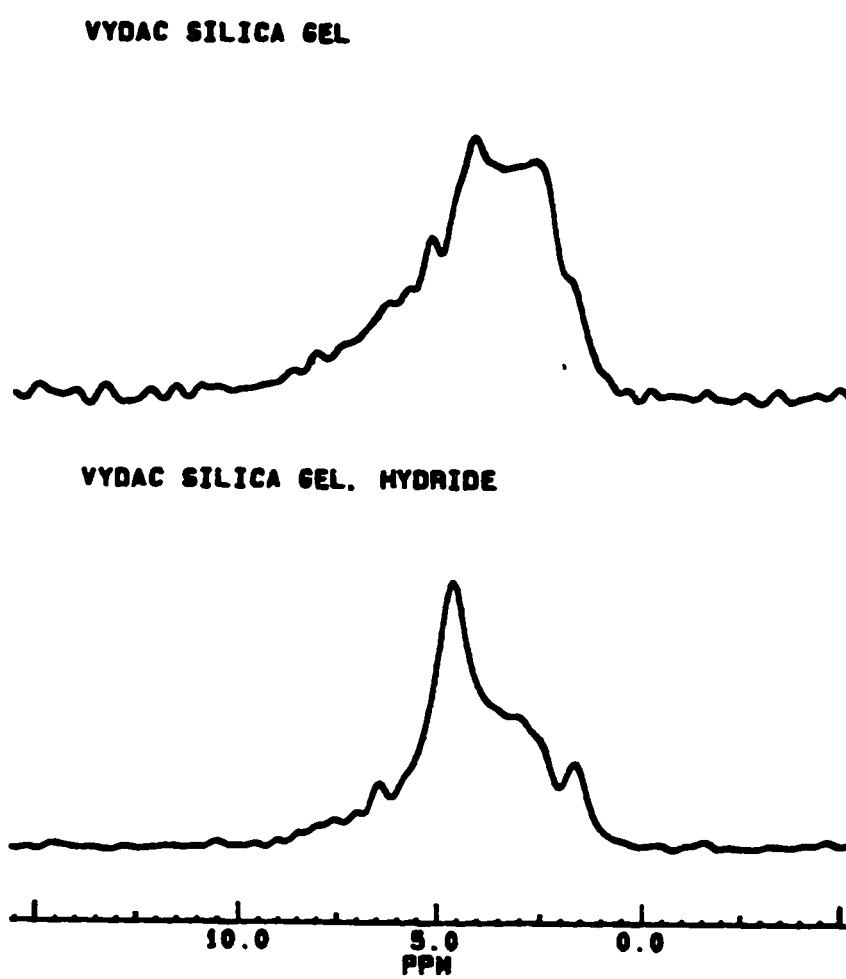
Figure 13: CRAMPS Spectra of Vydac-Bare Silica and Vydac Hydride

DAVISIL SILICA GEL. DRY

DAVISIL SILICA GEL. HYDRIDE

10.0   5.0   0.0
             PPM
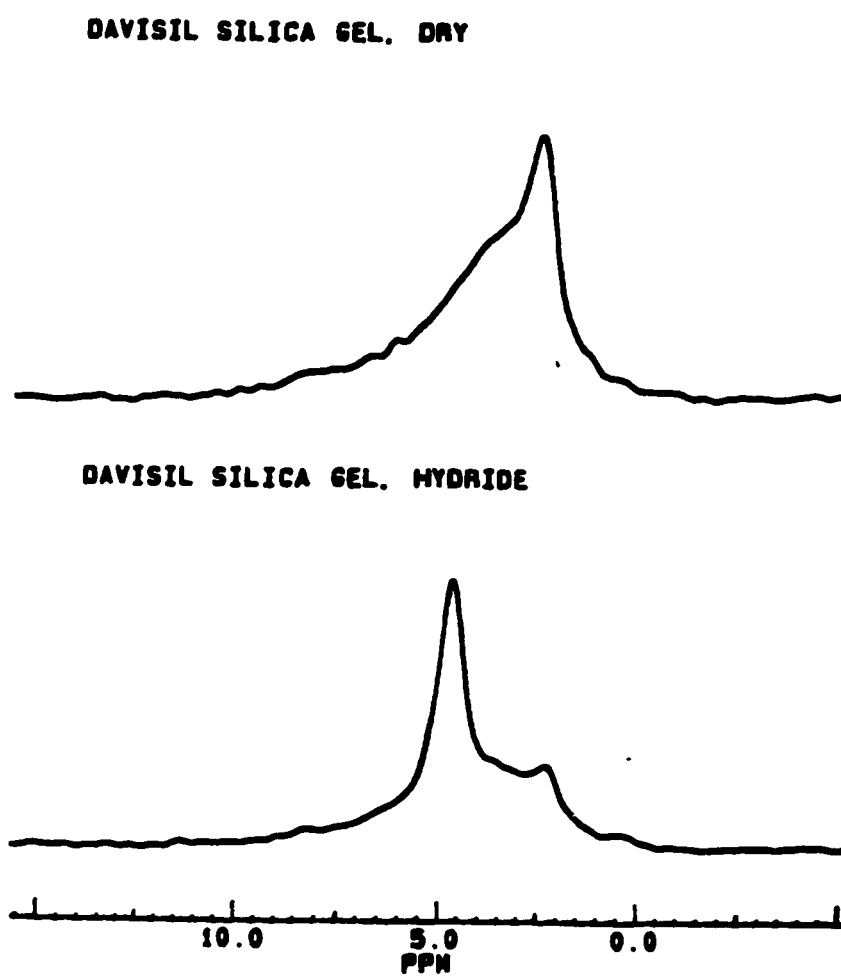
Figure 14: CRAMPS Spectra of Davisil-Bare Silica and Davisil Hydride

KROMASIL SILICA GEL, DRY

KROMASIL SILICA GEL, HYDRIDE

10.0   5.0   0.0
              PPM
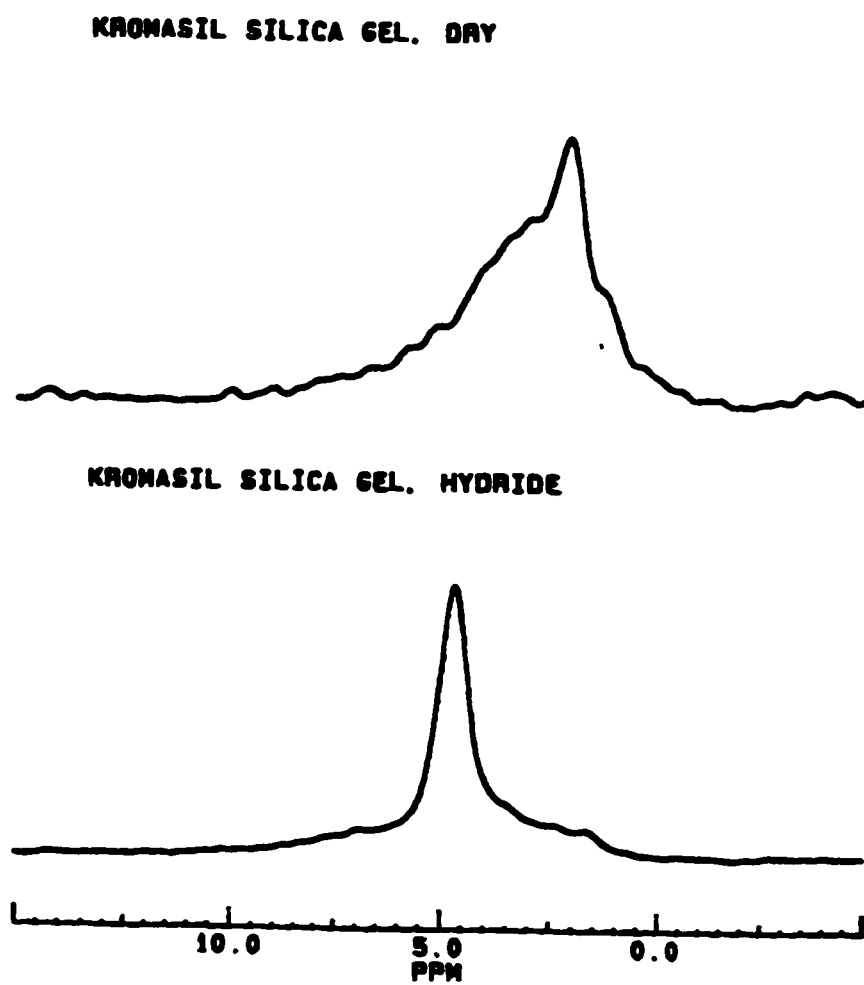
Figure 15: CRAMPS Spectra of Kromasil-Bare Silica and Kromasil Hydride

PDMS


```
    10.0        5.0        0.0
                PPM
```
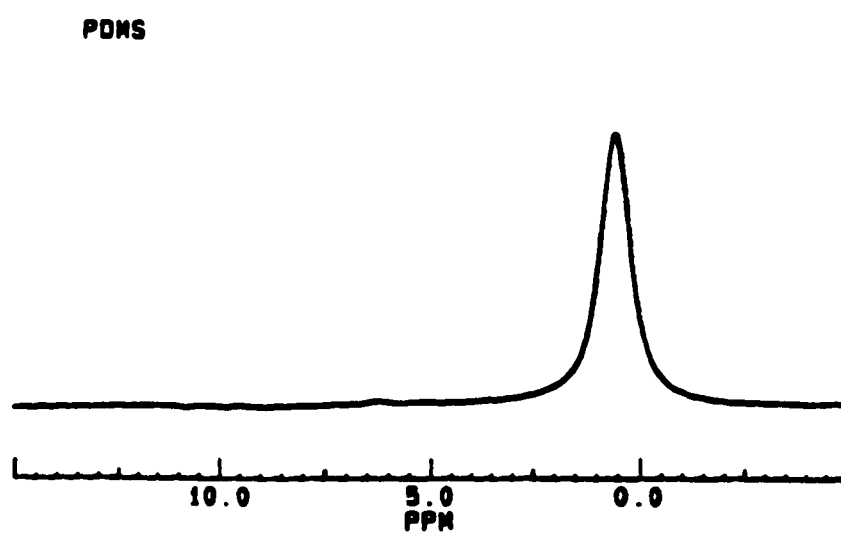
Figure 16: CRAMPS Spectrum of PDMS

ESCA Survey 18 Jan 94 Area: 1 Angle: 70 degrees Acquisition Time: 29.34 min
File: DAV61 DAVESIL DIOL (GRAY) #6
Scale Factor: 29.745 kc/s Offset: 0.378 kc/s Pass Energy: 187.850 eV Aperture: 5 Al 400in

Pt(4f) — 0.1 %
Si(2p) 32.6 %
Si(2s)
C(1s) 23.8 %
O(1s) 53.2 %
F(1s) 0.2 %
O(KLL)

N(E)/E

Binding Energy (eV)
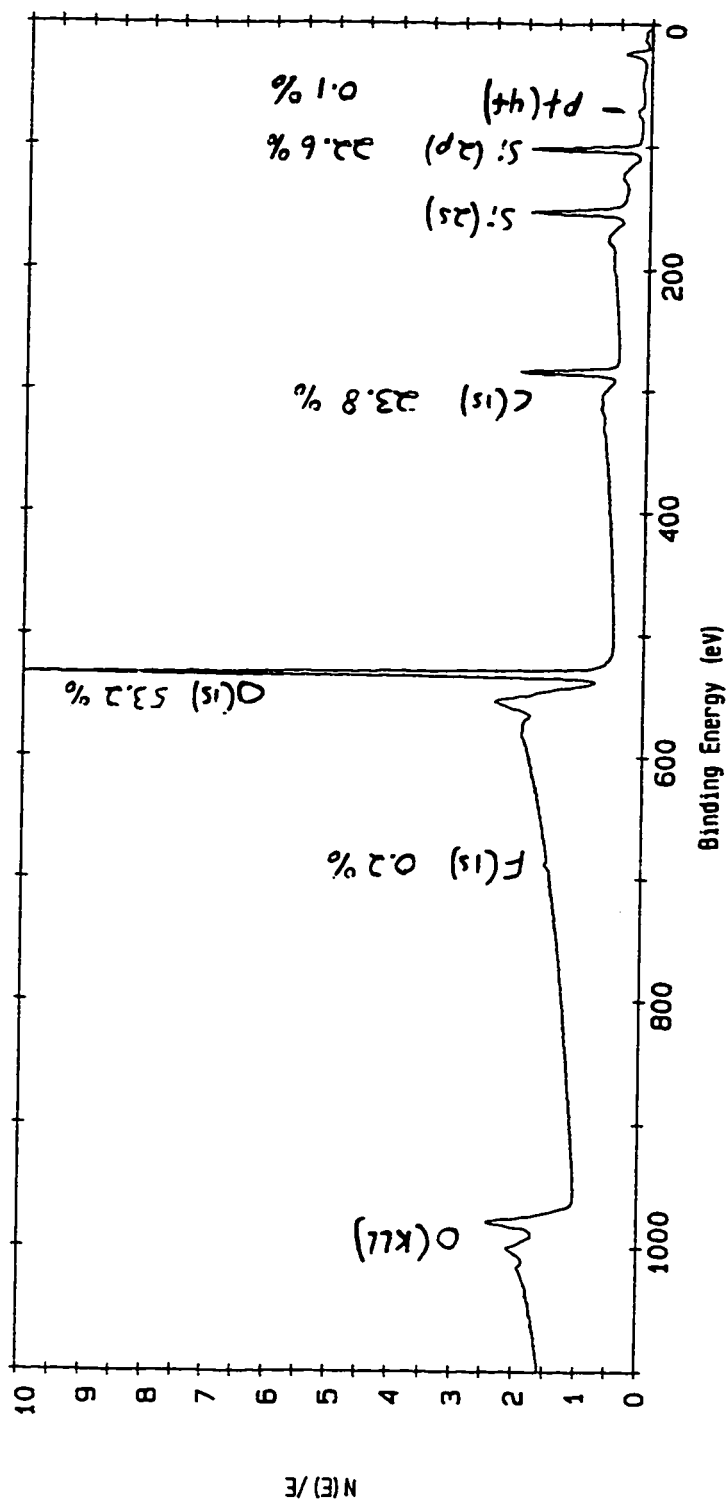
Figure 17: ESCA-Survey Spectrum of Davisil Diol (Gray) #6

ESCA Survey   18 Jan 94   Area: 1   Angle: 70 degrees   Acquisition Time: 29.34 min

File: DAV6A_2   DAVISIL DIOL ALLYL GLYCIDYL ETHER 6A

Scale Factor: 30.303 kc/s   Offset: 0.120 kc/s   Pass Energy: 187.850 eV   Aperture: 5   Al   400ln
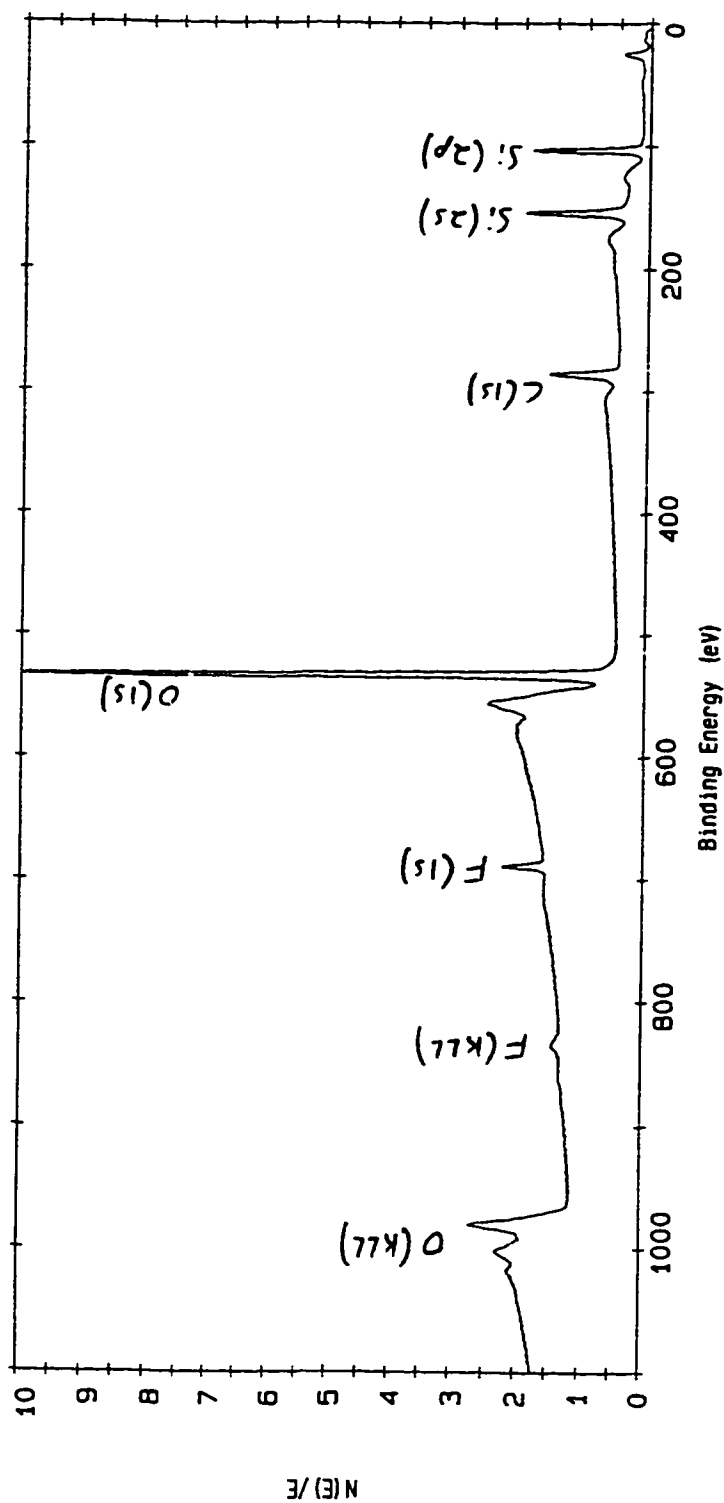
Figure 18: ESCA-Survey Spectrum of Davisil Diol Allyl Glycidyl Ether 6A

ESCA Survey   18 Jan 94   Area: 1   Angle: 70 degrees   Acquisition Time: 29.34 min
File: DAV68_3   DAVISIL DIOL 7-OCTENE-1,2,-DIOL 6B
Scale Factor: 29.897 kc/s   Offset: 0.169 kc/s   Pass Energy: 187.850 eV   Aperture: 5   Al 400in

Pt (4f)
Si (2p)
Si (2s)
C (1s)
O (1s)
F (1s)
O (KLL)

Binding Energy (eV)

N (E)/E
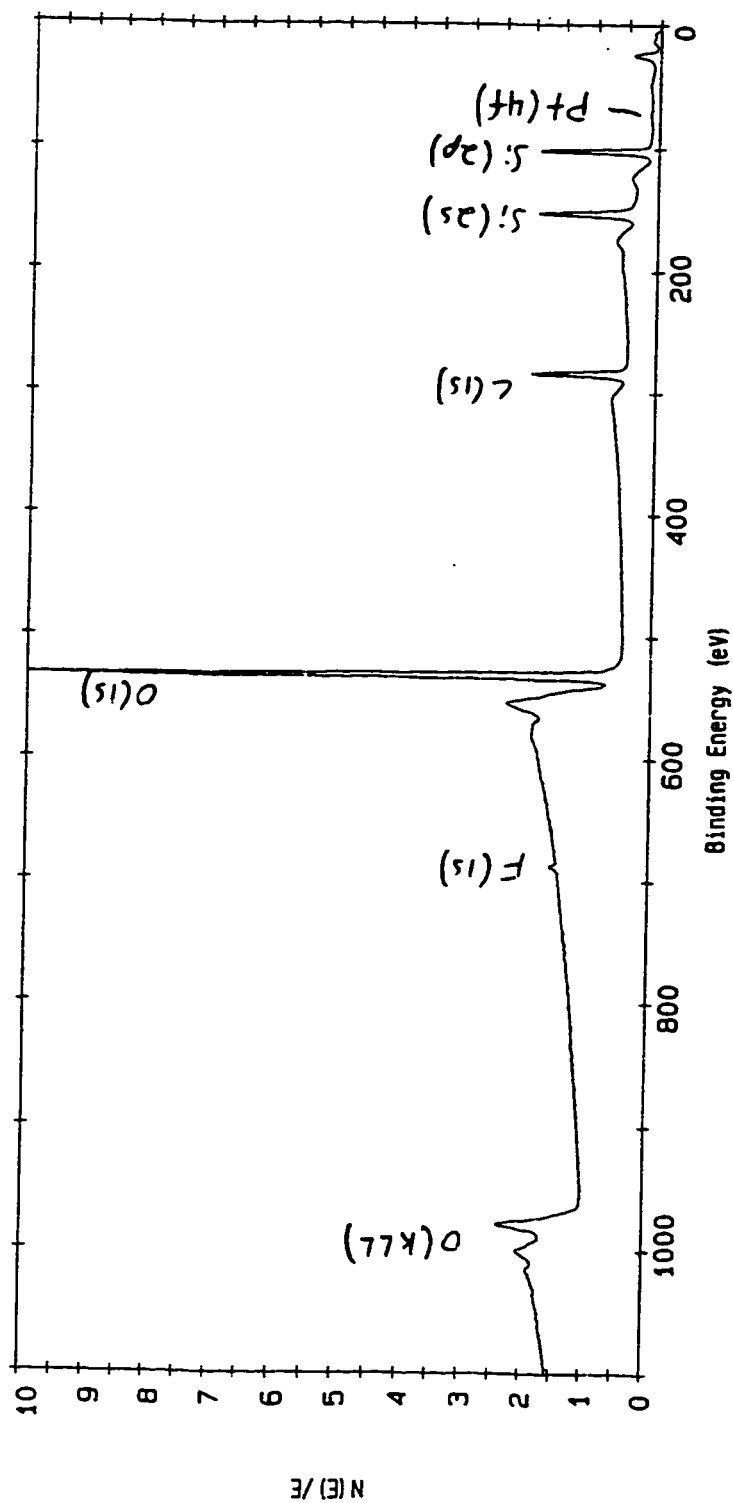
Figure 19: ESCA-Survey Spectrum of Davisil Diol 7-Octene-1,2-Diol 6B

73

ESCA Survey 25 Jan 94 Area: 1 Angle: 70 degrees Acquisition Time: 29.34 min
File: DAVE6C_4 DAVISIL DIOL 7-OCTENE-1,2,-DIOL 6C
Scale Factor: 43.811 kc/s Offset: 0.319 kc/s Pass Energy: 187.850 eV Aperture: 5 Al 400mi

Si(2p)

Si(2s)

C(1s)

O(1s)

F(1s)

O(KLL)

N(E)/E

Binding Energy (eV)
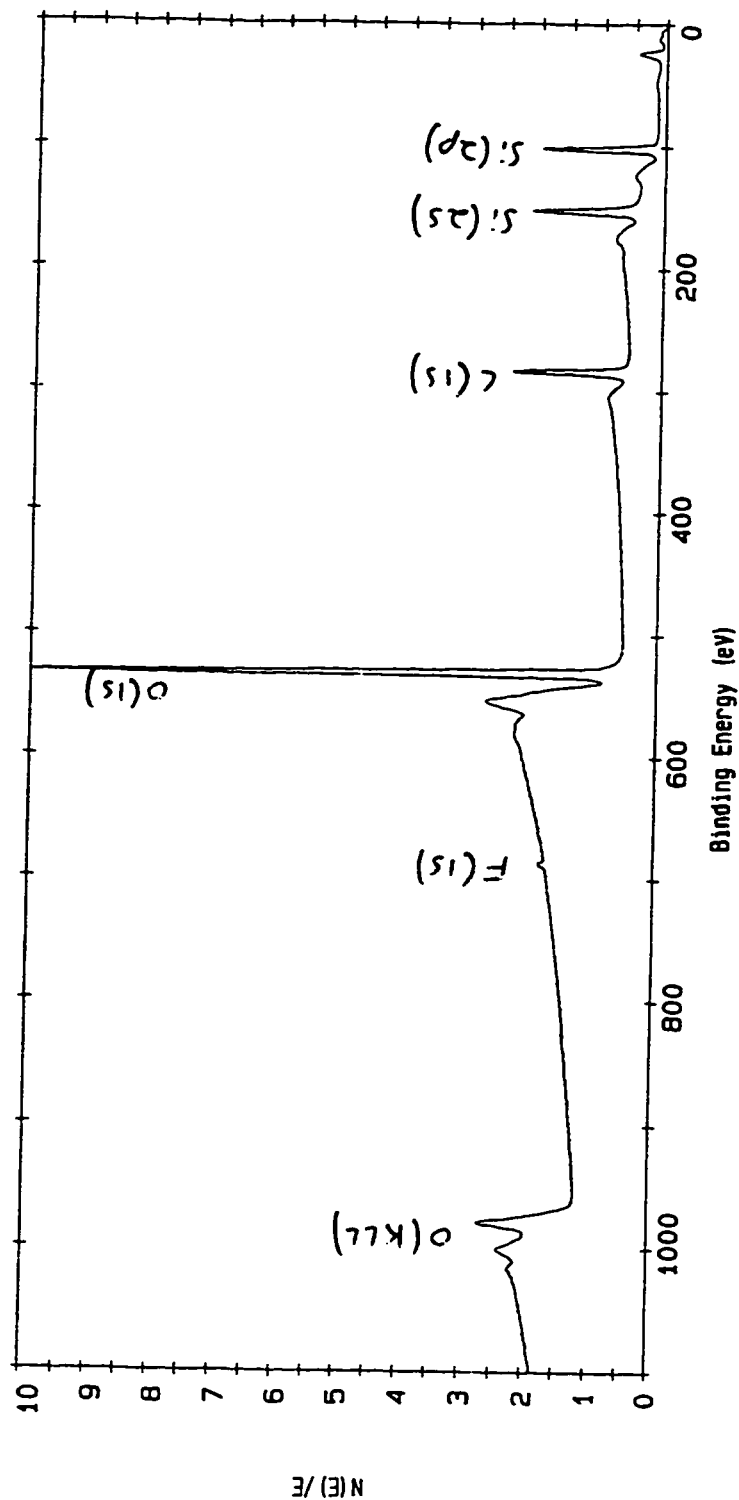
Figure 20: ESCA-Survey Spectrum of Davisil Diol 7-Octene-1,2-Diol 6C

ESCA Survey 17 Feb 94 Area: 1 Angle: 70 degrees Acquisition Time: 29.34 min
File: DAV_5 DAVISIL DIOL ALLYL GLYCIDYL ETHER BONDED 0.05 M HCL #1
Scale Factor: 34.951 kc/s Offset: 0.198 kc/s Pass Energy: 187.850 eV Aperture: 5 Al 400W

Si (2p)

Si (2s)

C (1s)

O (1s)

F (1s)

F (KLL)

O (KLL)

N(E)/E

Binding Energy (eV)
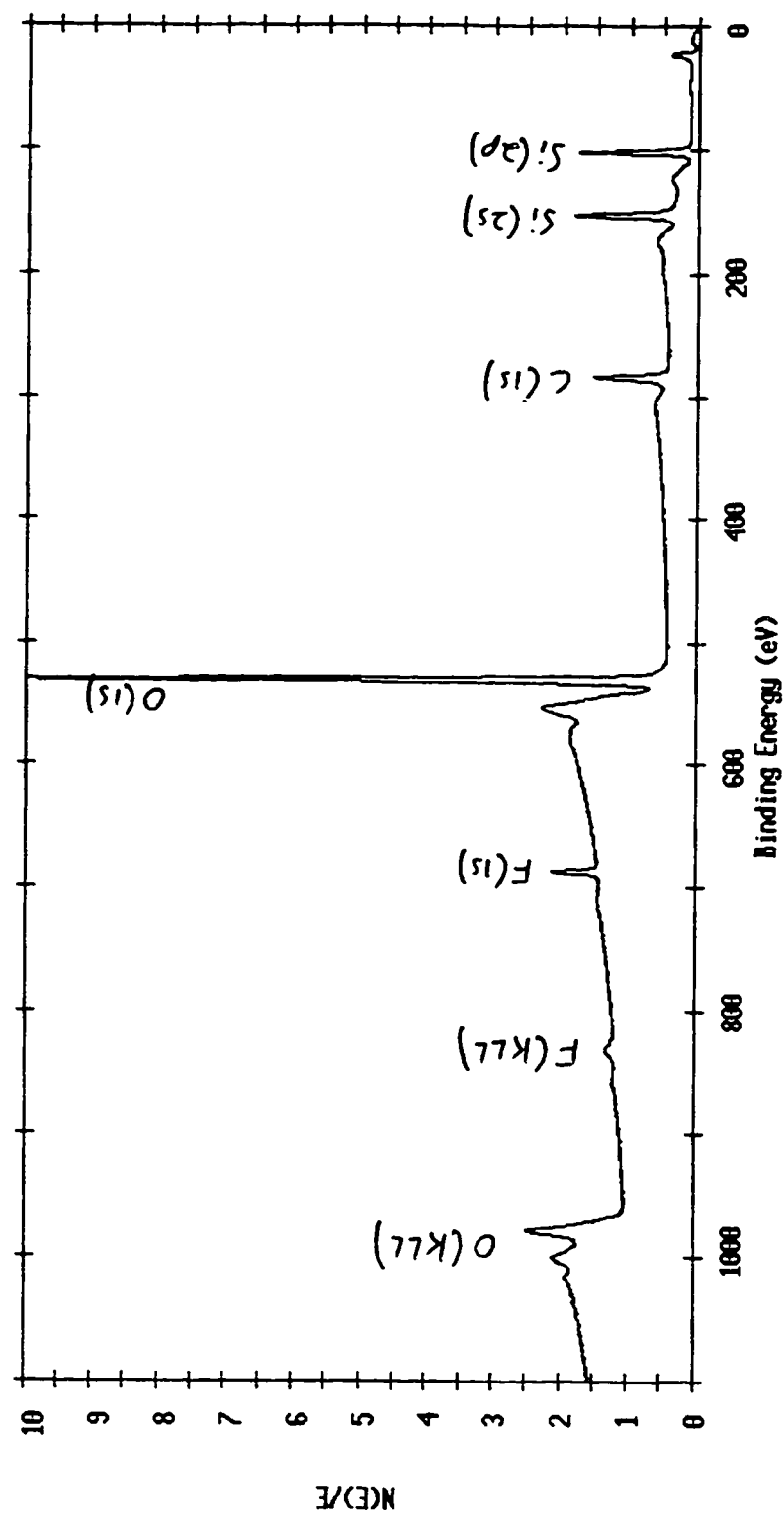
Figure 21: ESCA-Survey Spectrum of Davisil Diol Allyl Glycidyl Ether

ESCA Survey 19 Feb 94 Area: 1 Angle: 70 degrees Acquisition Time: 29.34 min
File: DAV_8 DAVISIL DIOL ALLYL GLYCEDYL ETHER BONDED 0.05M HCL-RUN2
Scale Factor: 29.908 kc/s Offset: 0.167 kc/s Pass Energy: 187.850 eV Aperture: 5 Al 400m
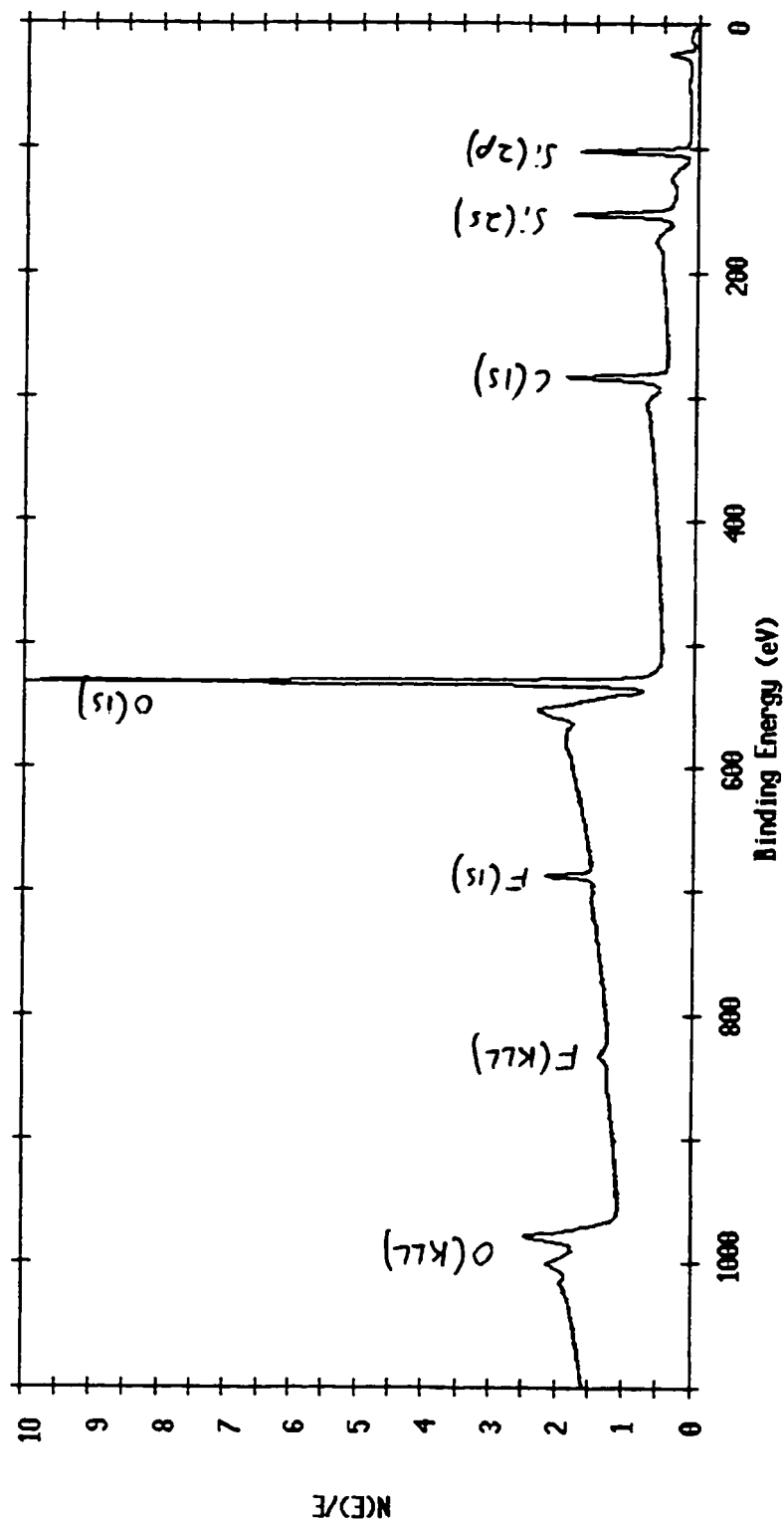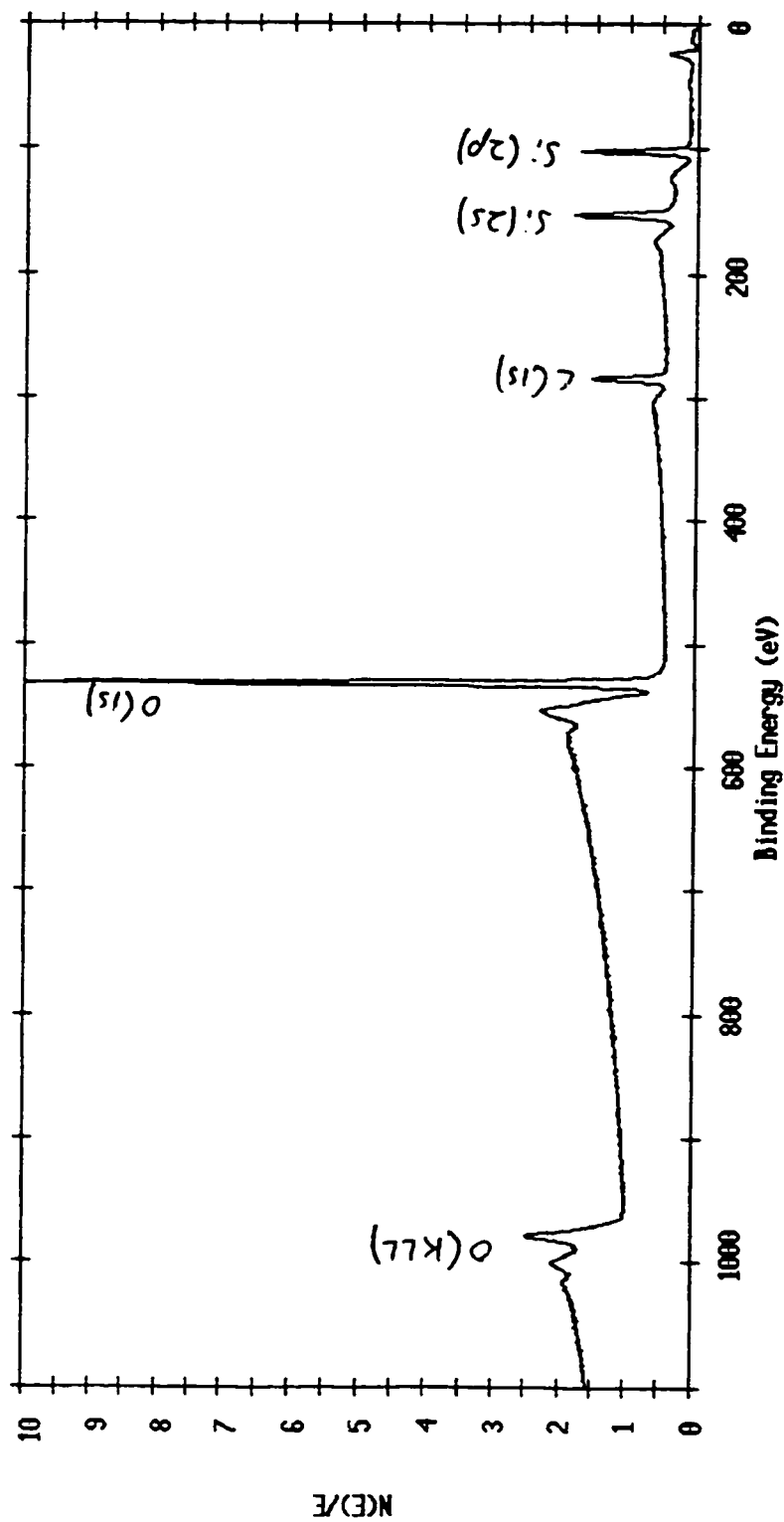

Figure 22: ESCA-Survey Spectrum of Davisil Diol Allyl Glycidyl Ether

ESCA Survey 17 Mar 94 Area: 1 Angle: 70 degrees Acquisition Time: 29.34 min
File: DAV_9 DAVISIL DIOL ALLYL GLYCIDYL ETHER BONDED 0.05M HCL RUN3
Scale Factor: 12.389 kc/s Offset: 0.055 kc/s Pass Energy: 187.850 eV Aperture: 4 Al 400m
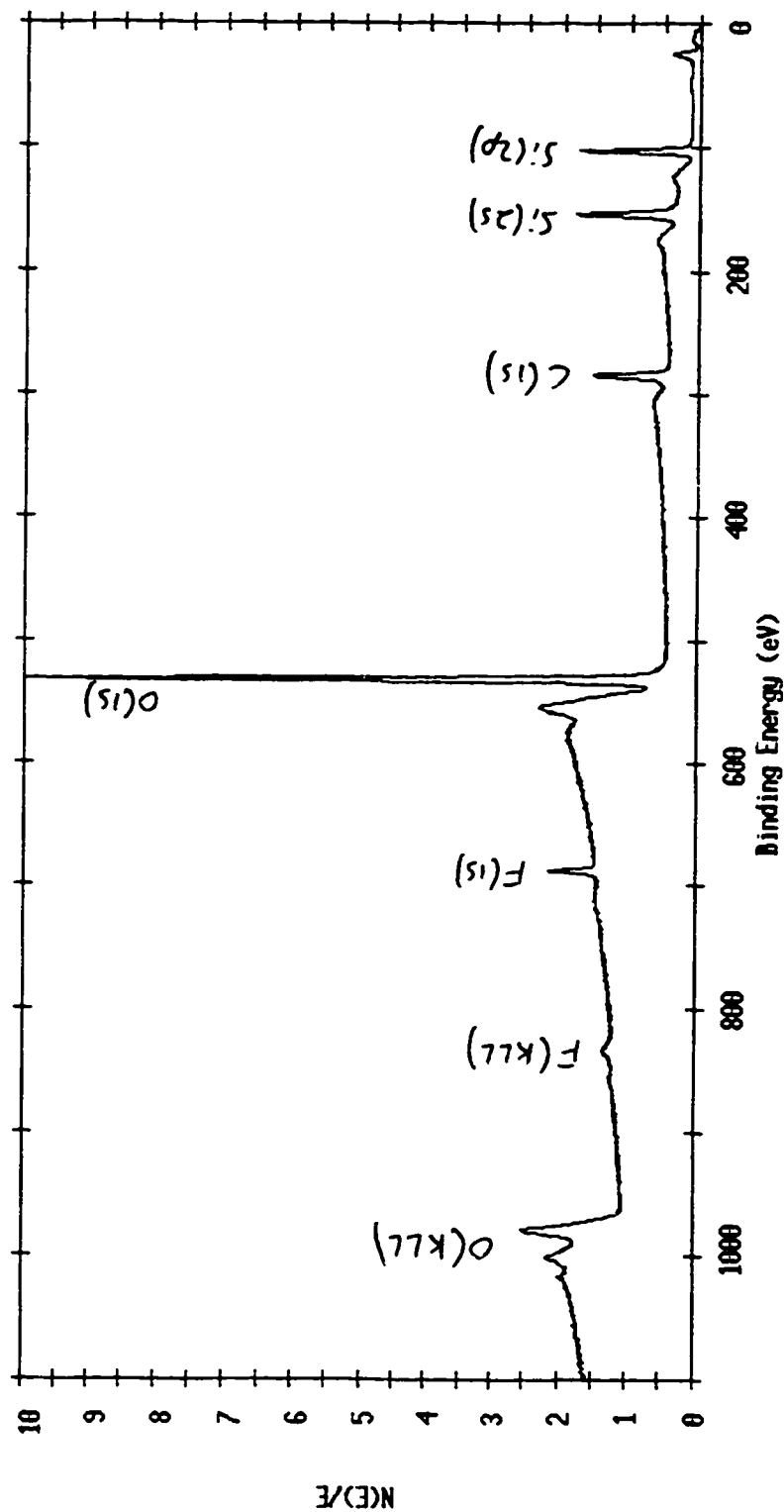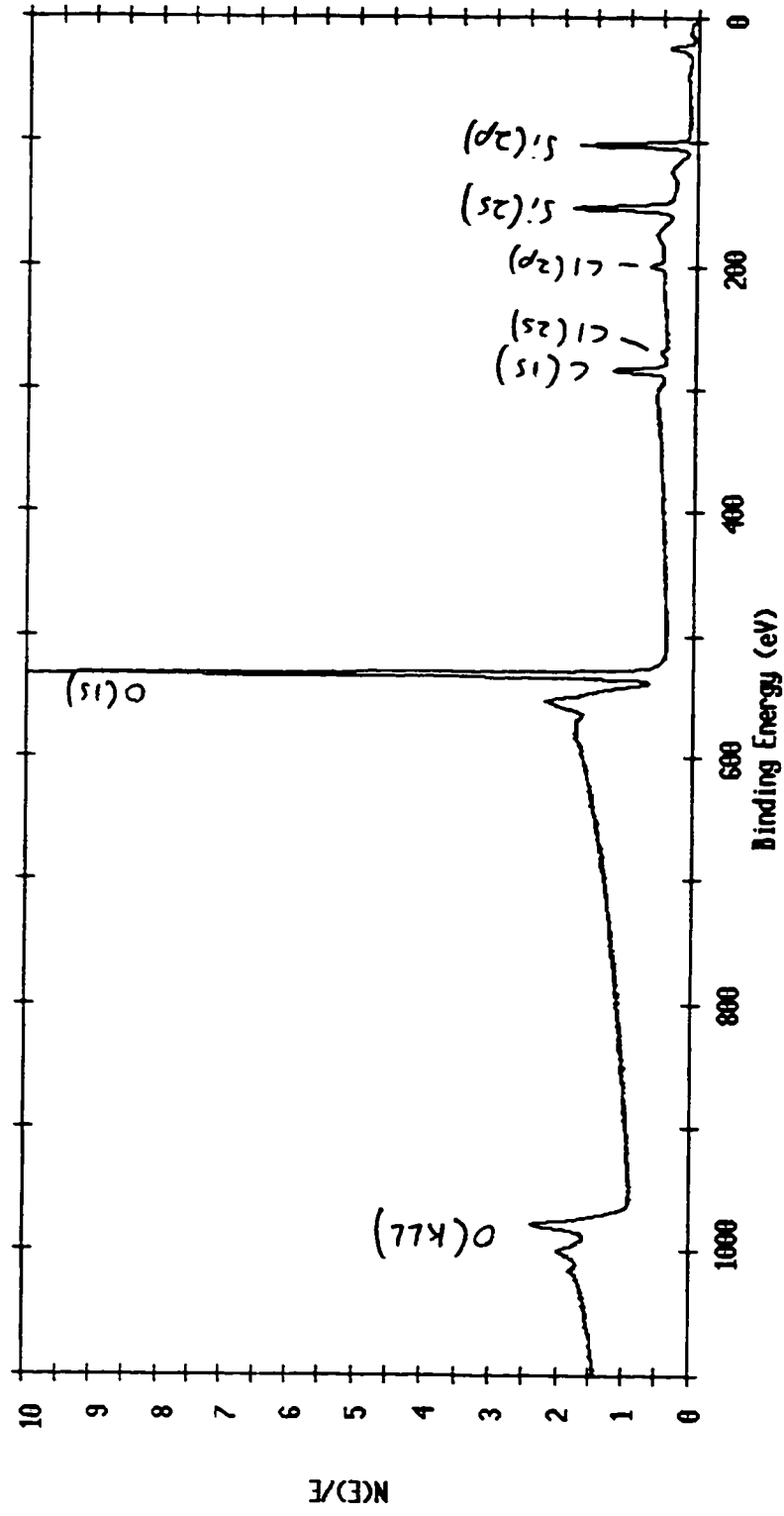
Figure 23: ESCA-Survey Spectrum of Davisil Diol Allyl Glycidyl Ether

ESCA Survey   17 Feb 94   Area: 1   Angle: 70 degrees   Acquisition Time: 29.34 min
File: DAV_6   DAVISIL + 1H, 1H, 2H-PERFLUOROOCTENE   RUN# 1
Scale Factor: 42.108 kc/s   Offset: 0.198 kc/s   Pass Energy: 187.850 eV   Aperture: 5   Al   4000m
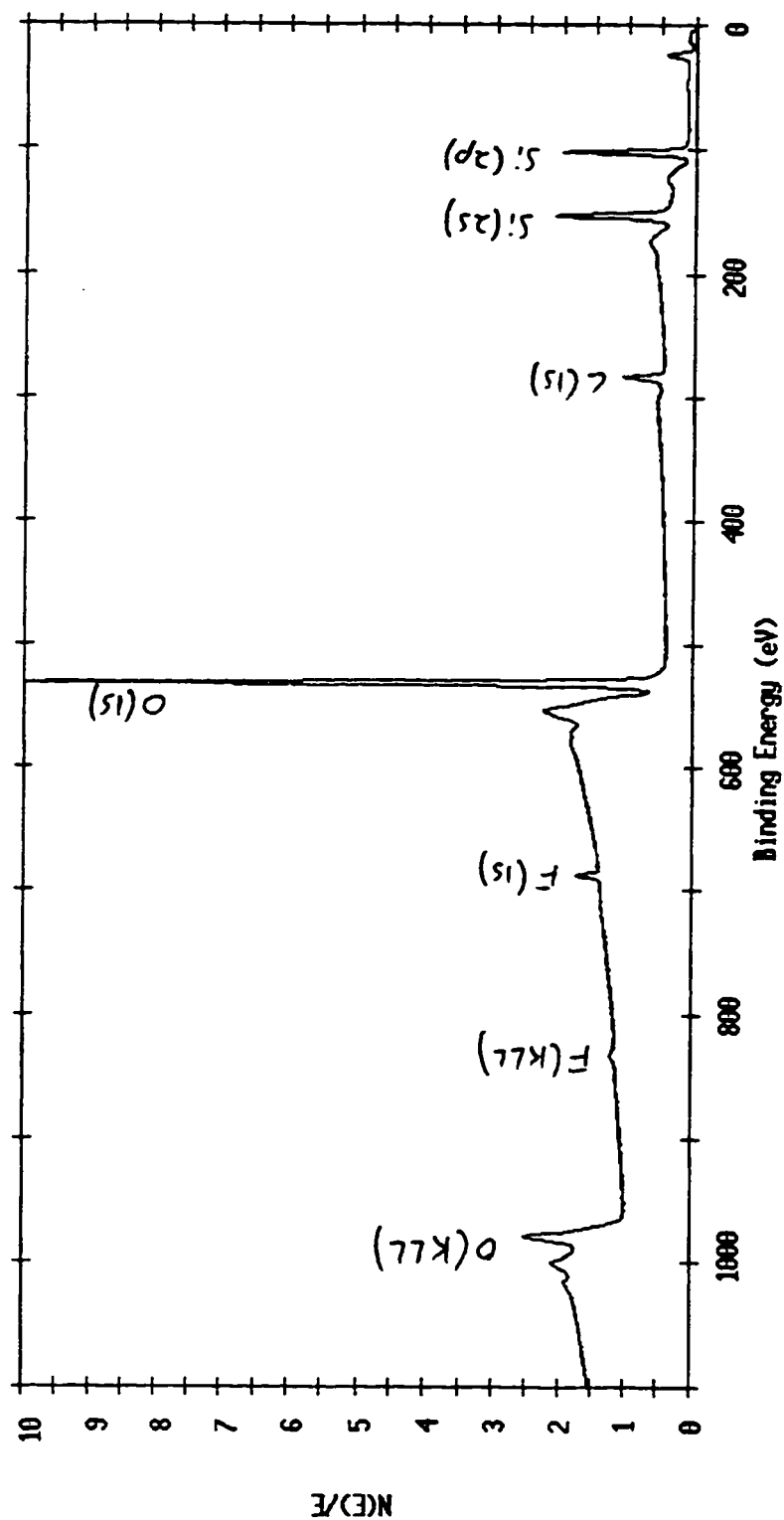
Figure 24:   ESCA-Survey Spectrum of Davisil + 1H, 1H, 2H-Perfluorooctene

ESCA Survey 17 Feb 94 Area: 1 Angle: 70 degrees Acquisition Time: 29.34 min
File: DAV_7 DAVISIL + 4-PHENYL-1-BUTENE (RUN 1)
Scale Factor: 31.073 kc/s Offset: 0.159 kc/s Pass Energy: 187.850 eV Aperture: 5 Al 400m

O(1s)

C(1s)

Si(2s)

Si(2p)

F(1s)

F(KLL)

O(KLL)

N(E)/E

10 9 8 7 6 5 4 3 2 1 0

0   200   400   600   800   1000

Binding Energy (eV)
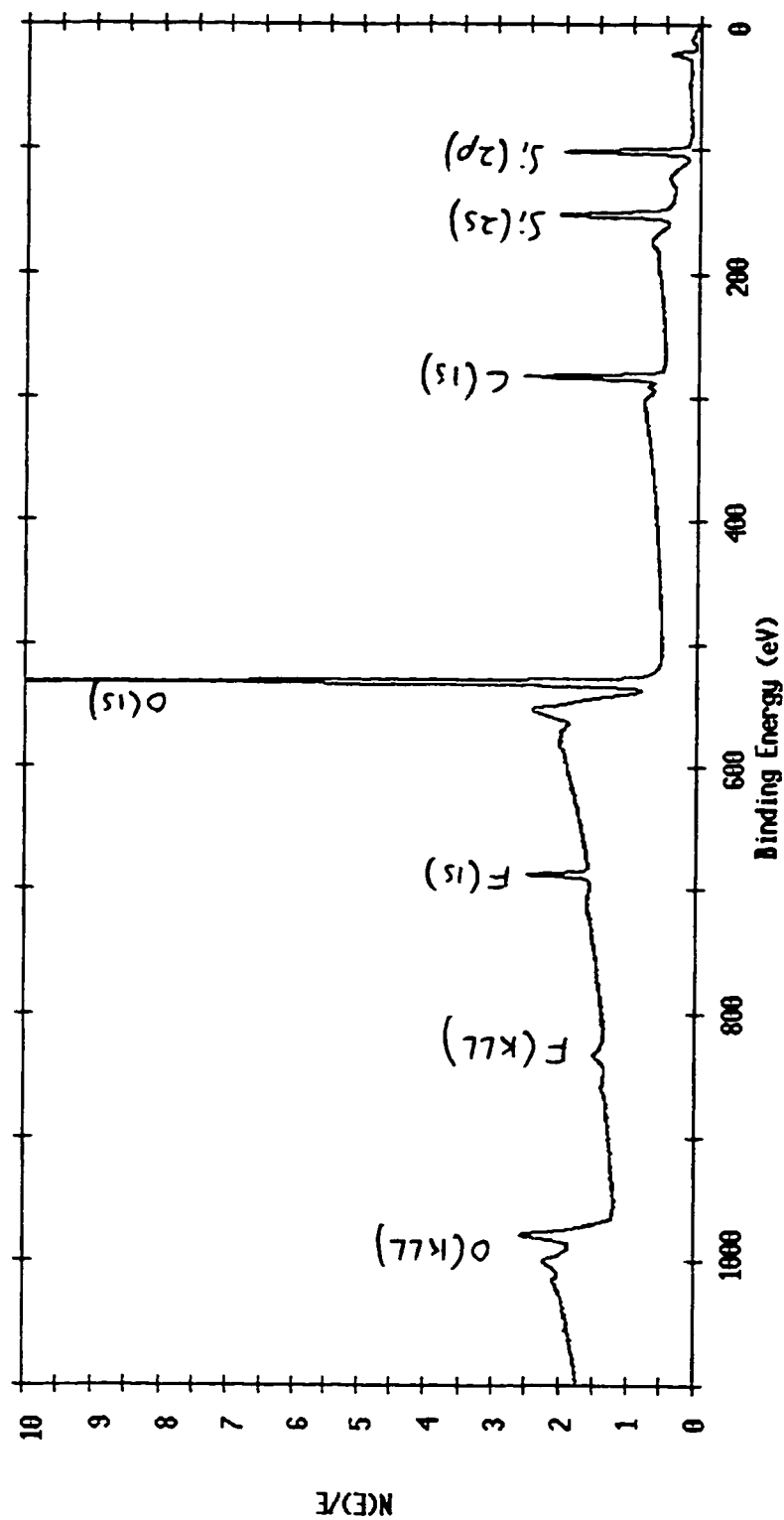
Figure 25: ESCA-Survey Spectrum of Davisil + 4-Phenyl-1-Butene Run 1

ESCA Survey 17 Mar 94 Area: 1 Angle: 70 degrees Acquisition Time: 29.34 min
File: DAV_10 DAVISIL + 4-PHENYL-1-BUTENE RUN2
Scale Factor: 10.584 kc/s Offset: 0.081 kc/s Pass Energy: 187.850 eV Aperture: 4 Al 4000n

N(E)/E

Si(2p)

Si(2s)

C(1s)

O(1s)

F(1s)

F(KLL)

O(KLL)

Binding Energy (eV)
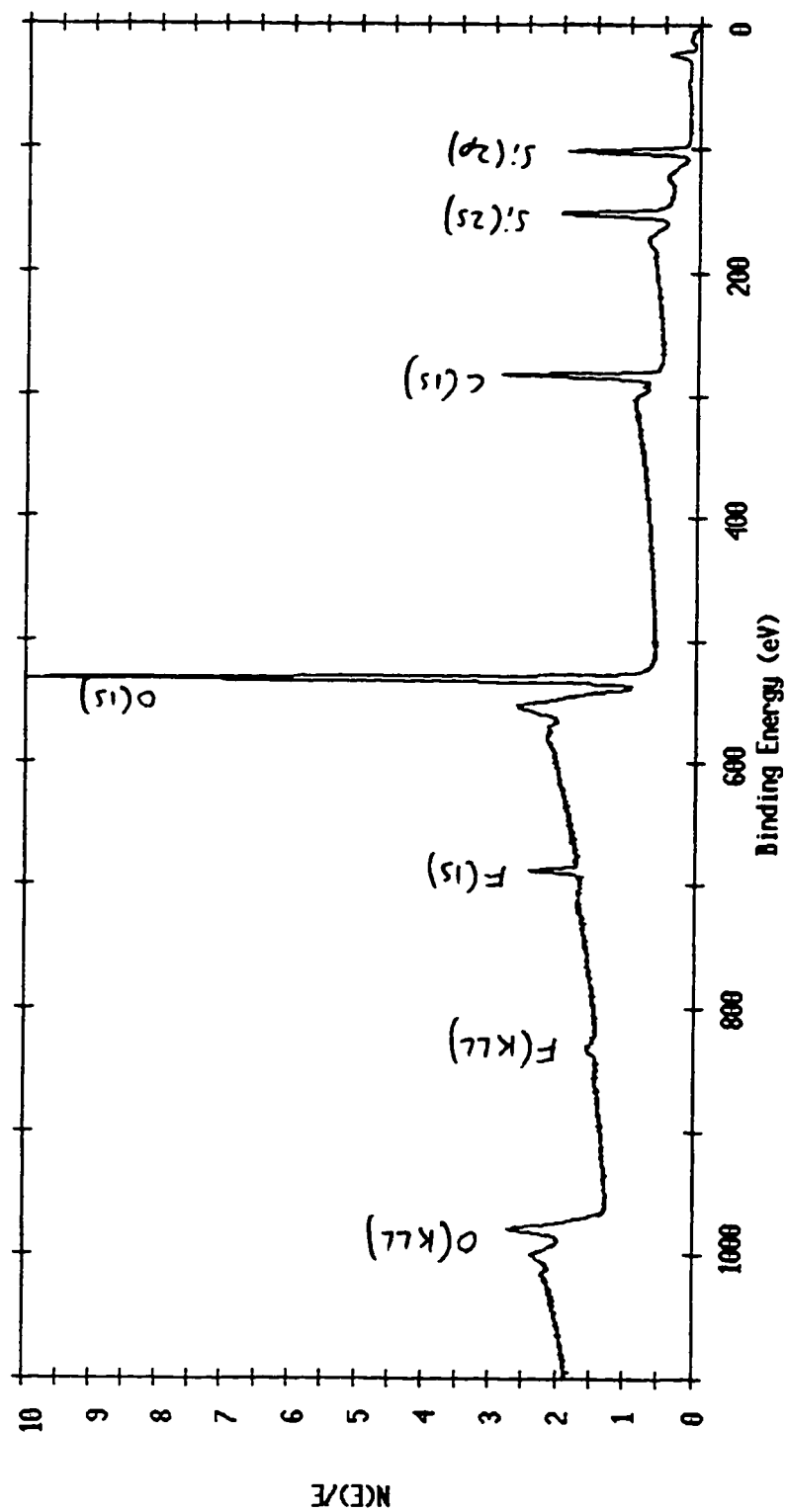
Figure 26: ESCA-Survey Spectrum of Davisil + 4-Phenyl-1-Butene Run 2

ESCA Survey 15 May 94 Area: 1 Angle: 70 degrees Acquisition Time: 29.34 min
File: DAV_13 DAVISIL BARE SILICA RUN 1
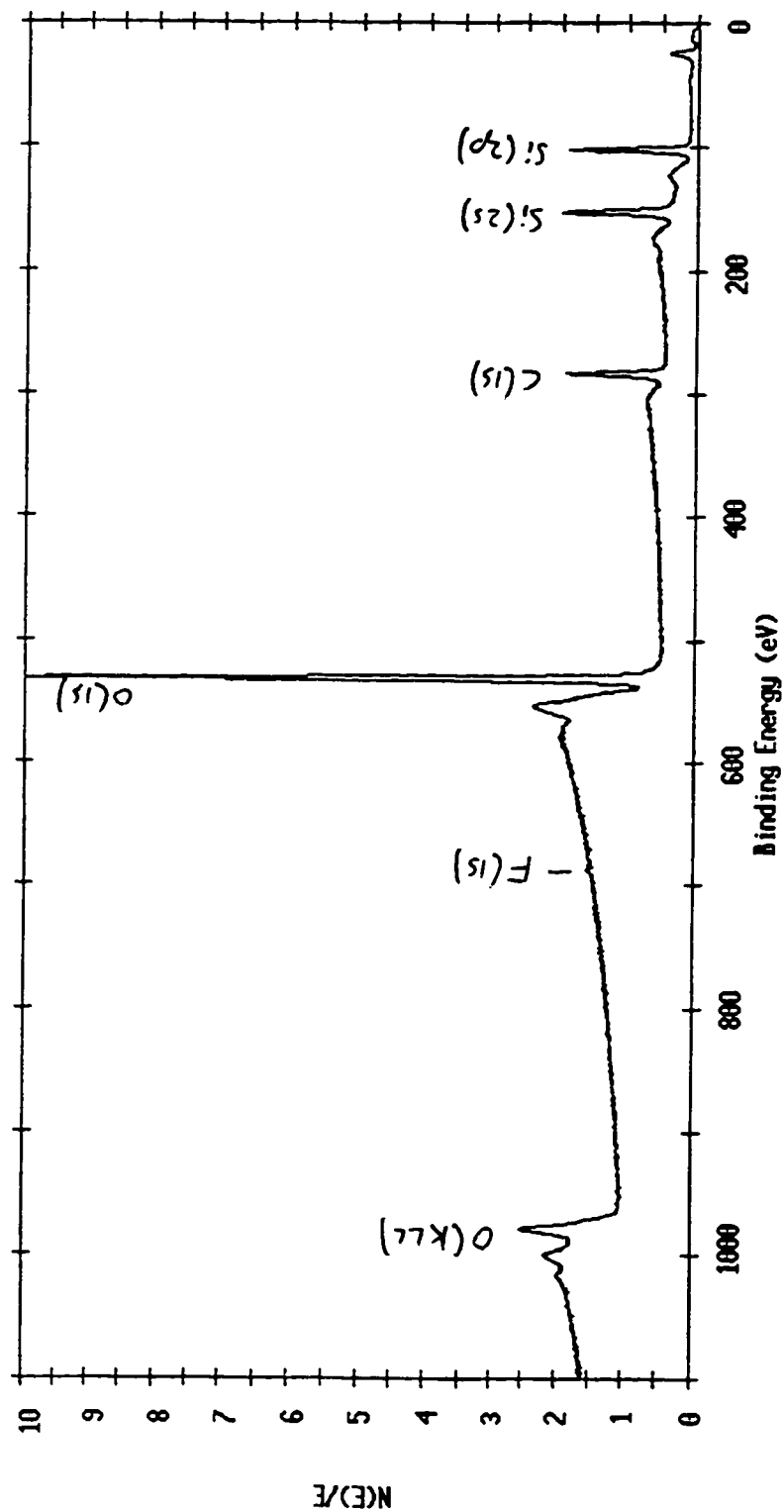Scale Factor: 16.361 kc/s Offset: 0.055 kc/s Pass Energy: 187.850 eV Aperture: 4 Al 4000m
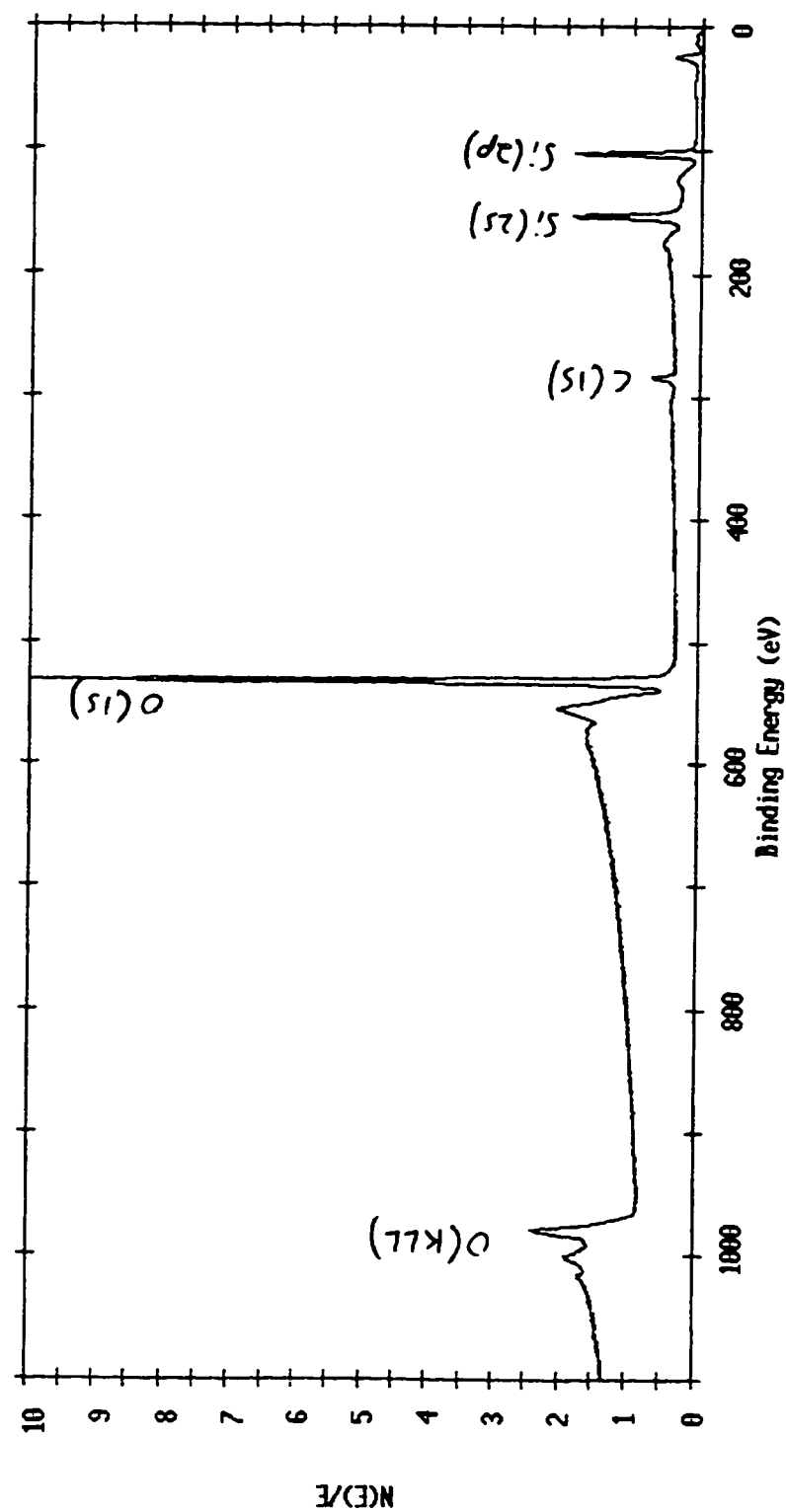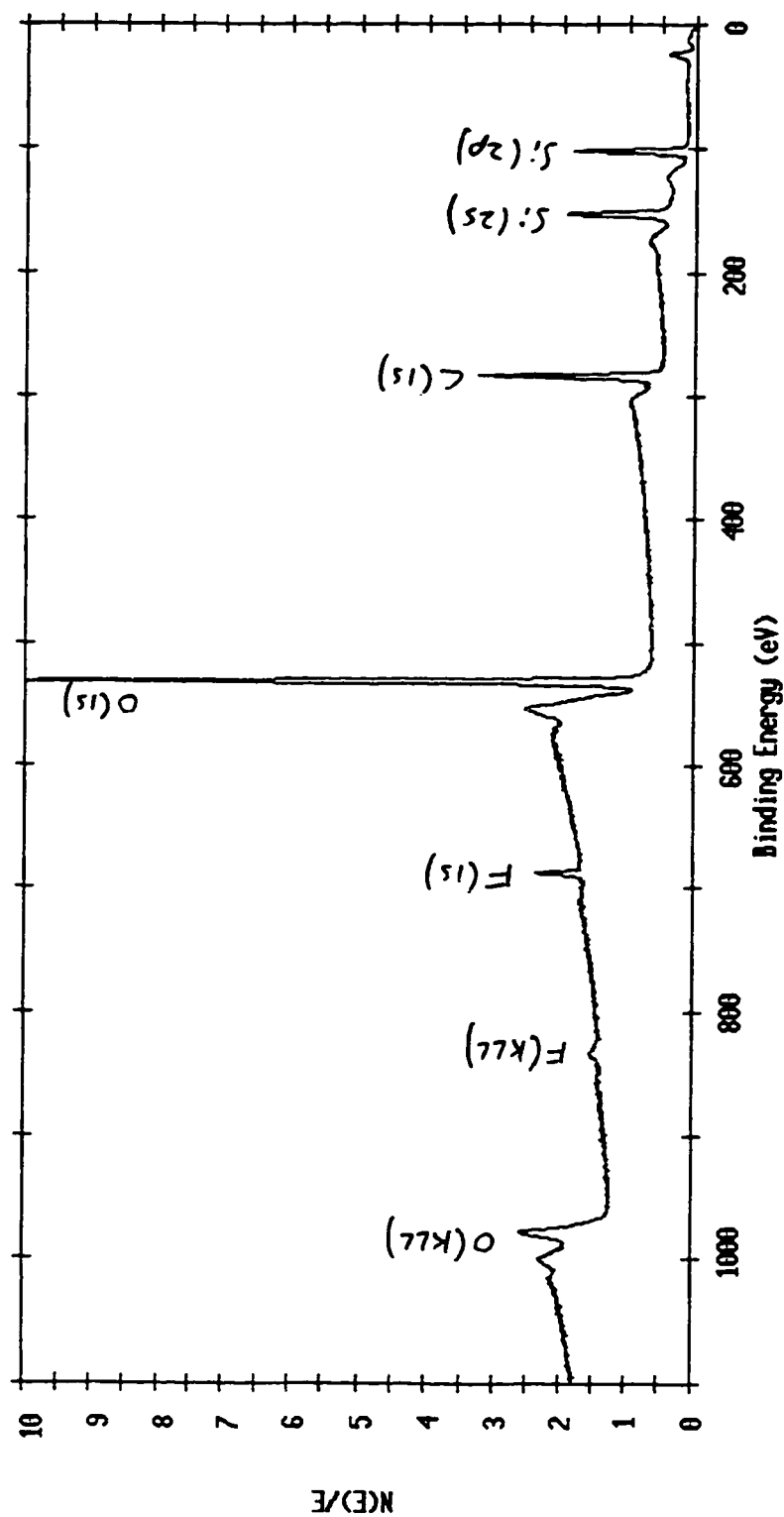
Figure 27: ESCA-Survey Spectrum of Davisil Bare Silica Run 1

ESCA Survey 15 May 94 Area: 1 Angle: 70 degrees Acquisition Time: 29.34 min
File: DAV_14 DAVISIL HYDRIDE RUN 1
Scale Factor: 13.494 kc/s Offset: 0.059 kc/s Pass Energy: 187.850 eV Aperture: 4 Al 4000m

Binding Energy (eV)

N(E)/E

Si(2p)

Si(2s)

C(1s)

O(1s)

O(KLL)
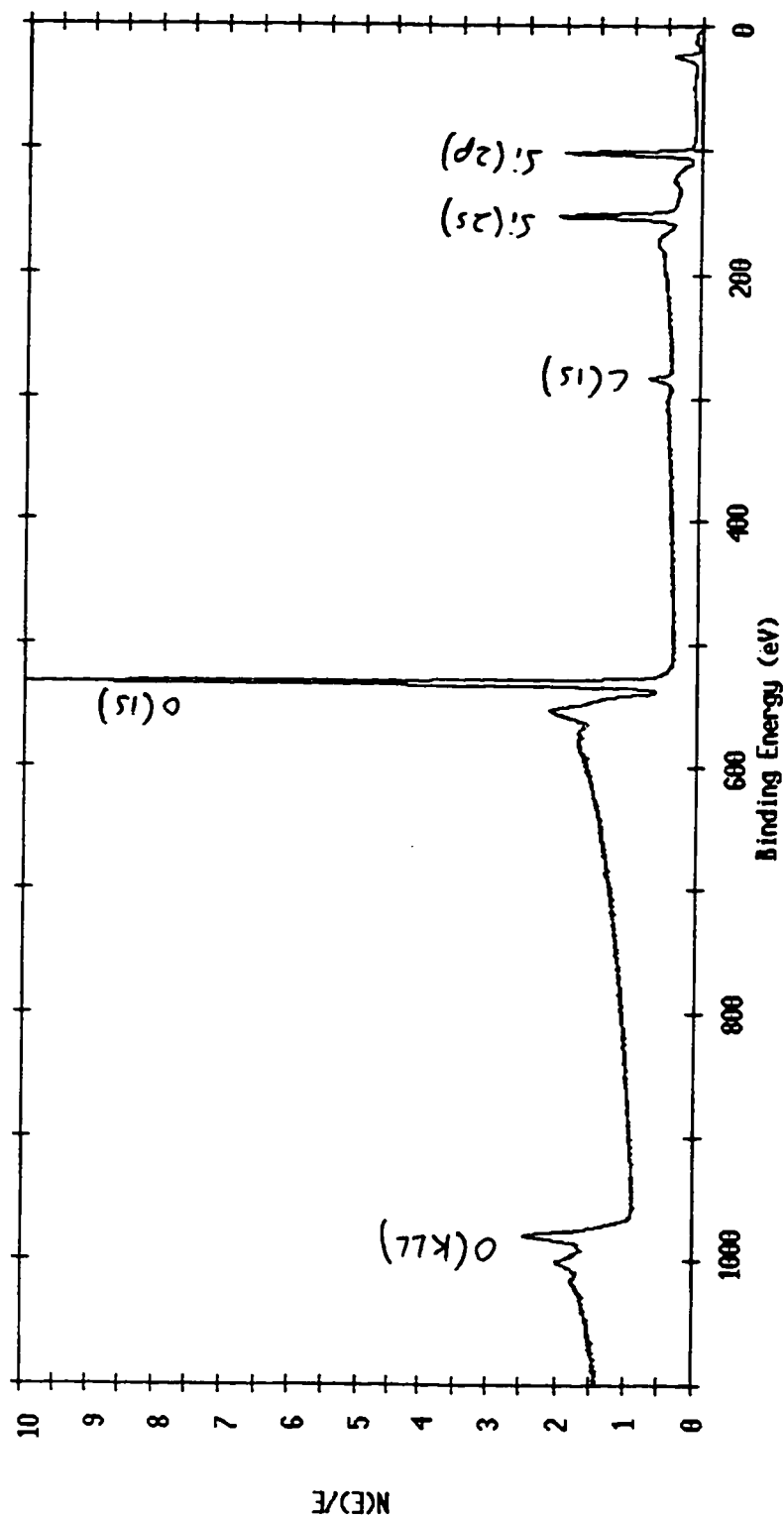
Figure 28: ESCA-Survey Spectrum of Davisil Hydride Run 1

ESCA Survey   15 May 94 Area: 1 Angle: 70 degrees Acquisition Time: 29.34 min
File: DAV_15 DAVISIL DIOL RD 377 H RUN 1
Scale Factor: 11.915 kc/s   Offset: 0.066 kc/s   Pass Energy: 187.850 eV Aperture: 4 Al 400M

Si (2p)

Si (2s)

C (1s)

O (1s)

O (KLL)

N(E)/E

Binding Energy (eV)

Figure 29: ESCA-Survey Spectrum of Davisil Diol RD 377 H Run 1

ESCA Survey 15 May 94 Area: 1 Angle: 70 degrees Acquisition Time: 29.34 min
File: DAV_16 DAVISIL DIOL LOT# 141614 RUN 1
Scale Factor: 11.718 kc/s Offset: 0.048 kc/s Pass Energy: 187.850 eV Aperture: 4 Al 400m

N(E)/E

10
9
8
7
6
5
4
3
2
1
0

O(1s)

O(KLL)

Si(2p)

Si(2s)

Cl(2p)

Cl(2s)

C(1s)

0   200   400   600   800   1000

Binding Energy (eV)

Figure 30: ESCA-Survey Spectrum of Davisil Diol Lot# 141614 Run 1

ESCA Survey 12 Jun 94 Area: 1 Angle: 70 degrees Acquisition Time: 29.34 min
File: DAV_17 DAVISIL AGE (SET 2) RUN 1
Scale Factor: 10.906 kc/s Offset: 0.048 kc/s Pass Energy: 187.850 eV Aperture: 4 Al 4000m

O(1s)

Si(2p)

Si(2s)

C(1s)
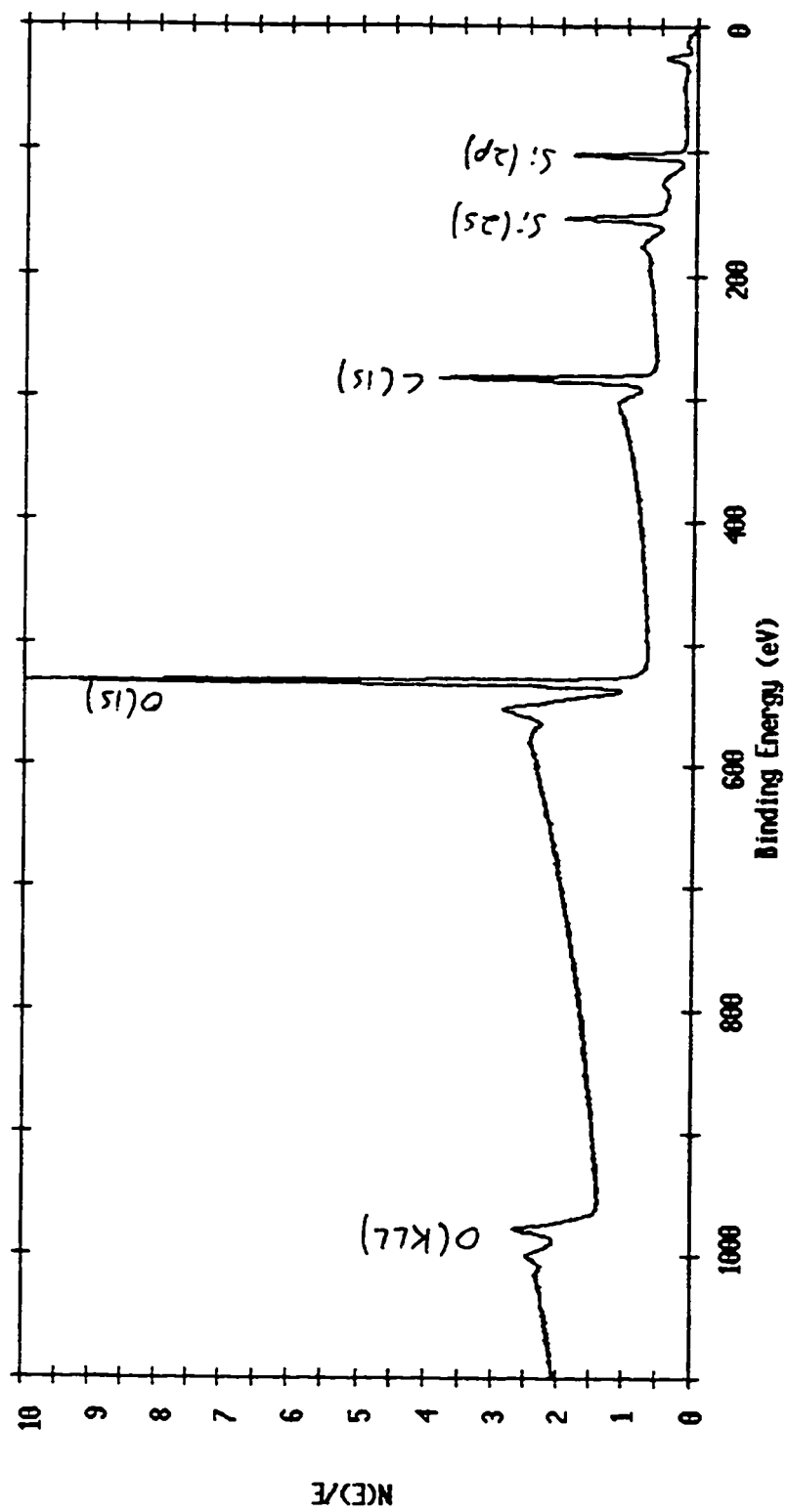
F(1s)

F(KLL)

O(KLL)

N(E)/E

Binding Energy (eV)
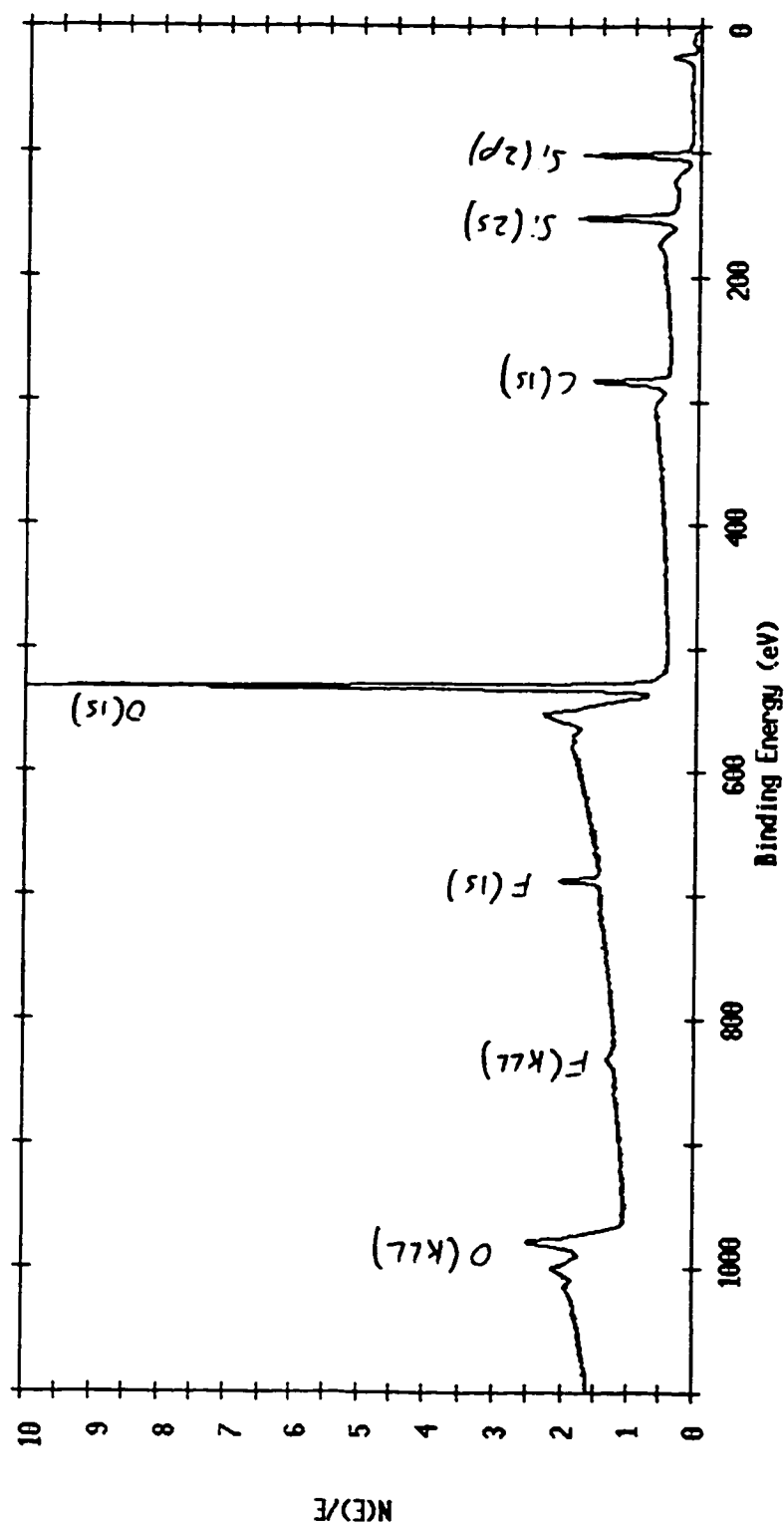
Figure 31: ESCA-Survey Spectrum of Davisil AGE (Set 2)

ESCA Survey   12 Jun 94   Area: 1   Angle: 70 degrees   Acquisition Time: 29.34 min
File: DAV_18   DAVISIL MPAB RUN 1
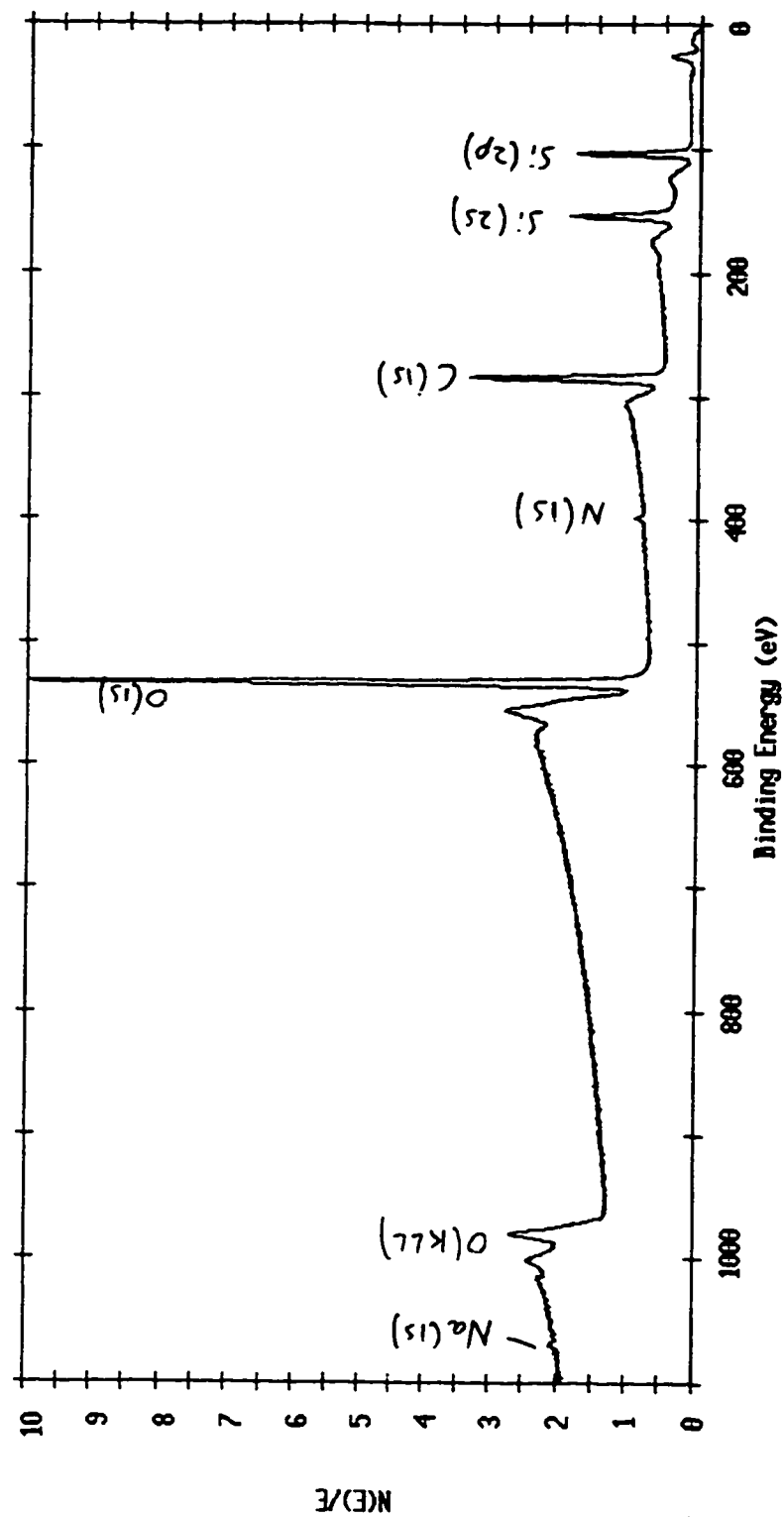Scale Factor: 11.710 kc/s   Offset: 0.073 kc/s   Pass Energy: 187.850 eV   Aperture: 4   Al 4000A

Figure 32: ESCA-Survey Spectrum of Davisil MPAB Run 1

ESCA Survey 12 Jun 94 Area: 1 Angle: 70 degrees Acquisition Time: 29.34 min
File: DAV_19 DAVISIL PHENYL RUN 1
Scale Factor: 9.470 kc/s Offset: 0.047 kc/s Pass Energy: 187.850 eV Aperture: 4 Al 4000m

Figure 33: ESCA-Survey Spectrum of Davisil Phenyl Run 1

ESCA Survey 4 Aug 94 Area: 1 Angle: 70 degrees Acquisition Time: 29.80 min
File: DAV_20 DAVISIL C-18
Scale Factor: 17.240 kc/s Offset: 0.074 kc/s Pass Energy: 187.850 eV Aperture: 5 Al 400m

O(1s)

C(1s)

Si(2s)

Si(2p)

Cl(2p)

F(1s)

O(KLL)

N(E)/E

Binding Energy (eV)
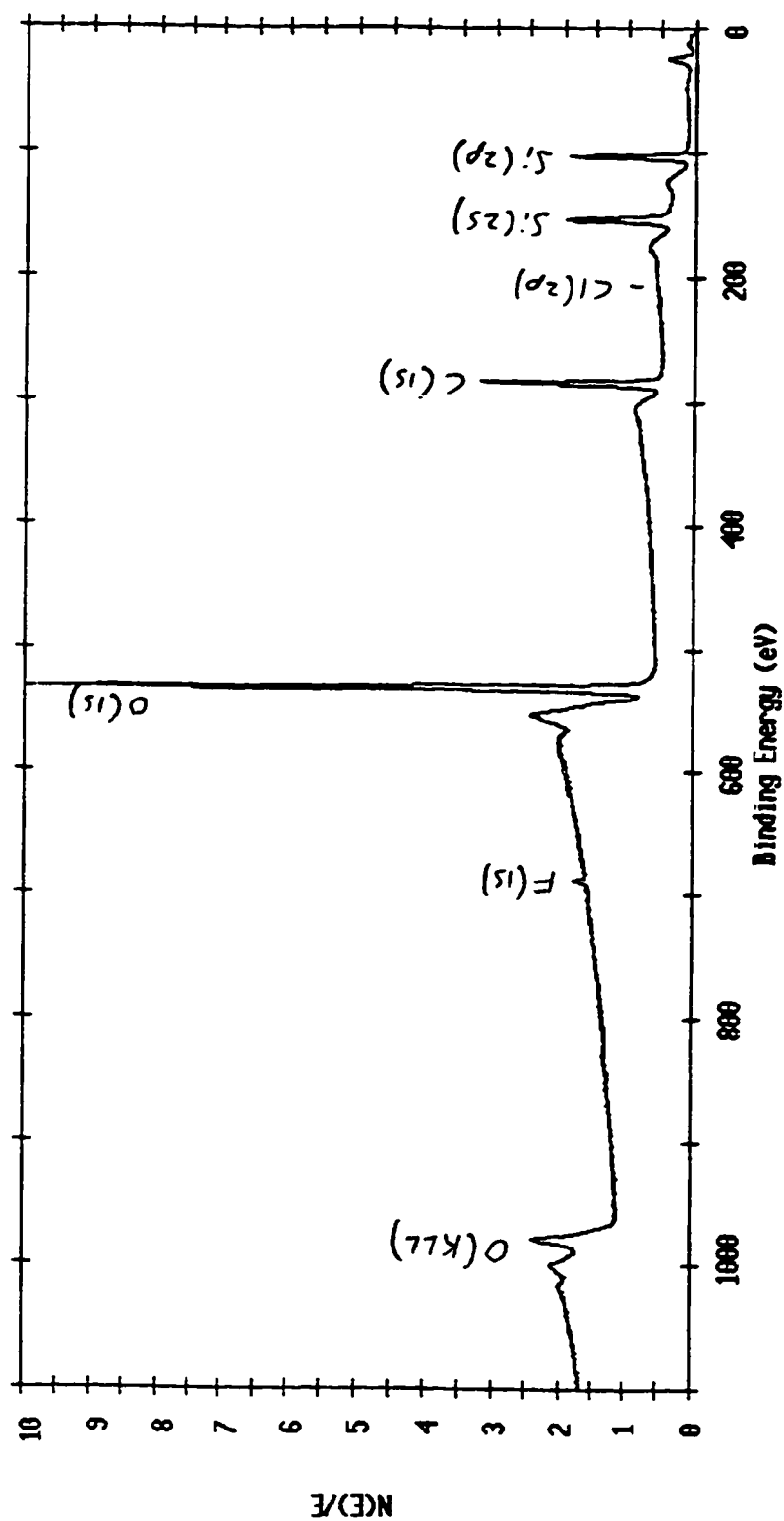
Figure 34: ESCA-Survey Spectrum of Davisil C-18

ESCA Survey 4 Sep 94   Area: 1 Angle: 70 degrees Acquisition Time: 29.80 min
File: DAV_21 Davisil — cholesterol
Scale Factor: 30.240 kc/s Offset: 0.355 kc/s Pass Energy: 187.850 eV Aperture: 5 Al 1000m

Binding Energy (eV)

N(E)/E
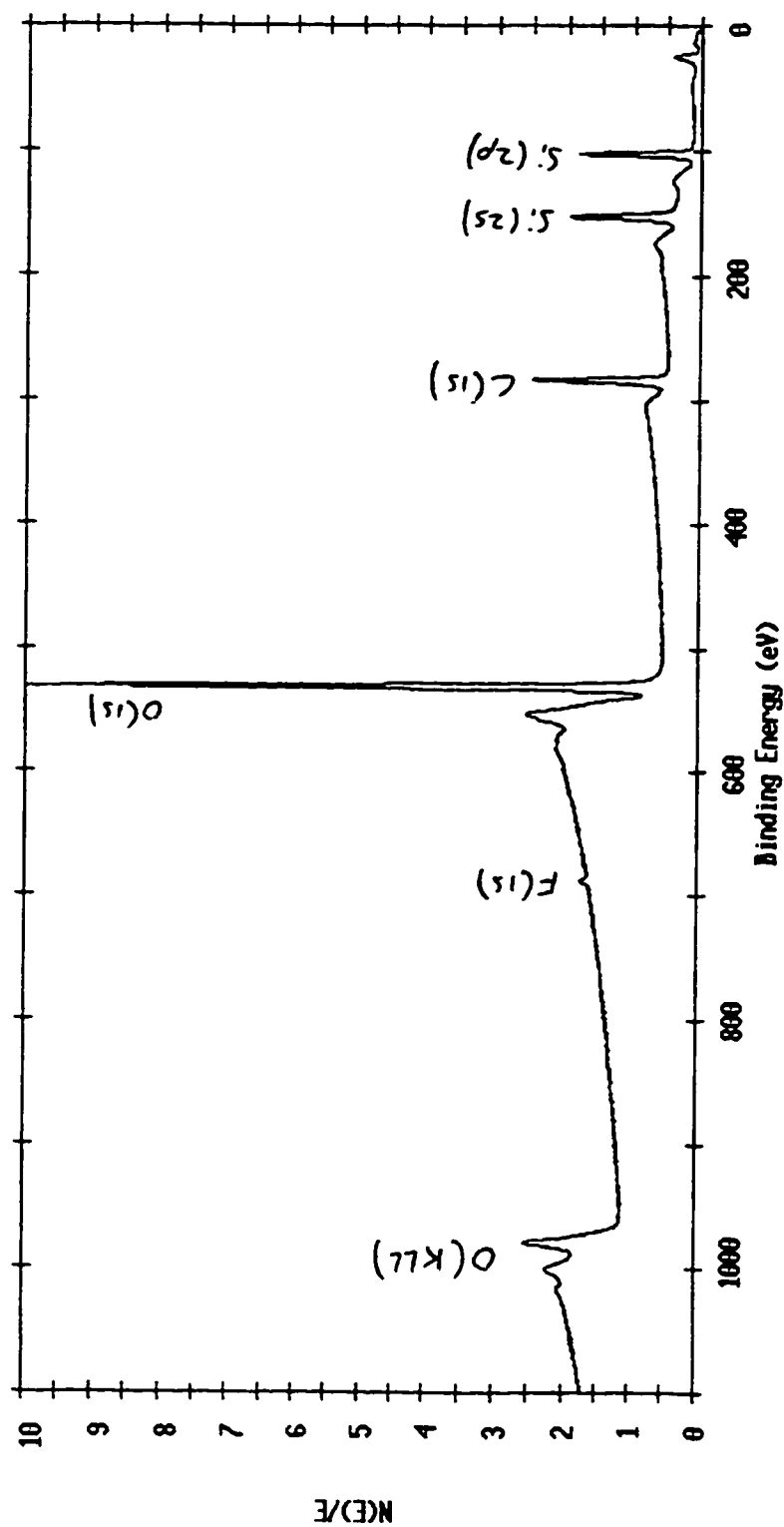
Figure 35: ESCA-Survey Spectrum of Davisil Cholesterol

ESCA Survey 4 Sep 94 Area: 1 Angle: 70 degrees Acquisition Time: 29.80 min
File: DAV_22 Davisil — MPAB, 149300
Scale Factor: 46.115 kc/s Offset: 0.488 kc/s Pass Energy: 187.850 eV Aperture: 5 Al 400W
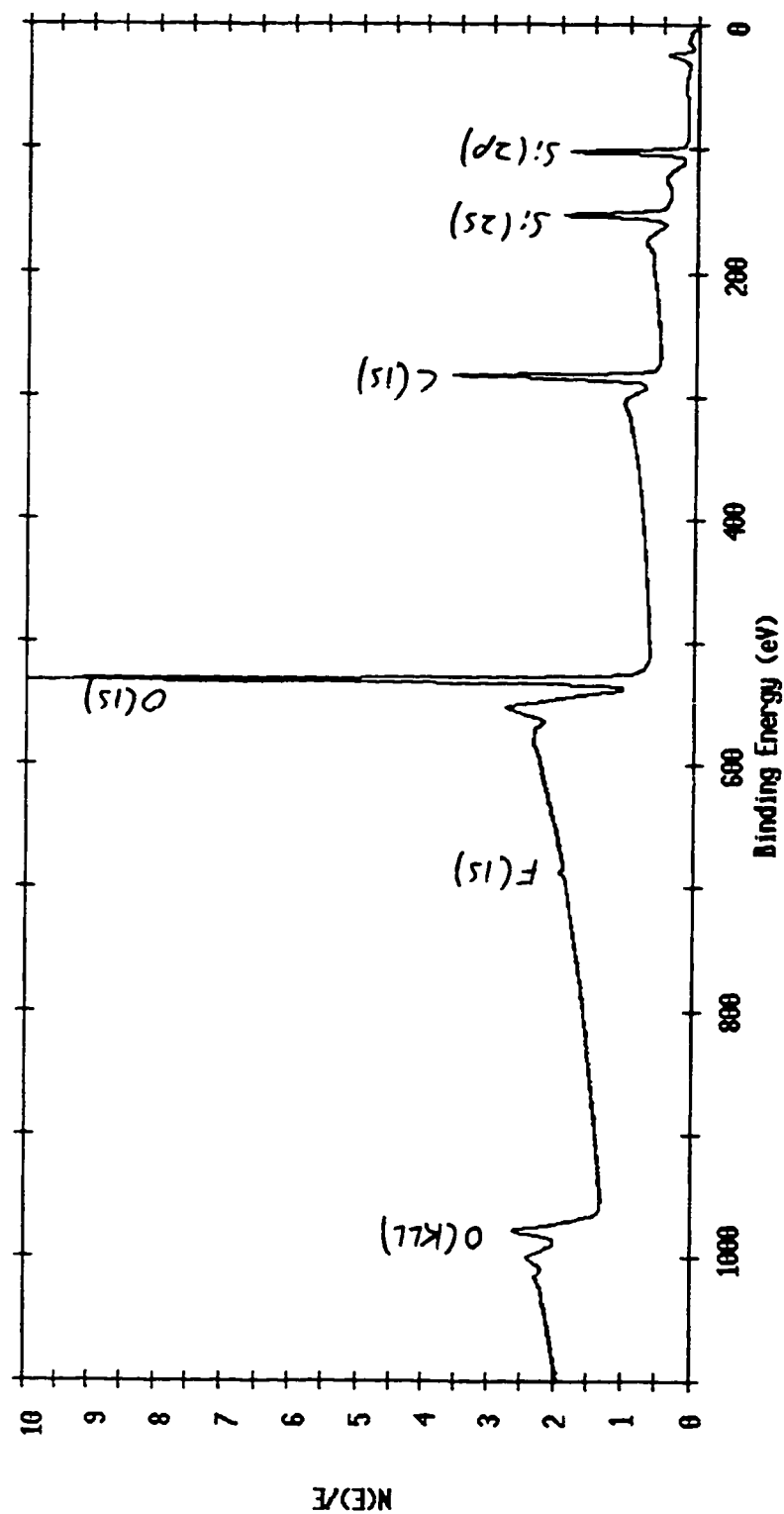
Figure 36: ESCA-Survey Spectrum of Davisil MPAB, 149300

ESCA Survey 5 Feb 95   Area: 1 Angle: 70 degrees Acquisition Time: 29.88 min
File: DAV_36   Davisil MPAB-silica (13100), Pt cat.
Scale Factor: 13.584 kc/s   Offset: 0.069 kc/s   Pass Energy: 187.850 eV   Aperture: 4 Al   400um

O(1s)

C(1s)

Si(2s)

Si(2p)

O(KLL)

N(E)/E

10
9
8
7
6
5
4
3
2
1
0

0   200   400   600   800   1000

Binding Energy (eV)

Figure 37: ESCA-Survey Spectrum of Davisil MPAB-Silica (13100)

ESCA Survey 5 Feb 95   Area: 1 Angle: 70 degrees   Acquisition Time: 29.80 min
File: DAV_37 Davisil MPAB-silica (15300), Pt cat., (control sample)
Scale Factor: 13.324 kc/s   Offset: 0.049 kc/s   Pass Energy: 187.850 eV   Aperture: 4 Al 4000n

Si (2p)

Si (2s)

C (1s)

N (1s)

O (1s)

O (KLL)

Na (1s)

Binding Energy (eV)

N(E)/E

Figure 38: ESCA-Survey Spectrum of Davisil MPAB-silica (15300)

ESCA Survey 25 Jan 94 Area: 1 Angle: 70 degrees Acquisition Time: 29.34 min
File: VYDAC5_1 VYDAC DIOL (GREY) 5
Scale Factor: 78.071 kc/s   Offset: 0.336 kc/s   Pass Energy: 187.850 eV Aperture: 5 Al 400 W

N(E)/E

Binding Energy (eV)

O(1s)

O(KLL)

C(1s)

S(2s)

S(2p)

Pt(4f)
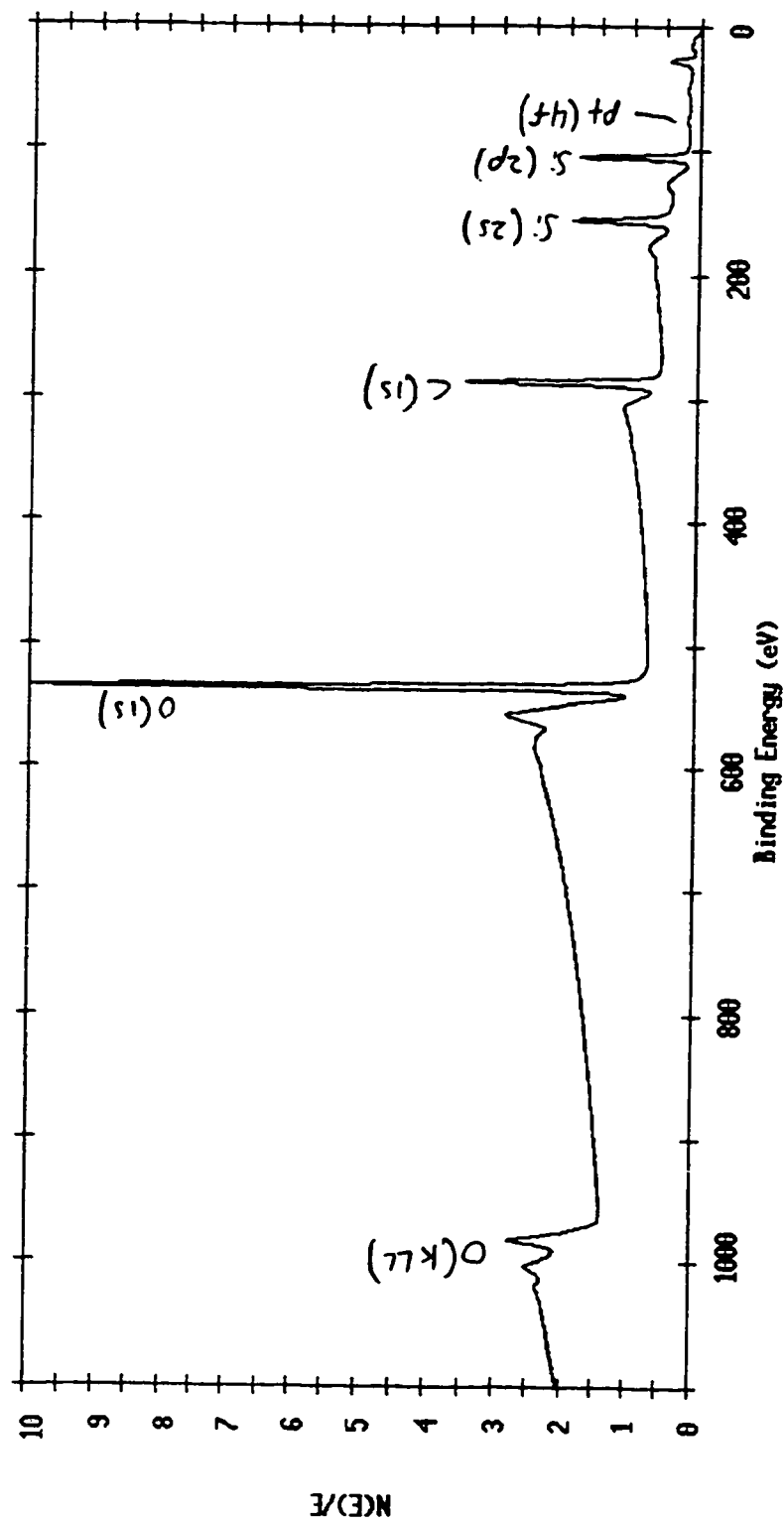
Figure 39: ESCA-Survey Spectrum of Vydac Diol (Gray) #5

ESCA Survey 25 Jan 94 Area: 1 Angle: 70 degrees Acquisition Time: 20.34 min
File: VYDAC5A_2 VYDAC DIOL ALLYL GLYCIDYL ETHER #5A
Scale Factor: 76.848 kc/s Offset: 0.506 kc/s Pass Energy: 187.850 eV Aperture: 5 Al 400 W
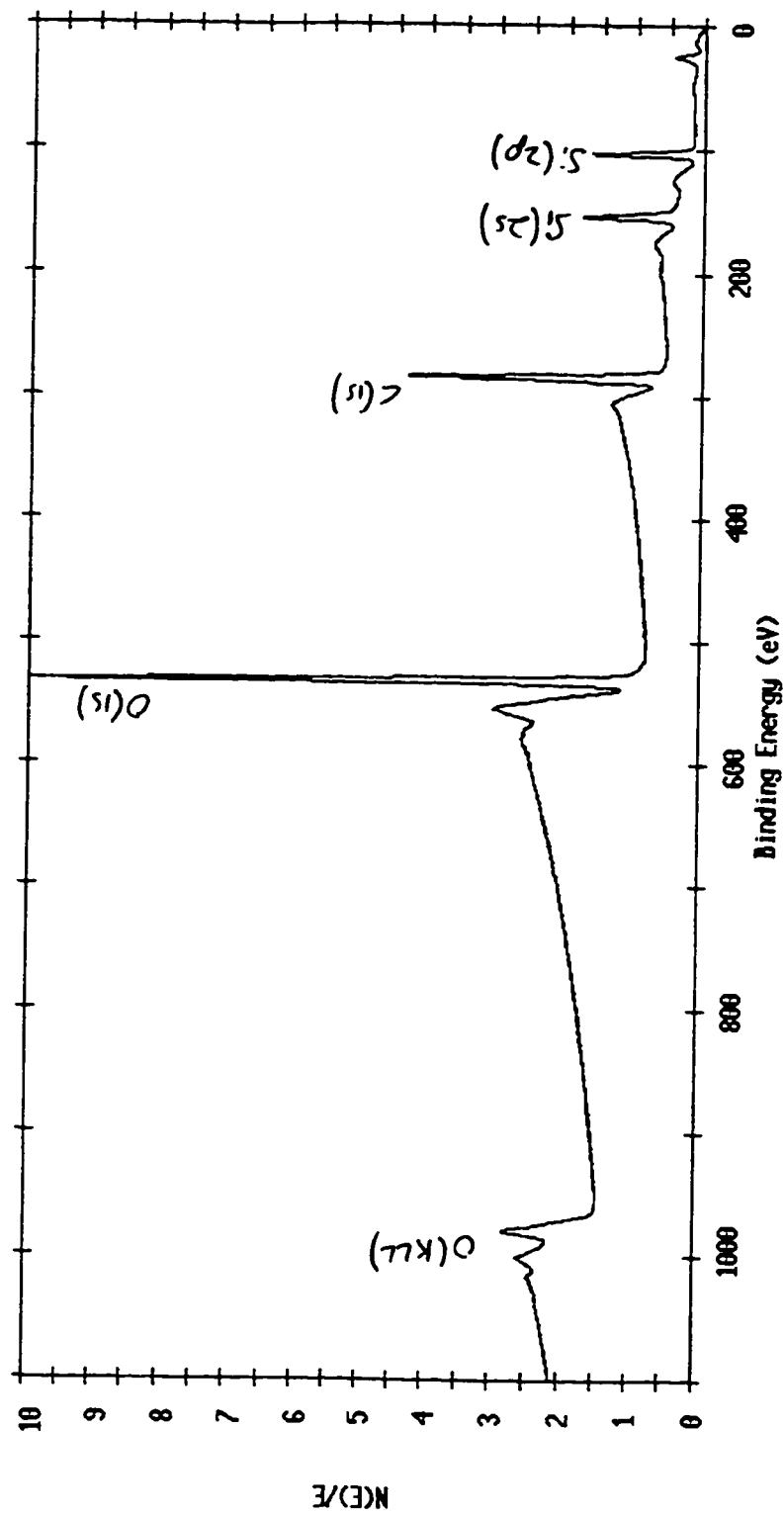
Figure 40: ESCA-Survey Spectrum of Vydac Diol Allyl Glycidyl Ether #5A

ESCA Survey 26 Jan 94 Area: 1 Angle: 70 degrees Acquisition Time: 29.34 min
File: VYDAC5B_3 VYDAC DIOL 7-OCTENE-1,2-DIOL 5B (RUN 1)
Scale Factor: 51.439 kc/s Offset: 0.325 kc/s Pass Energy: 187.850 eV Aperture: 5 Al 400 W
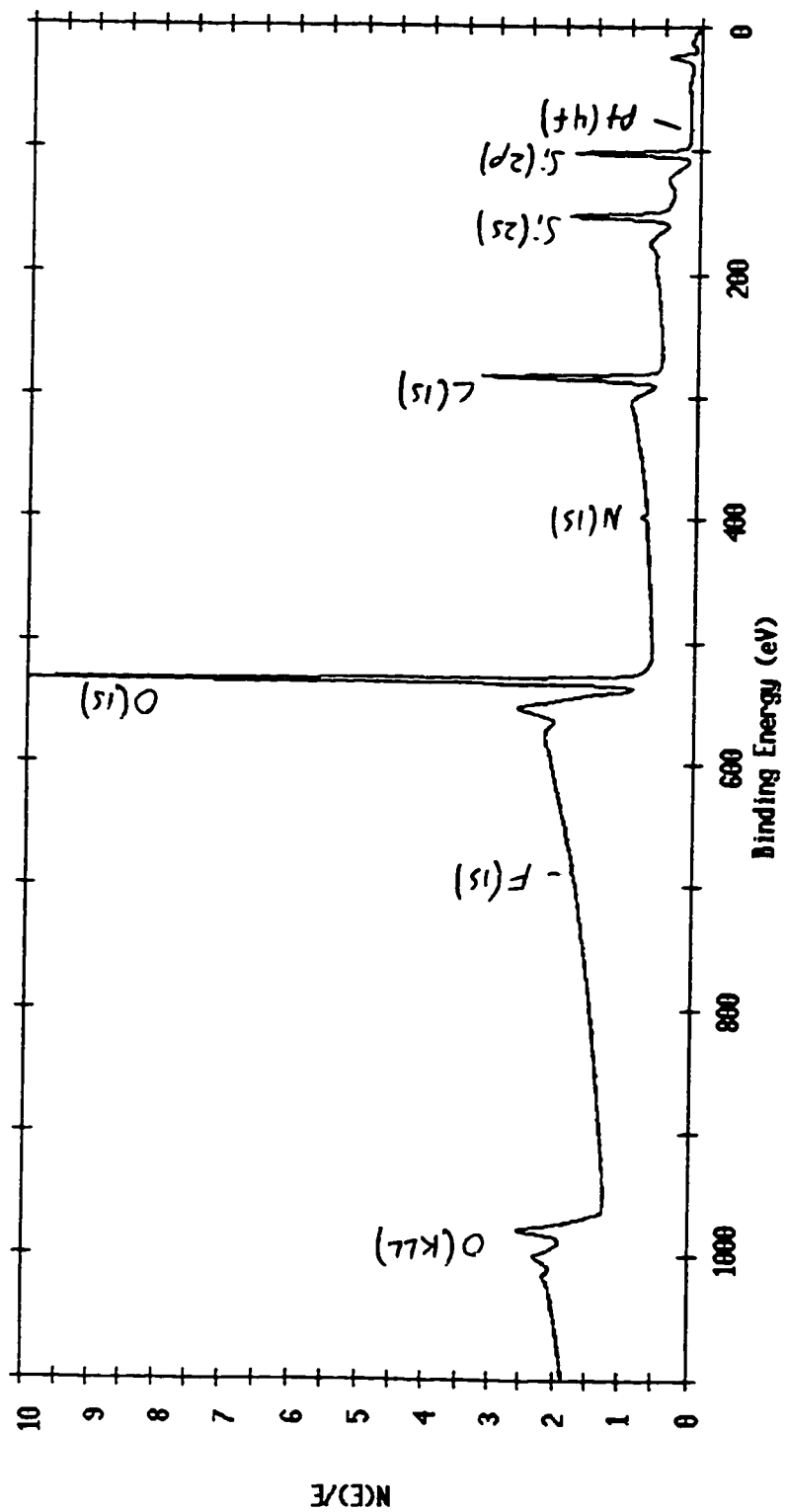
Figure 41: ESCA-Survey Spectrum of Vydac Diol 7-Octene-1,2-Diol 5B

ESCA Survey 26 Jan 94 Area: 1 Angle: 70 degrees Acquisition Time: 29.34 min
File: VYDAC5C_4 VYDAC DIOL 7-OCTENE-1,2-DIOL 5C (RUN 1)
Scale Factor: 45.971 kc/s Offset: 0.322 kc/s Pass Energy: 187.850 eV Aperture: 5 Al 400 W
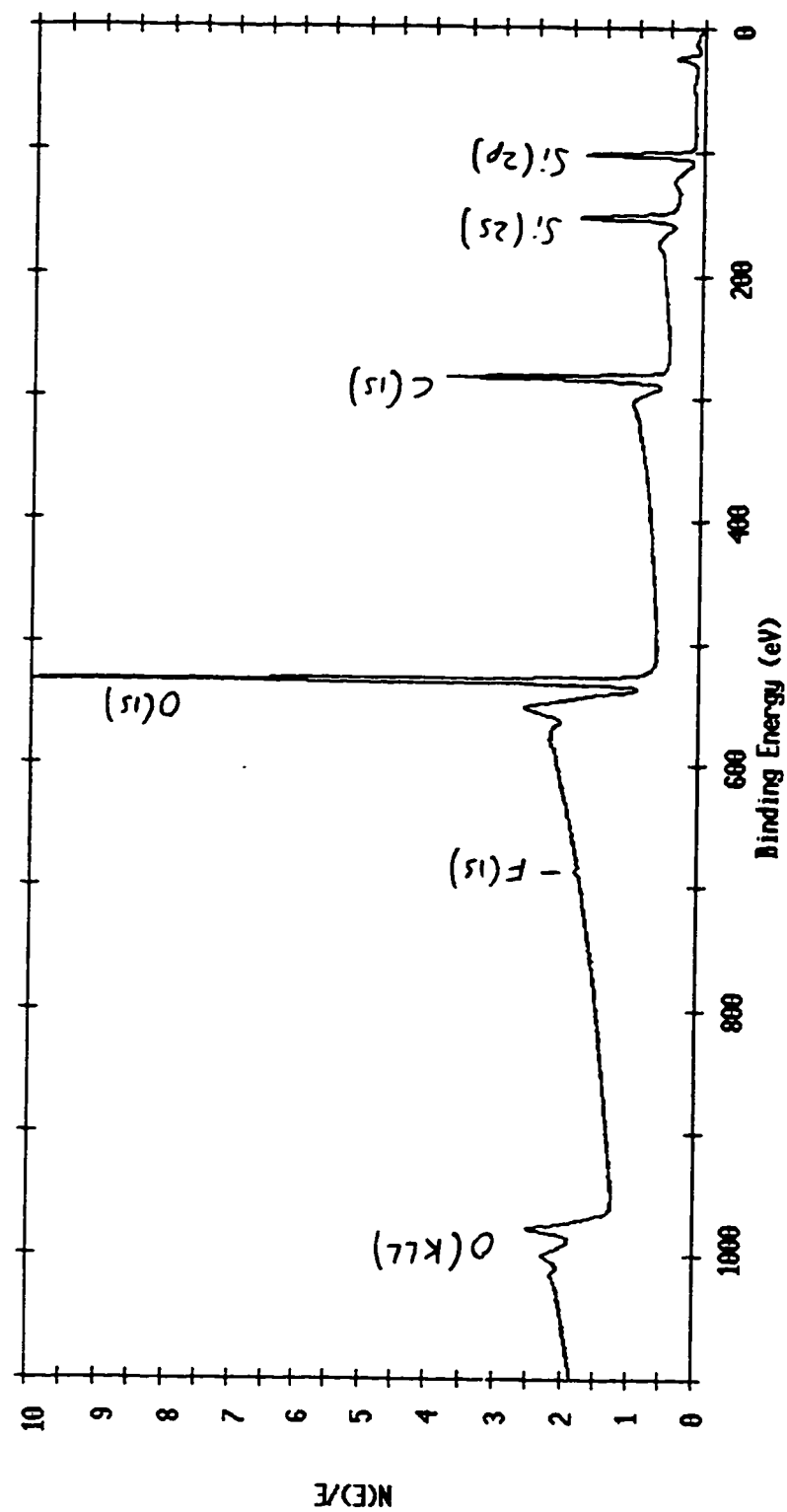
Figure 42: ESCA-Survey Spectrum of Vydac Diol 7-Octene1,2-Diol 5C

ESCA Survey 19 Feb 94 Area: 1 Angle: 70 degrees Acquisition Time: 29.34 min
File: VYDAC_5 VYDAC DIOL ALLYL GLYCIDYL ETHER BONDED 0.05M HCL (RUN1)
Scale Factor: 50.766 kc/s Offset: 0.344 kc/s Pass Energy: 187.850 eV Aperture: 5 Al 400 W
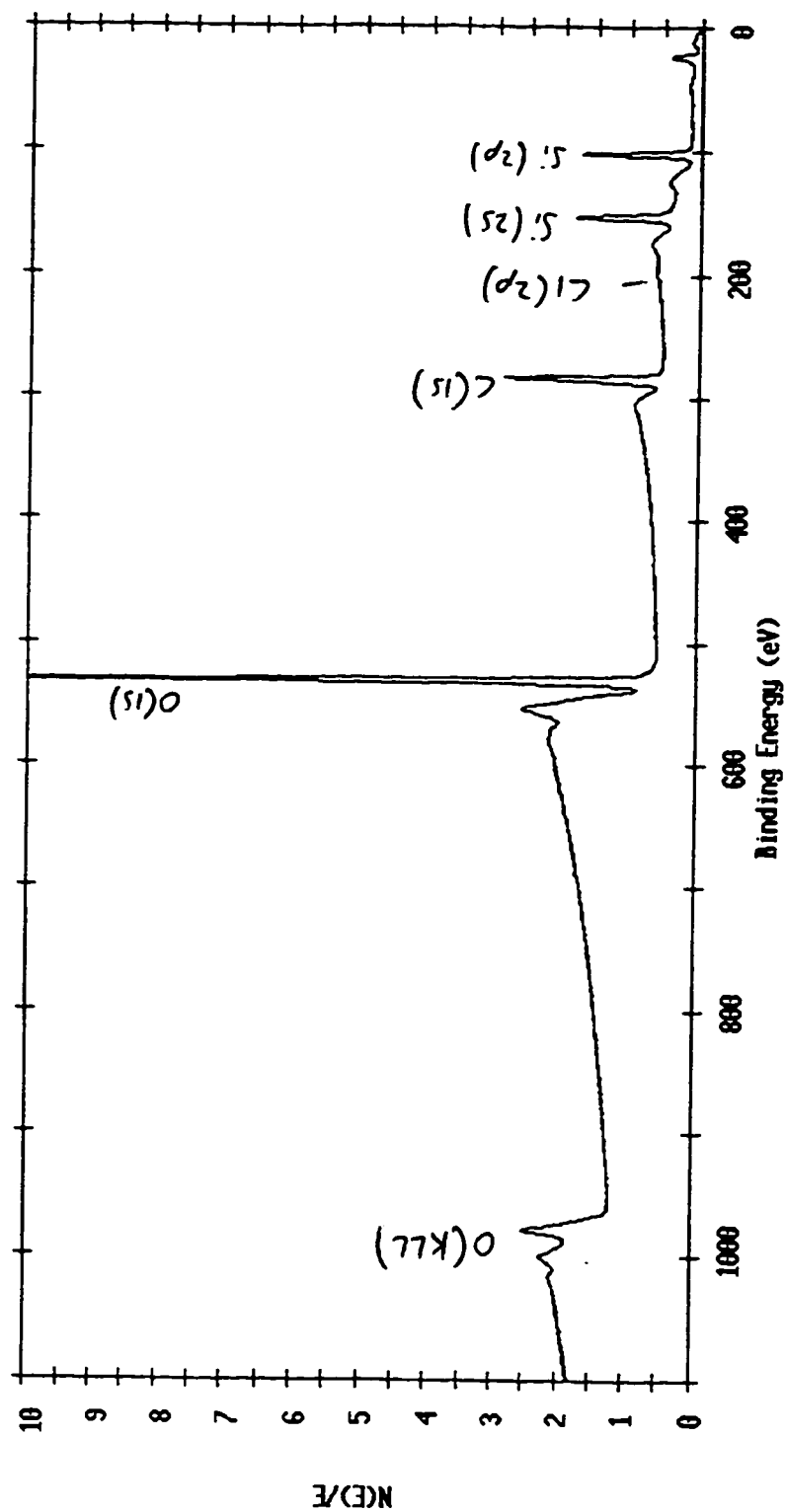
Figure 43: ESCA-Survey Spectrum of Vydac Diol Allyl Glycidyl Ether

ESCA Survey 19 Feb 94 Area: 1 Angle: 70 degrees Acquisition Time: 29.34 min
File: VYDAC_6 VYDAC +1H, 1H, 2H-PERFLUOROOCTENE (RUN 1)
Scale Factor: 63.885 kc/s Offset: 0.350 kc/s Pass Energy: 187.850 eV Aperture: 5 Al 400 W
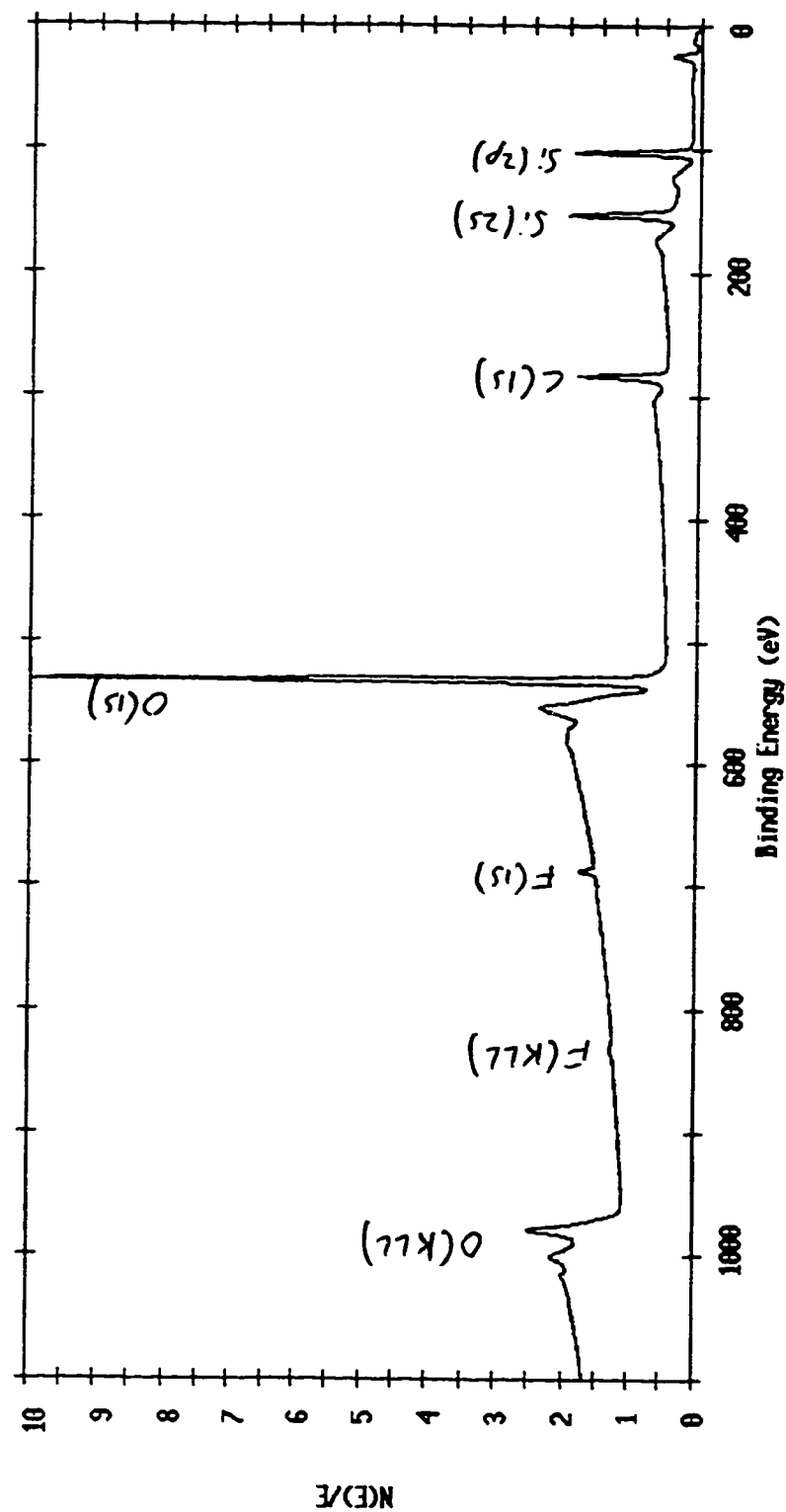
Figure 44: ESCA-Survey Spectrum of Vydac + 1H, 1H, 2H-Perfluorooctene

ESCA Survey 19 Feb 94 Area: 1 Angle: 70 degrees Acquisition Time: 29.34 min
File: VYDAC_7 VYDAC + 4-PHENYL-1-BUTENE (RUN 1)
Scale Factor: 45.227 kc/s Offset: 0.298 kc/s Pass Energy: 187.850 eV Aperture: 5 Al 400 W

Si (2p)

Si (2s)

C(1s)

O(1s)

O(KLL)

N(E)/E

Binding Energy (eV)
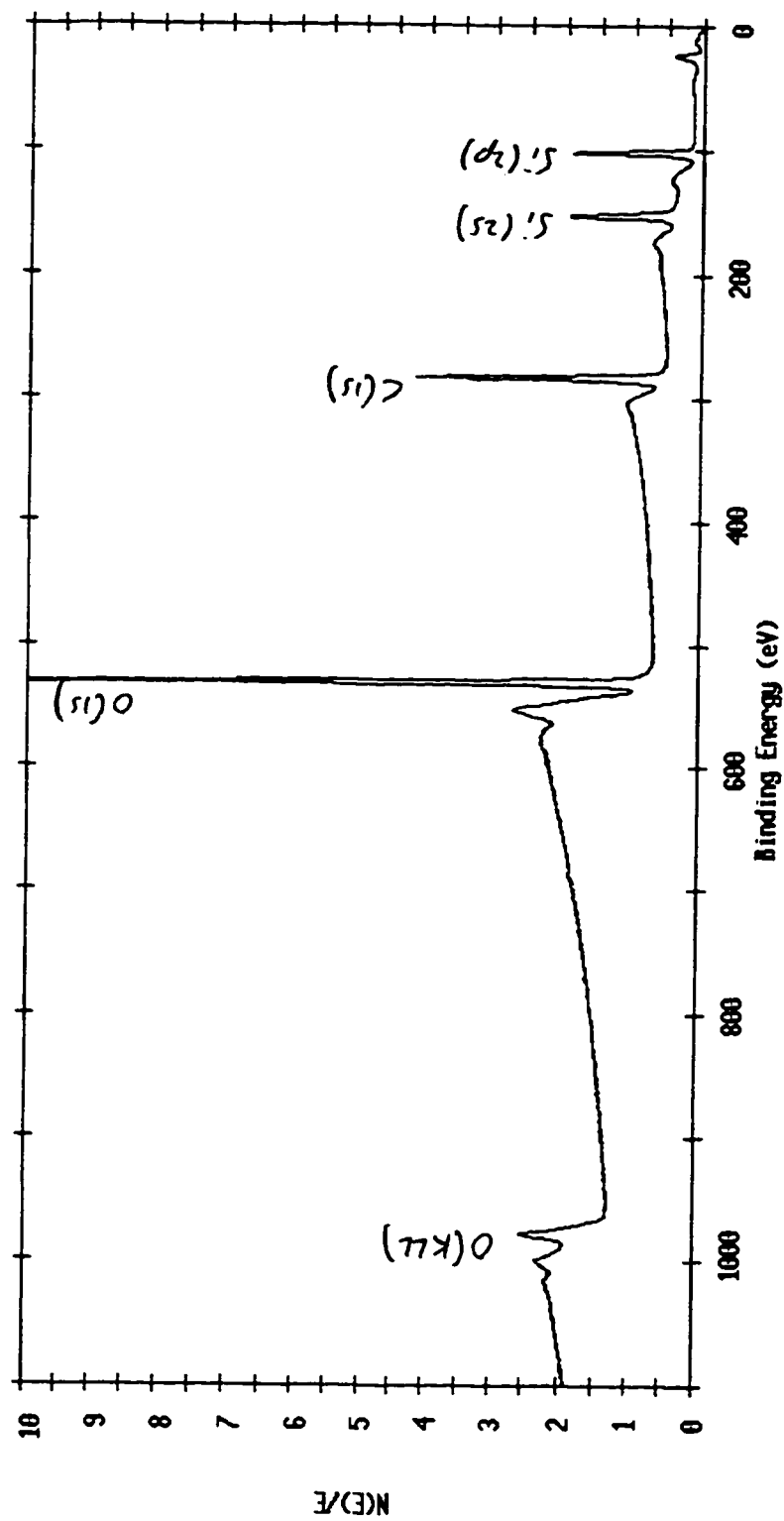
Figure 45: ESCA-Survey Spectrum of Vydac + 4-Phenyl-1-Butene

ESCA Survey 19 Feb 94 Area: 1 Angle: 70 degrees Acquisition Time: 29.34 min
File: VYDAC_8 VYDAC-HYDRIDE (RUN 1)
Scale Factor: 59.837 kc/s Offset: 0.302 kc/s Pass Energy: 187.850 eV Aperture: 5 Al 400 M

Si(2p)
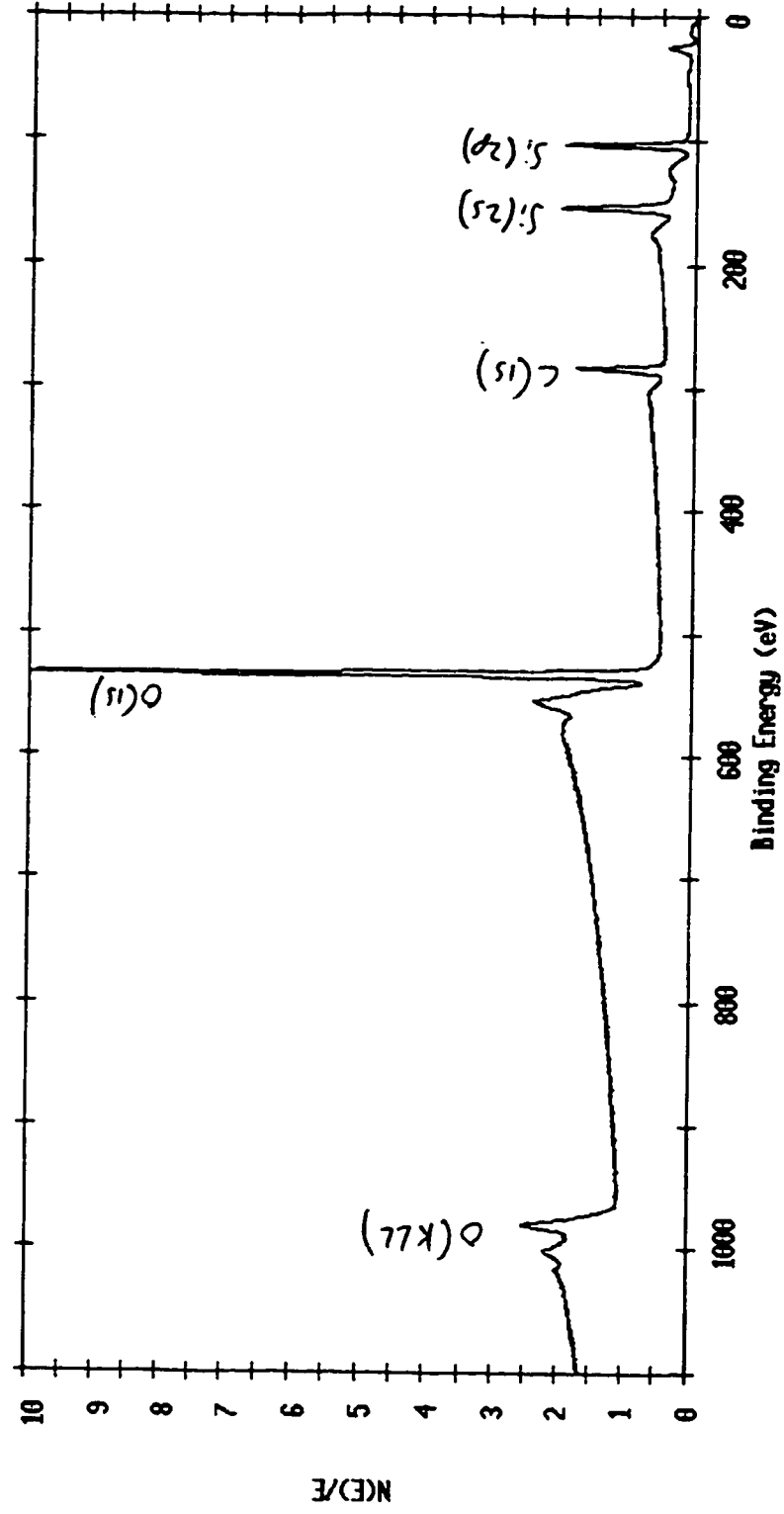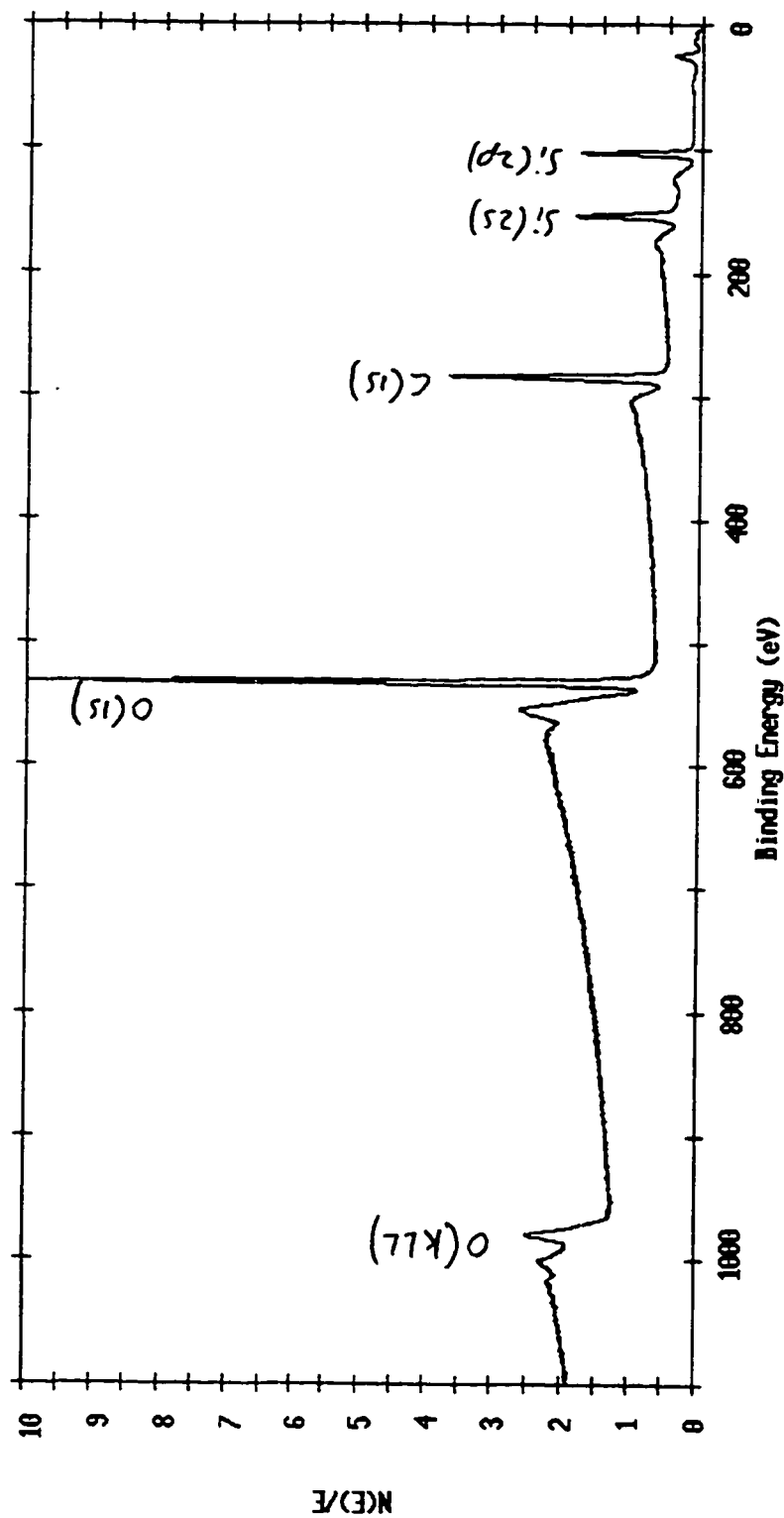
Si(2s)

C(1s)

O(1s)

O(KLL)

Binding Energy (eV)

N(E)/E
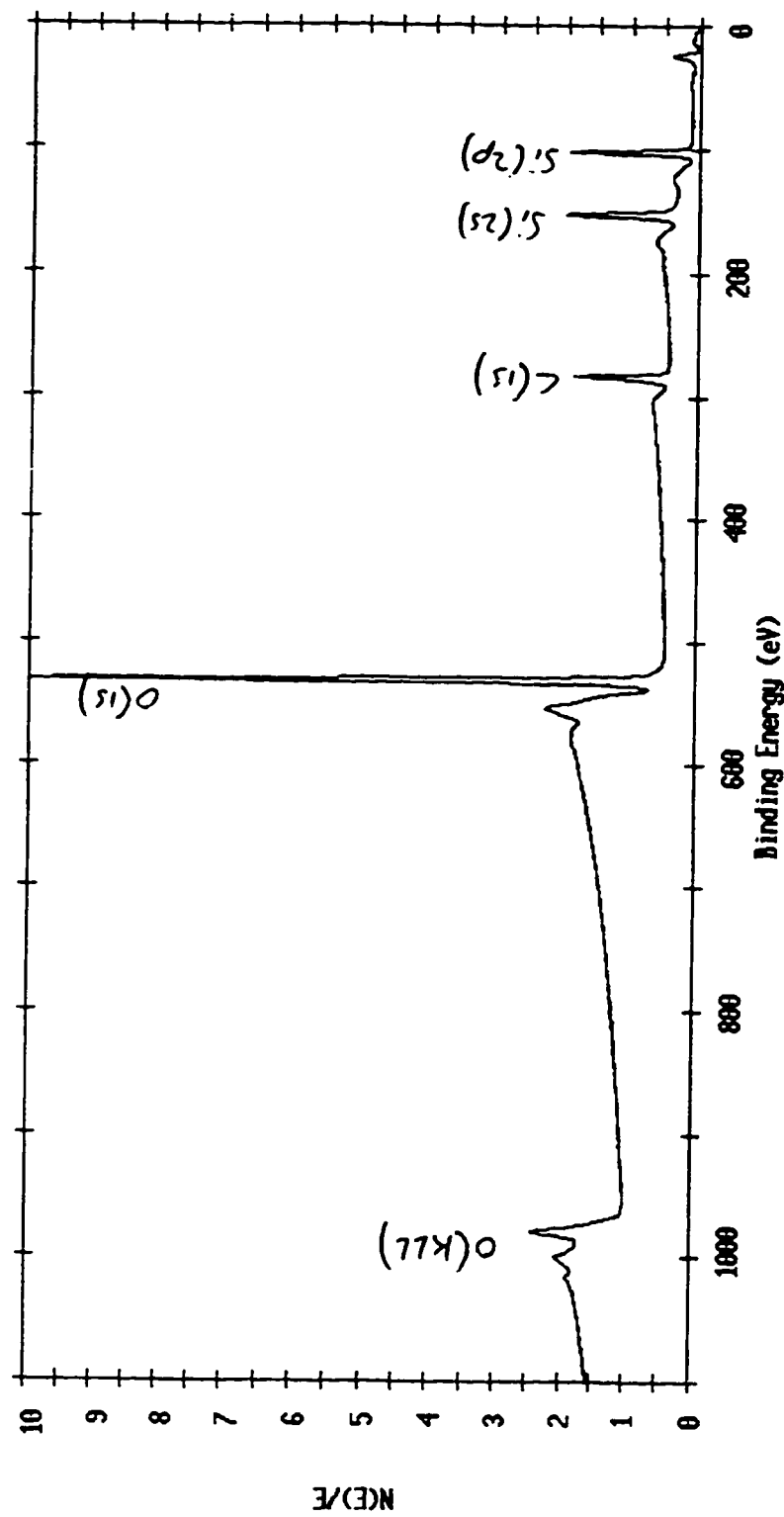
Figure 46: ESCA-Survey Spectrum of Vydac Hydride Run 1

ESCA Survey 18 Mar 94 Area: 1 Angle: 70 degrees Acquisition Time: 29.34 min
File: VYDAC_12 VYDAC BARE SILICA RUN1
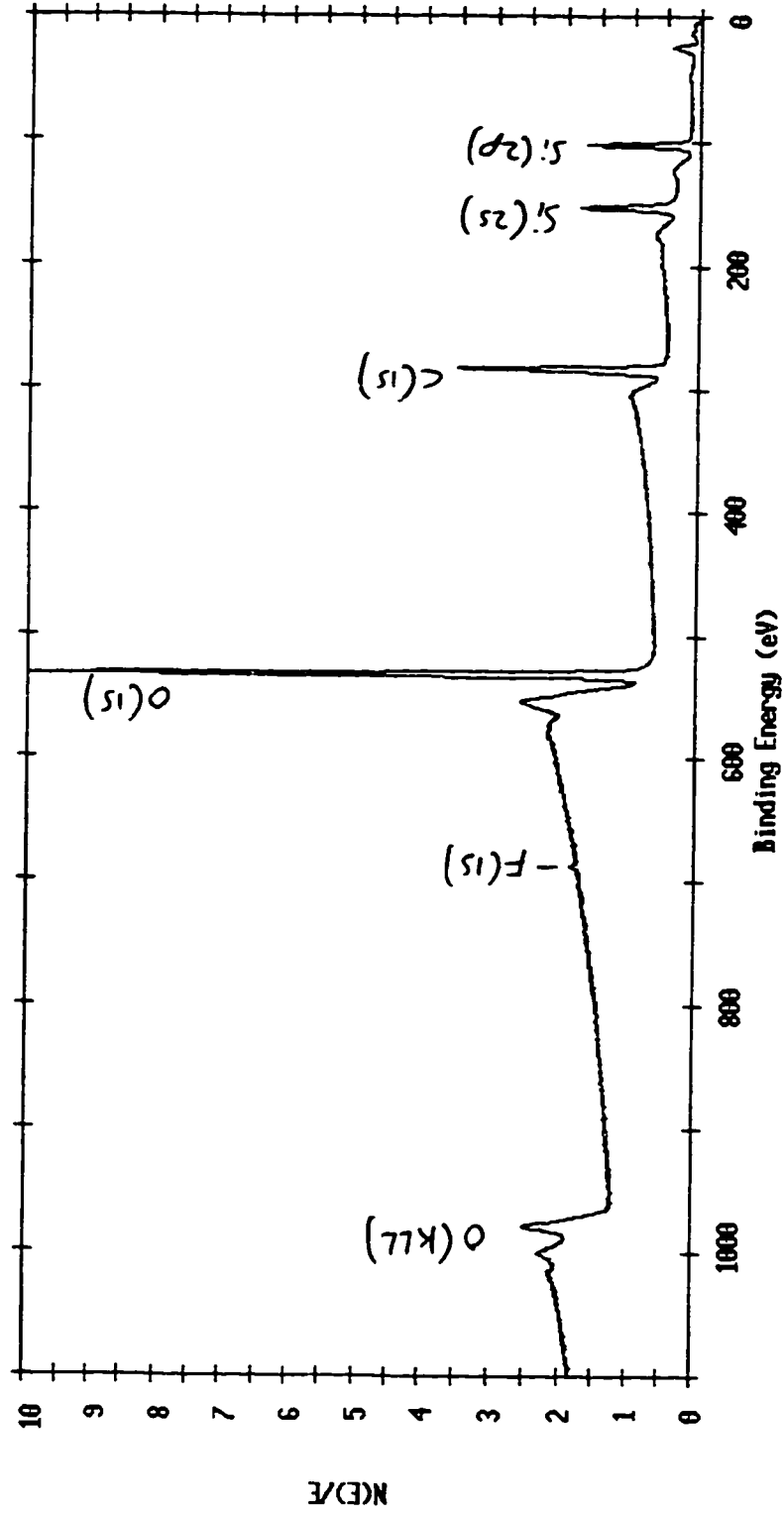Scale Factor: 20.320 kc/s Offset: 0.081 kc/s Pass Energy: 187.850 eV Aperture: 4 Al 400 W
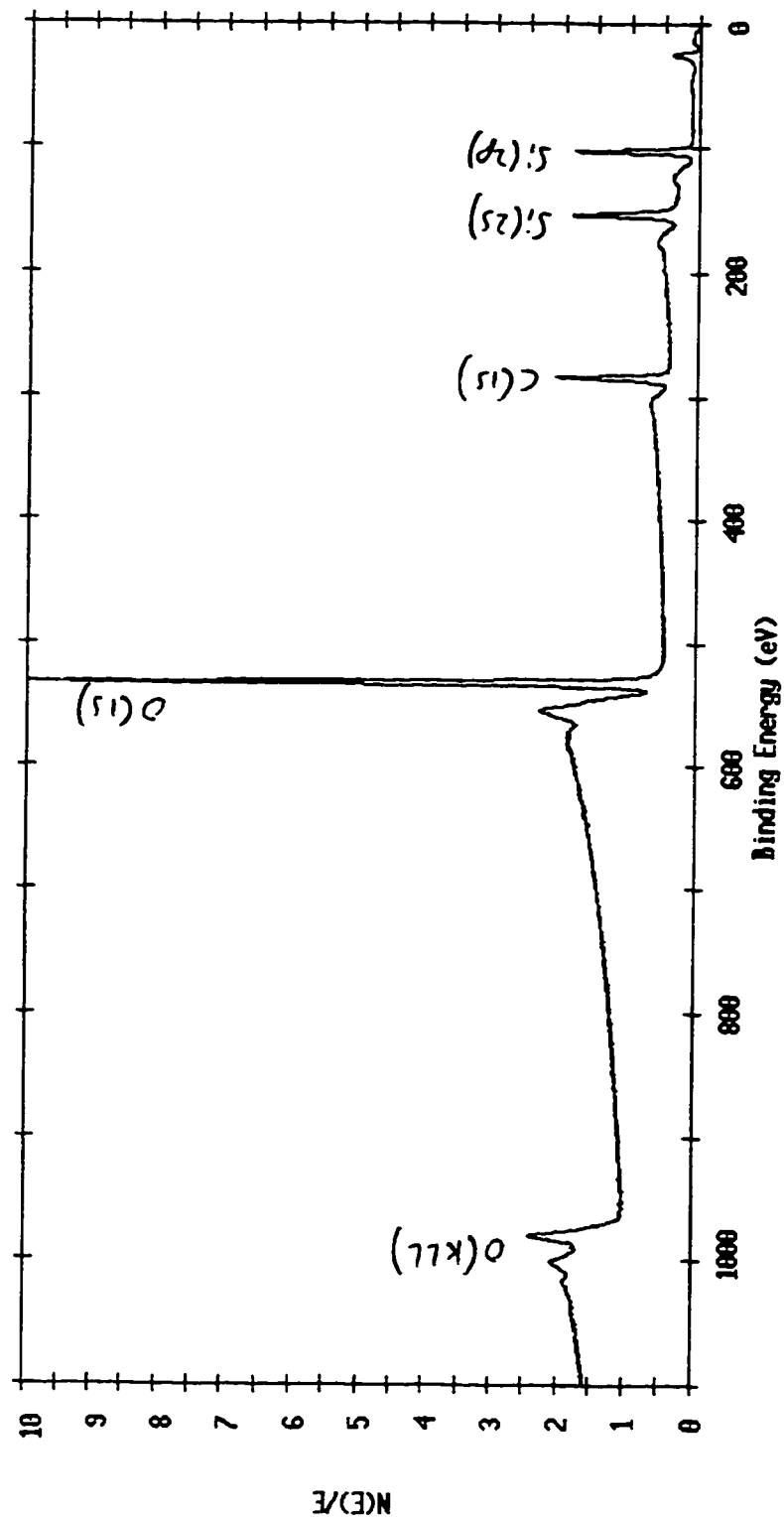
Figure 47: ESCA-Survey Spectrum of Vydac Bare Silica Run 1

ESCA Survey 18 Mar 94 Area: 1 Angle: 70 degrees Acquisition Time: 29.34 min
File: VYDAC_13 VYDAC HYDRID BATCH# 2 RUN 1
Scale Factor: 18.016 kc/s Offset: 0.006 kc/s Pass Energy: 187.850 eV Aperture: 4 Al 400 W

N(E)/E

10
9
8
7
6
5
4
3
2
1
0

O(1s)

O(KLL)

C(1s)

Si(2s)

Si(2p)

0   200   400   600   800   1000

Binding Energy (eV)

Figure 48: ESCA-Survey Spectrum of Vydac Hydride Batch 2 Run 1

ESCA Survey 19 Mar 94 Area: 1 Angle: 70 degrees Acquisition Time: 29.34 min
File: VYDAC_15 VYDAC DIOL FROM VYDAC-H BATCH 2 RUN 1
Scale Factor: 16.603 kc/s Offset: 0.086 kc/s Pass Energy: 187.850 eV Aperture: 4 Al 400 H

Si(2p)
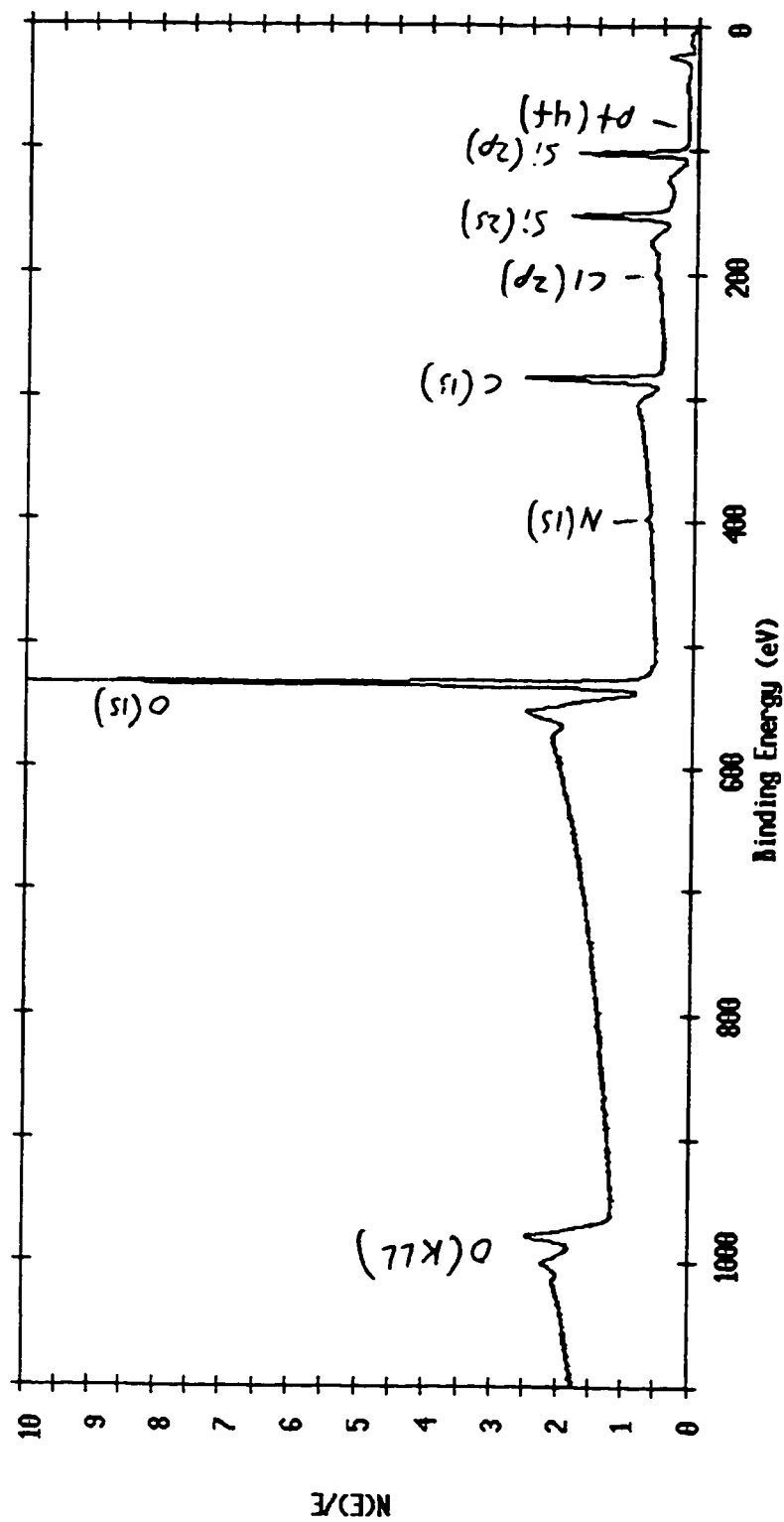
Si(2s)

C(1s)

O(1s)

O(KLL)

Binding Energy (eV)

N(E)/E

Figure 49: ESCA-Survey Spectrum of Vydac Diol from Vydac-H Batch 2 Run 1

ESCA Survey 19 Mar 94 Area: 1 Angle: 70 degrees Acquisition Time: 29.34 min
File: VYDAC_16 VYDAC + AGE SAMPLE 5D RUN 1
Scale Factor: 17.082 kc/s Offset: 0.103 kc/s Pass Energy: 187.850 eV Aperture: 4 Al 400 W

N(E)/E

Binding Energy (eV)

O(1s)

C(1s)
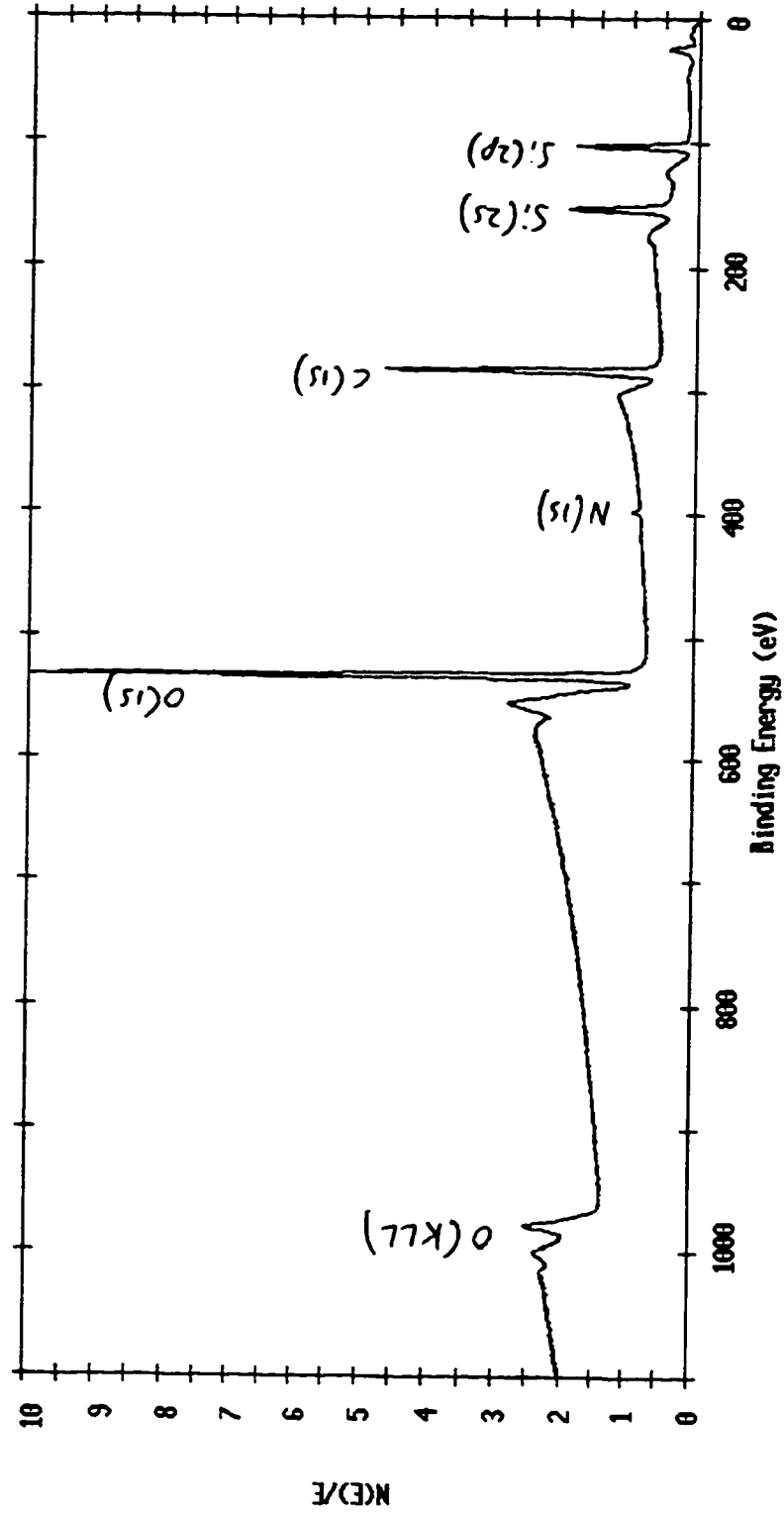
Si(2s)

Si(2p)

F(1s)

O(KLL)

Figure 50: ESCA-Survey Spectrum of Vydac + AGE Sample 5D Run 1

ESCA Survey 5 Jul 94 Area: 1 Angle: 70 degrees Acquisition Time: 29.80 min
File: VYDAC_17 AGE-DIOL (VYDAC-H) -- batch# 2, run 1
Scale Factor: 13.639 kc/s Offset: 0.077 kc/s Pass Energy: 187.850 eV Aperture: 4 Al 400 W

Binding Energy (eV)

N(E)/E

O(1s)

N(1s)

C(1s)

Cl(2p)

Si(2s)

Si(2p)

P(4f)

O(KLL)

Figure 51: ESCA-Survey Spectrum of Vydac AGE-Diol from Vydac-H Batch 2 Run 1

ESCA Survey 18 Oct 94 Area: 1 Angle: 70 degrees Acquisition Time: 29.80 min
File: VYDAC_23 C18 ON VYDAC TP
Scale Factor: 27.096 kc/s Offset: 0.166 kc/s Pass Energy: 187.850 eV Aperture: 5 Al 400 W

O(1s)

C(1s)

N(1s)

Si(2s)

Si(2p)

O(KLL)

Binding Energy (eV)

N(E)/E

Figure 52: ESCA-Survey Spectrum of Vydac TP + C18

ESCA Survey 18 Oct 94 Area: 1 Angle: 70 degrees Acquisition Time: 29.80 min
File: VYDAC_24 C8 ON VYDAC TP
Scale Factor: 31.053 kc/s Offset: 0.186 kc/s Pass Energy: 187.850 eV Aperture: 5 Al 400 W
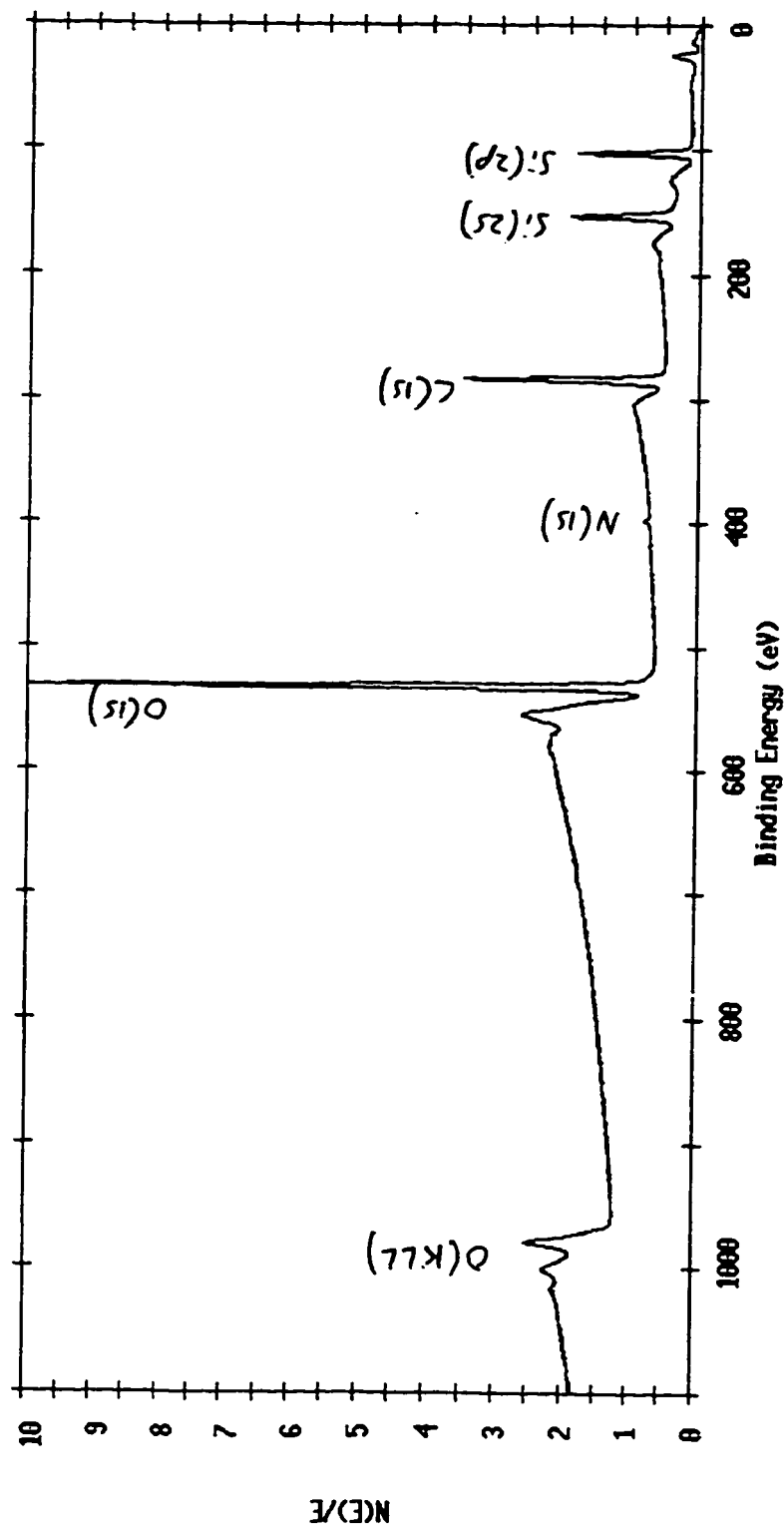
Figure 53: ESCA-Survey Spectrum of Vydac TP + C8

ESCA Survey   26 Jan 94   Area: 1   Angle: 70 degrees   Acquisition Time: 13.75 min
File: TAPE_1   ANALYSIS OF DOUBLE-STICKY TAPE RUN 1
Scale Factor: 45.228 kc/s   Offset: 0.363 kc/s   Pass Energy: 187.850 eV   Aperture: 5   Al 400 W
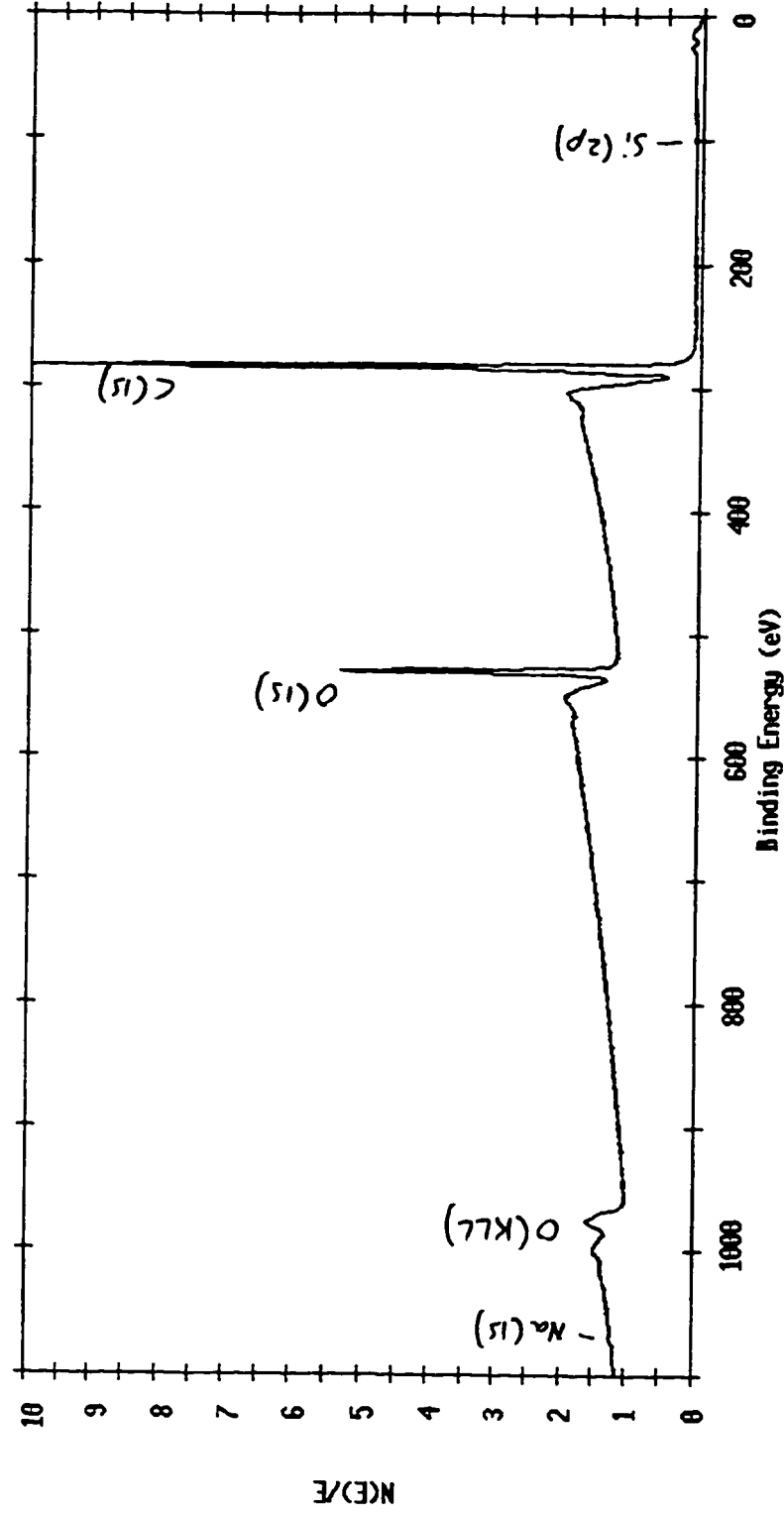
Figure 54: ESCA-Survey Spectrum of Double-Sticky Tape Run 1

ESCA Survey 5 Jul 94 Area: 1 Angle: 70 degrees Acquisition Time: 29.80 min
File: catal_1 H2PtCl6 (Platinum Catalyst)
Scale Factor: 5.249 kc/s Offset: 1.268 kc/s Pass Energy: 187.850 eV Aperture: 4 Al 400 W

Figure 55: ESCA-Survey Spectrum of Platinum Catalyst (H_2PtCl_6)

ESCA Survey 5 Sep 94   Area: 1 Angle: 70 degrees   Acquisition Time: 29.80 min
File: catal_7   fresh sample of H2PtCl6 on gold substrate, AR
Scale Factor: 14.004 kc/s   Offset: 7.354 kc/s   Pass Energy: 187.850 eV Aperture: 4 Al 400 W

Pt(4f)

Cl(2p)

Cl(2s)

C(1s)

Pt(4d5/2)

Pt(4d3/2)

N(1s)

Pt(4p3/2)

O(1s)

Pt(4p1/2)

F(1s)

Pt(4s)

O(KLL)

Binding Energy (eV)

N(E)/E
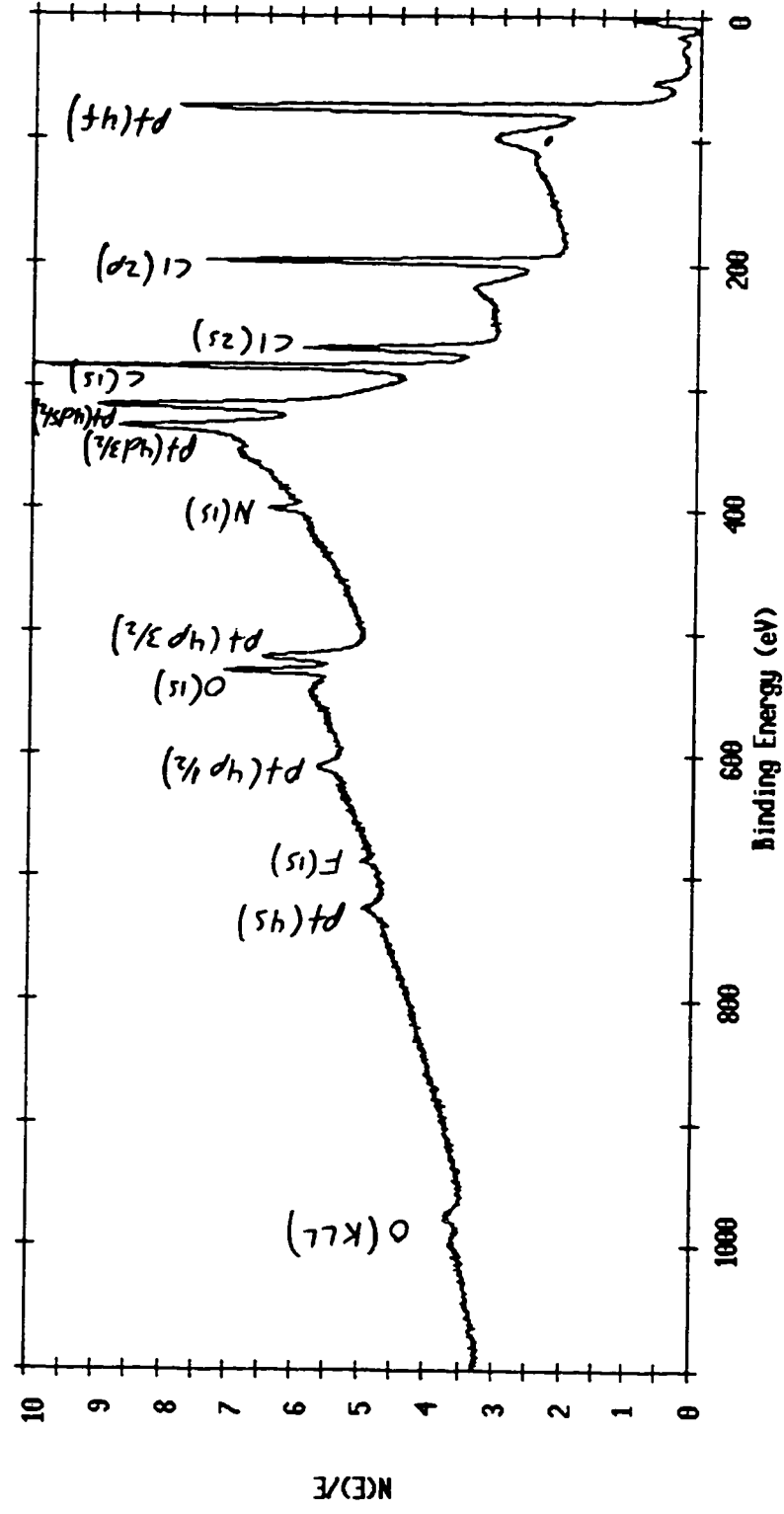
Figure 56: ESCA-Survey Spectrum of Platinum Catalyst (H_2PtCl_6)

ESCA Survey 18 Jul 95 Area: 1 Angle: 70 degrees Acquisition Time: 29.34 min
File: S01P31C_2 S01P31C SAMPLE

Scale Factor: 10.278 kc/s Offset: 0.850 kc/s Pass Energy: 187.850 eV Aperture: 5 Al 350 W

$Pt(4f)$

$Si(2p)$

$Si(2s)$

$C(1s)$

$Pt(4d5/2)$

$Pt(4d3/2)$

$Pt(4p3/2)$

$O(1s)$

$O(KLL)$

N(E)/E

10 9 8 7 6 5 4 3 2 1 0

0 200 400 600 800 1000

Binding Energy (eV)

Figure 57: ESCA-Survey Spectrum of S02P31C

ESCA Survey 18 Jul 95 Area: 1 Angle: 70 degrees Acquisition Time: 29.34 min
File: S01P34C_1 S01P34C SAMPLE
Scale Factor: 9.607 kc/s Offset: 0.492 kc/s Pass Energy: 187.850 eV Aperture: 5 Al 350 W
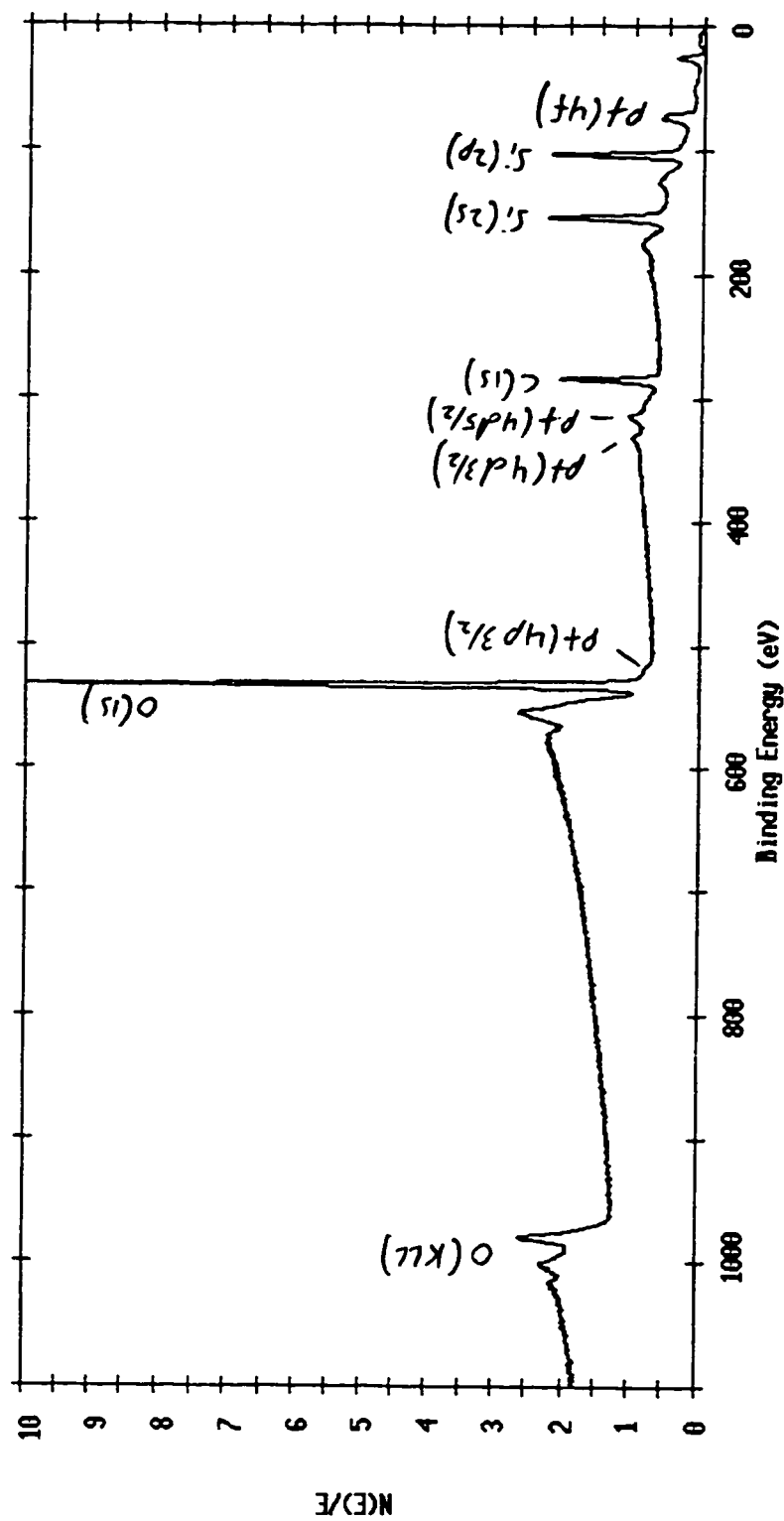
Figure 58: ESCA-Survey Spectrum of S01P34C

ESCA Survey 18 Jul 95 Area: 1 Angle: 70 degrees Acquisition Time: 29.34 min
File: S01P35C_1 S01P35C SAMPLE
Scale Factor: 4.728 kc/s Offset: 0.219 kc/s Pass Energy: 187.850 eV Aperture: 5 Al 350 W
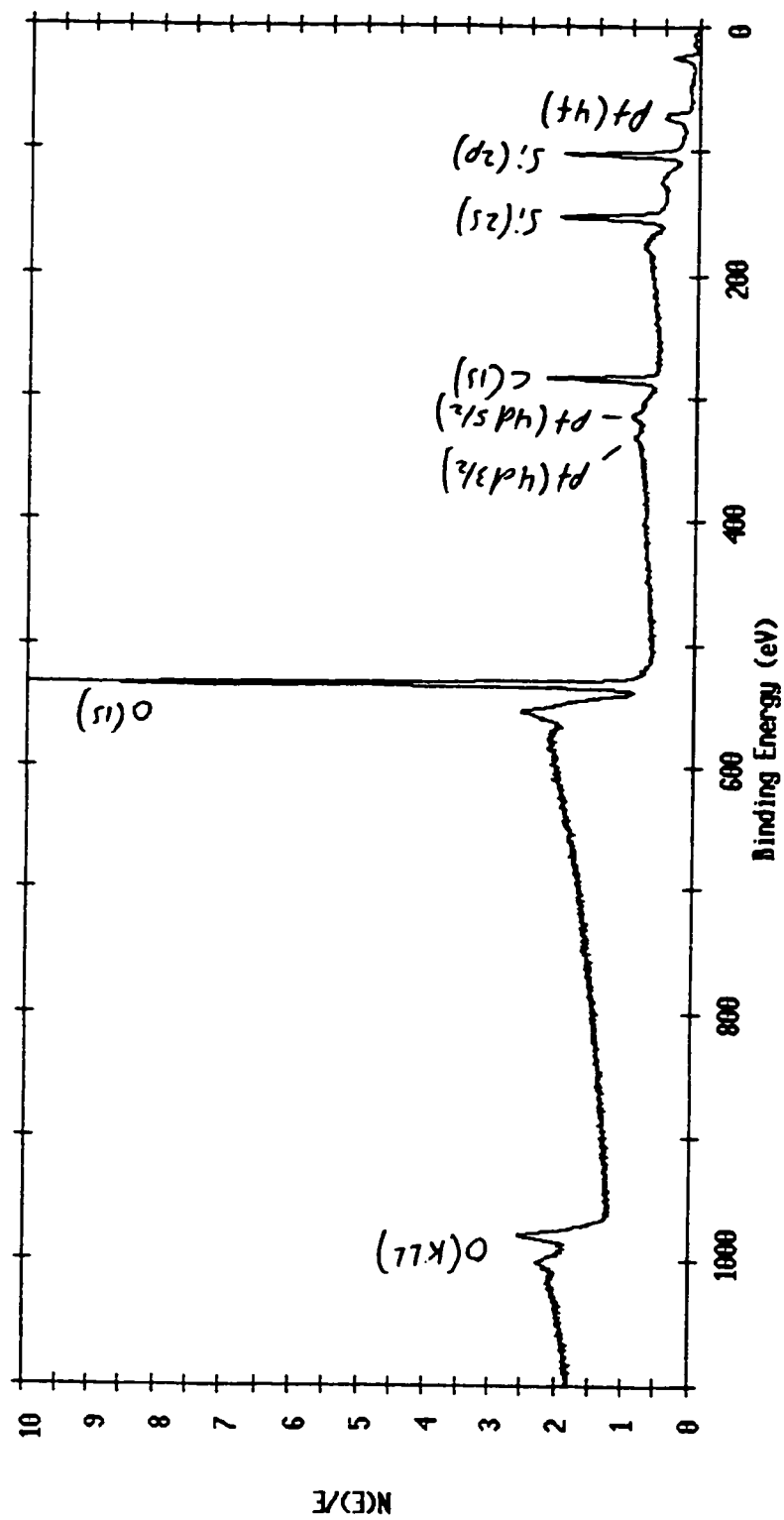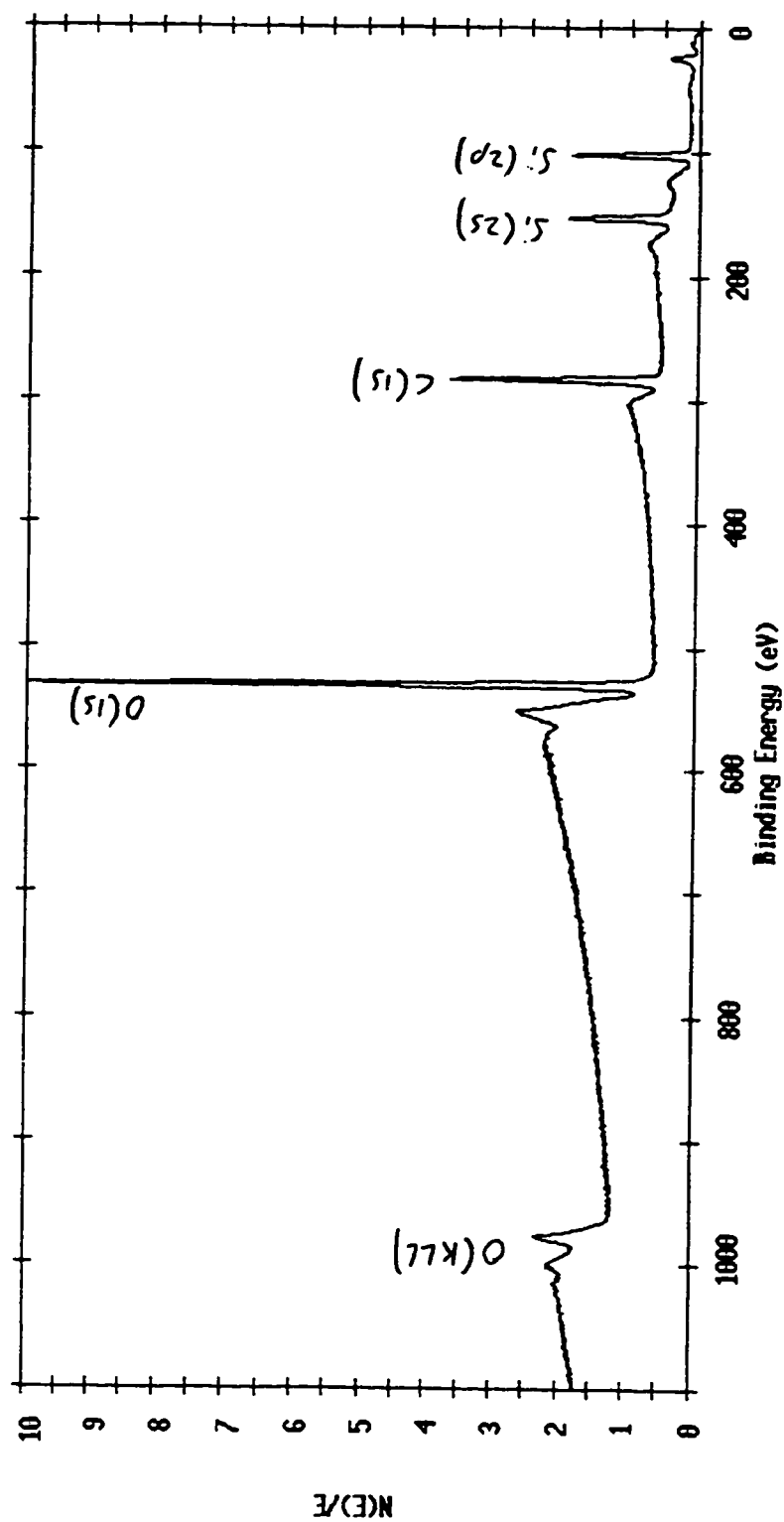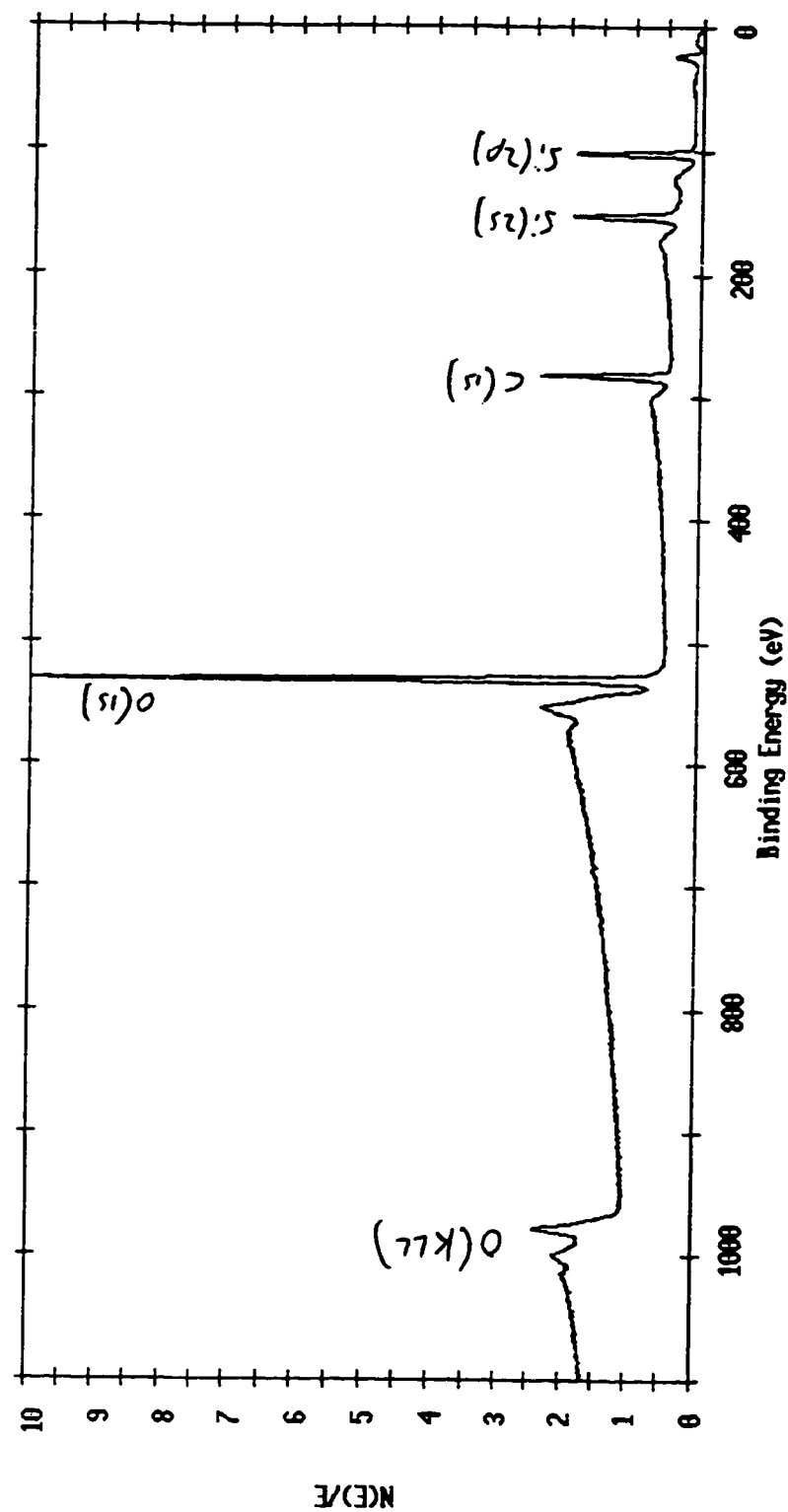

Figure 59: ESCA-Survey Spectrum of S01P35C

113

ESCA Survey 21 Feb 96 Area: 1 Angle: 70 degrees Acquisition Time: 33.93 min
File: titania_1 titania 3 days (batch# 2) dated 7-8-94
Scale Factor: 6.232 kc/s Offset: 0.159 kc/s Pass Energy: 187.850 eV Aperture: 4 Al 350 W

N(E)/E

Ti(3p)
Ti(3s)
Cl(2p)
Cl(2s)
C(1s)
Ti(2p1/2)
Ti(2p3/2)
O(1s)
Ti(2s)
O(1s)
Ti(LMM)

Binding Energy (eV)
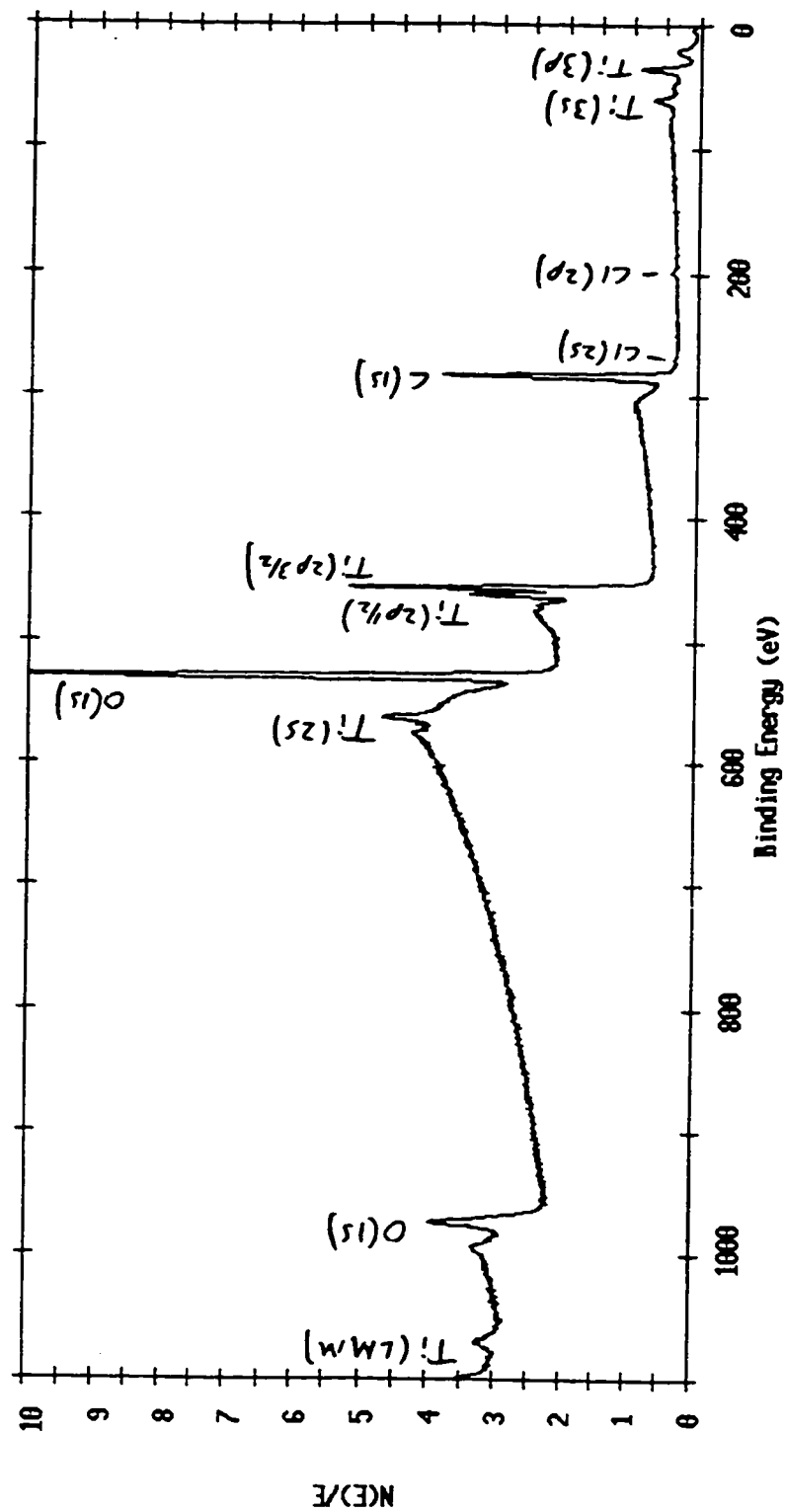
Figure 60: ESCA-Survey Spectrum of Titania 3 Days (Batch 2, dated 7/8/94)

ESCA Survey 21 Feb 96 Area: 1 Angle: 70 degrees Acquisition Time: 30.26 min
File: titania_2 titania 7 days (batch# 2) dated 7-15-94
Scale Factor: 4.841 kc/s Offset: 0.194 kc/s Pass Energy: 187.850 eV Aperture: 4 Al 350 W
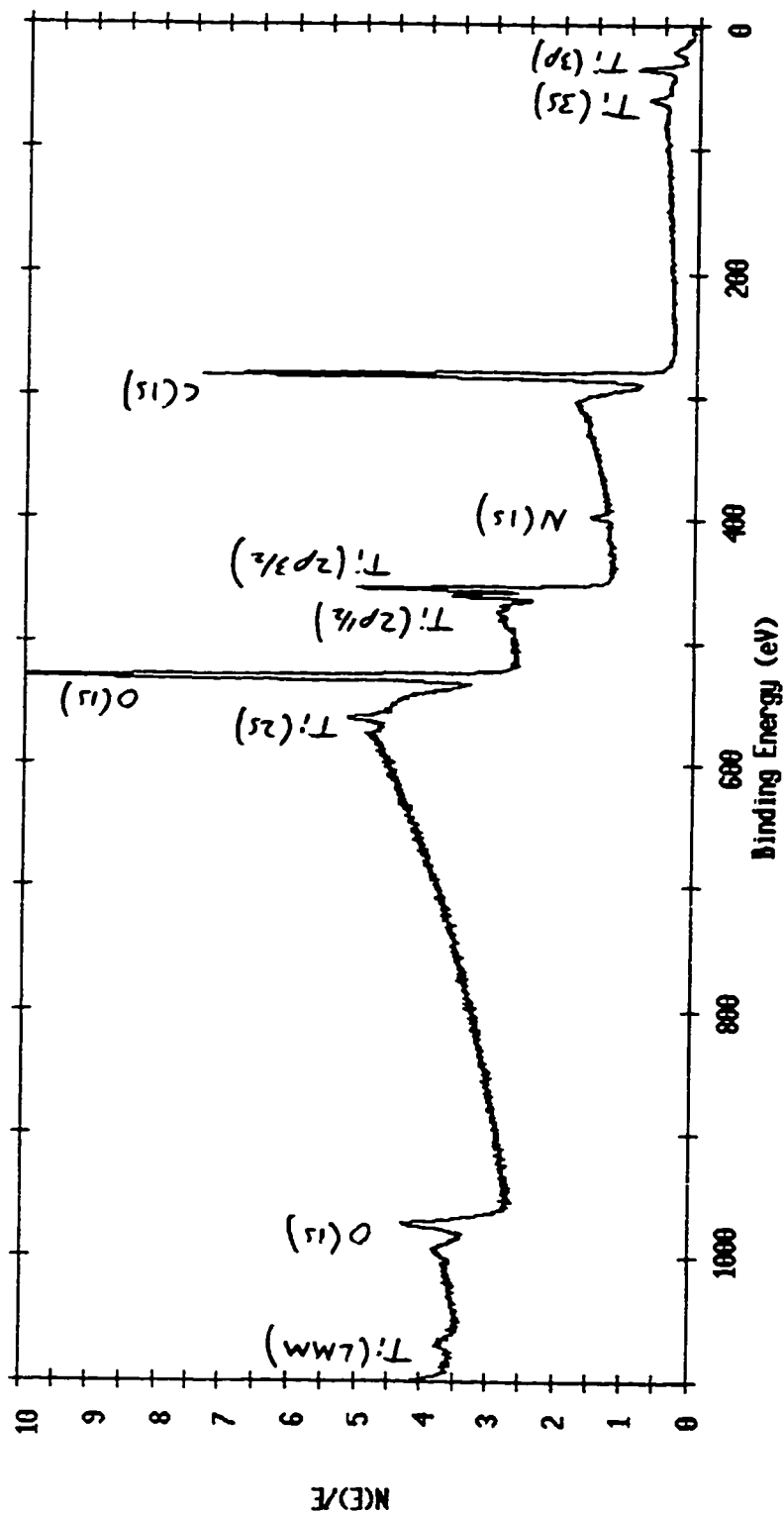
Figure 61: ESCA-Survey Spectrum of Titania 7 Days (Batch 2, dated 7/15/94)

ESCA Survey 12 Mar 96 Area: 1 Angle: 70 degrees Acquisition Time: 29.34 min
File: ST9031_1 C30 PT ST9031
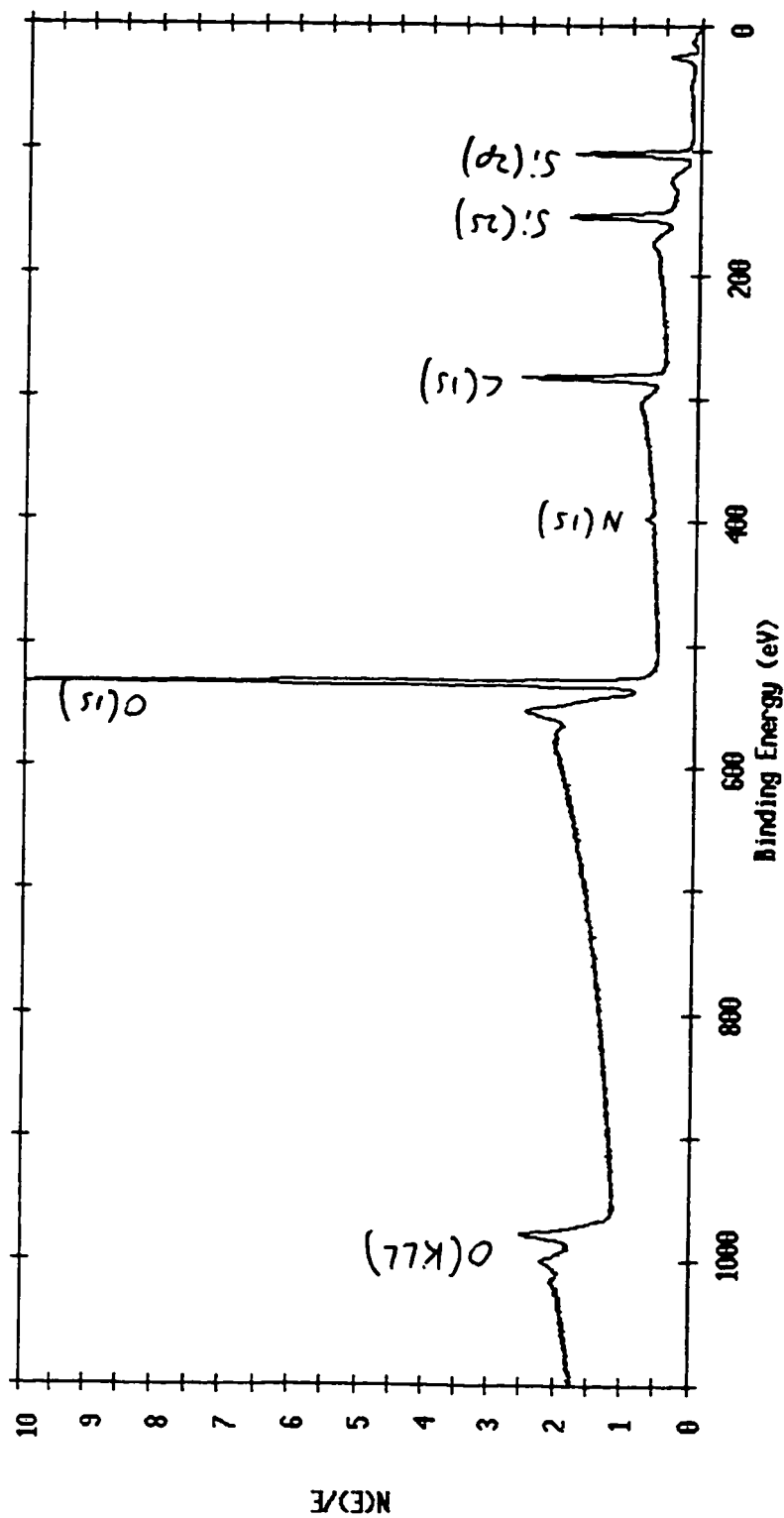Scale Factor: 9.713 kc/s Offset: 0.073 kc/s Pass Energy: 187.850 eV Aperture: 4 Al 350 W

Figure 62: ESCA-Survey Spectrum of C30 Pt ST9031

ESCA Survey 12 Mar 96 Area: 1 Angle: 70 degrees Acquisition Time: 29.34 min
File: STG032_1 C30 AIBN STG032
Scale Factor: 12.784 kc/s   Offset: 0.069 kc/s Pass Energy: 187.850 eV Aperture: 4 Al 350 W

Figure 63: ESCA-Survey Spectrum of C30 AIBN STG032

ESCA Survey 13 Mar 96 Area: 1 Angle: 70 degrees Acquisition Time: 29.34 min
File: RNEA_1 R(+) NEA
Scale Factor: 11.736 kc/s Offset: 0.058 kc/s Pass Energy: 187.850 eV Aperture: 4 Al 350 M

$N(E)/E$

$S:(2p)$
$S:(2s)$
$C(1s)$
$N(1s)$
$O(1s)$
$O(KLL)$

Binding Energy (eV)

Figure 64: ESCA-Survey Spectrum of R(+) NEA

ESCA Survey 13 Mar 96 Area: 1 Angle: 70 degrees Acquisition Time: 29.34 min
File: SNEA_1 S(-) NEA
Scale Factor: 10.680 kc/s Offset: 0.061 kc/s Pass Energy: 187.850 eV Aperture: 4 Al 350 W
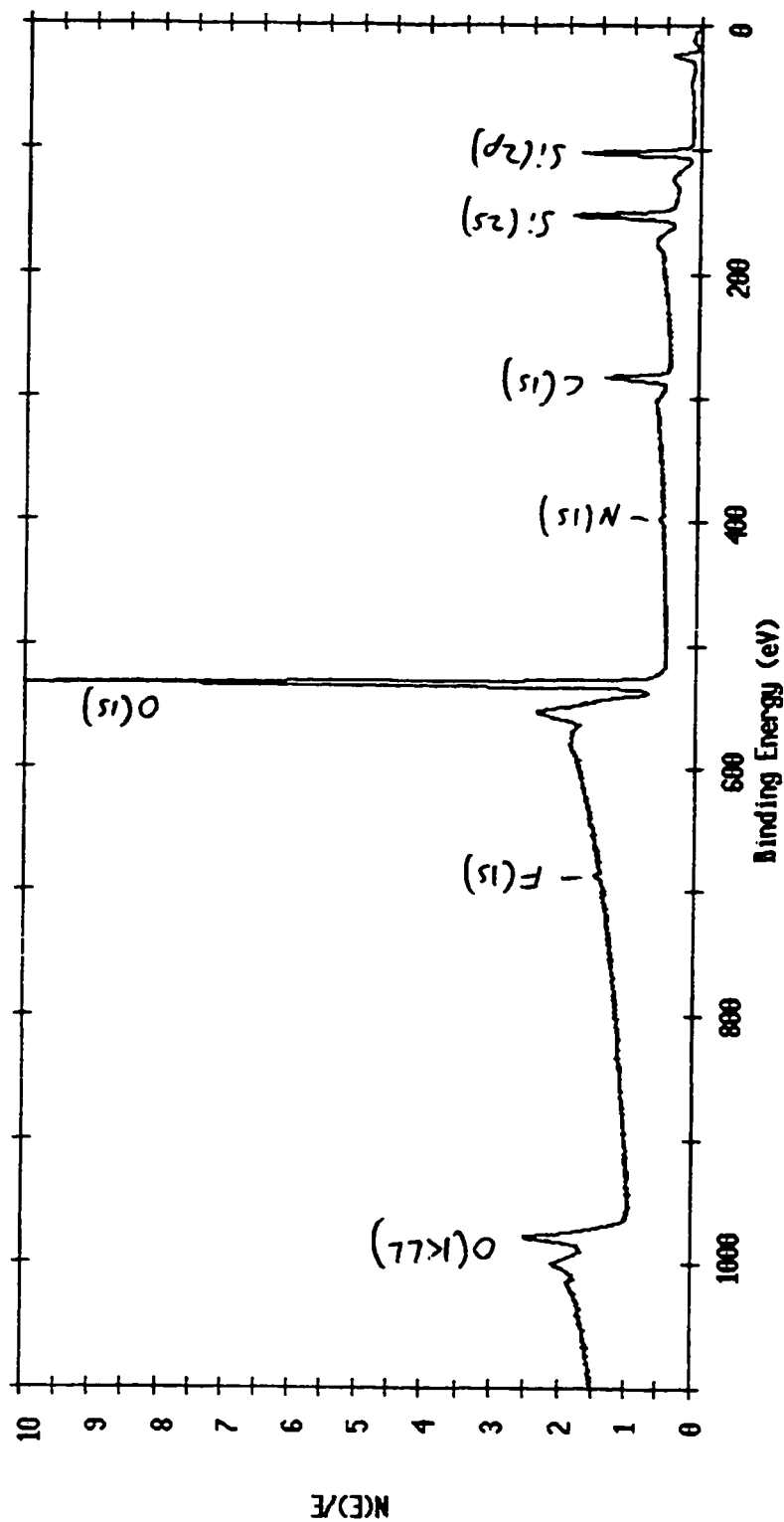
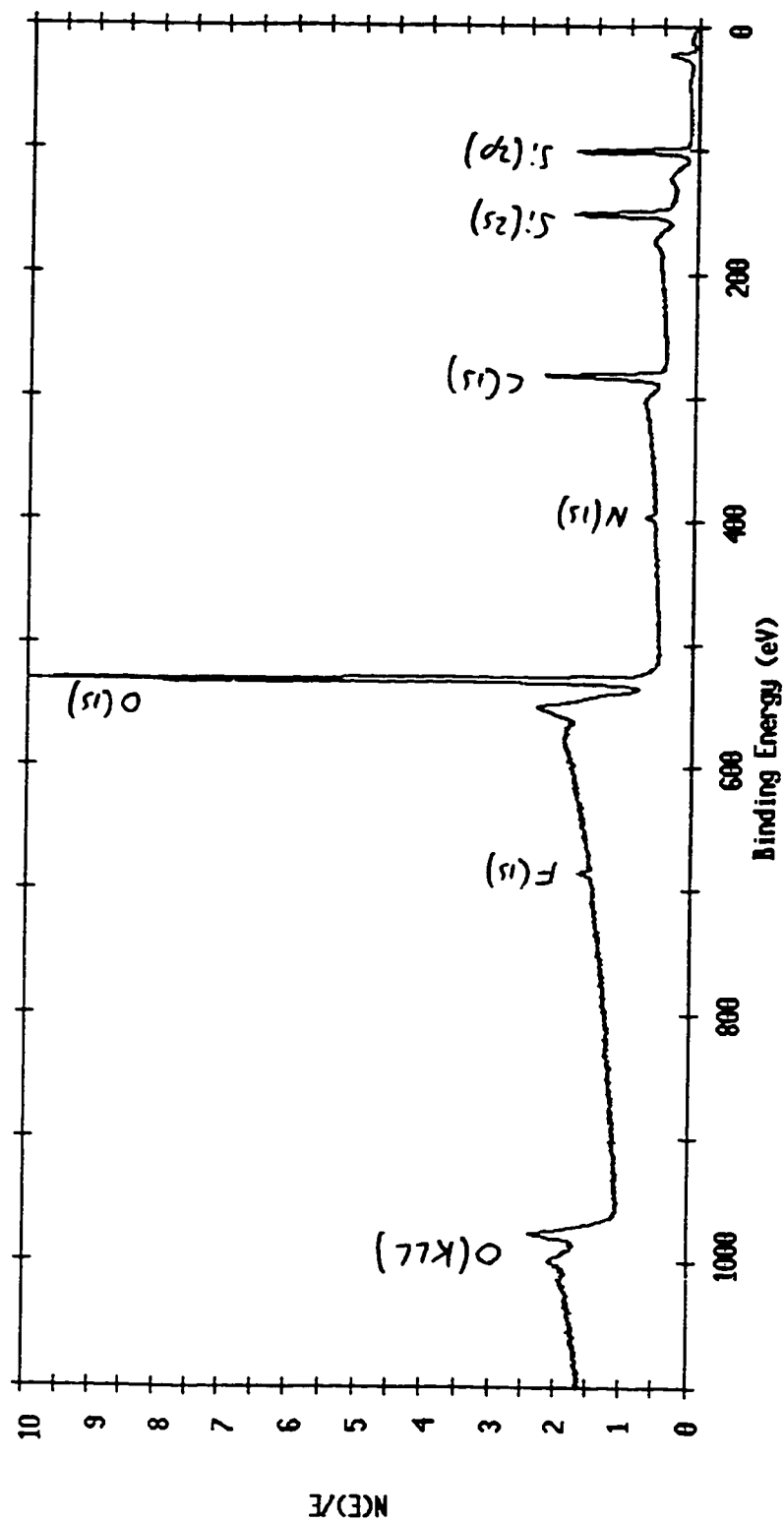Figure 65: ESCA-Survey Spectrum of S(-) NEA

ESCA Survey 8 Dec 93   Area: 1 Angle: 45 degrees   Acquisition Time: 29.34 min
File: BKSIOO4_1 BKSIOO4 SAMPLE (RHODIUM CATALYST)   RUN1
Scale Factor: 47.812 kc/s   Offset: 0.195 kc/s   Pass Energy: 187.850 eV Aperture: 5 Al 400 W
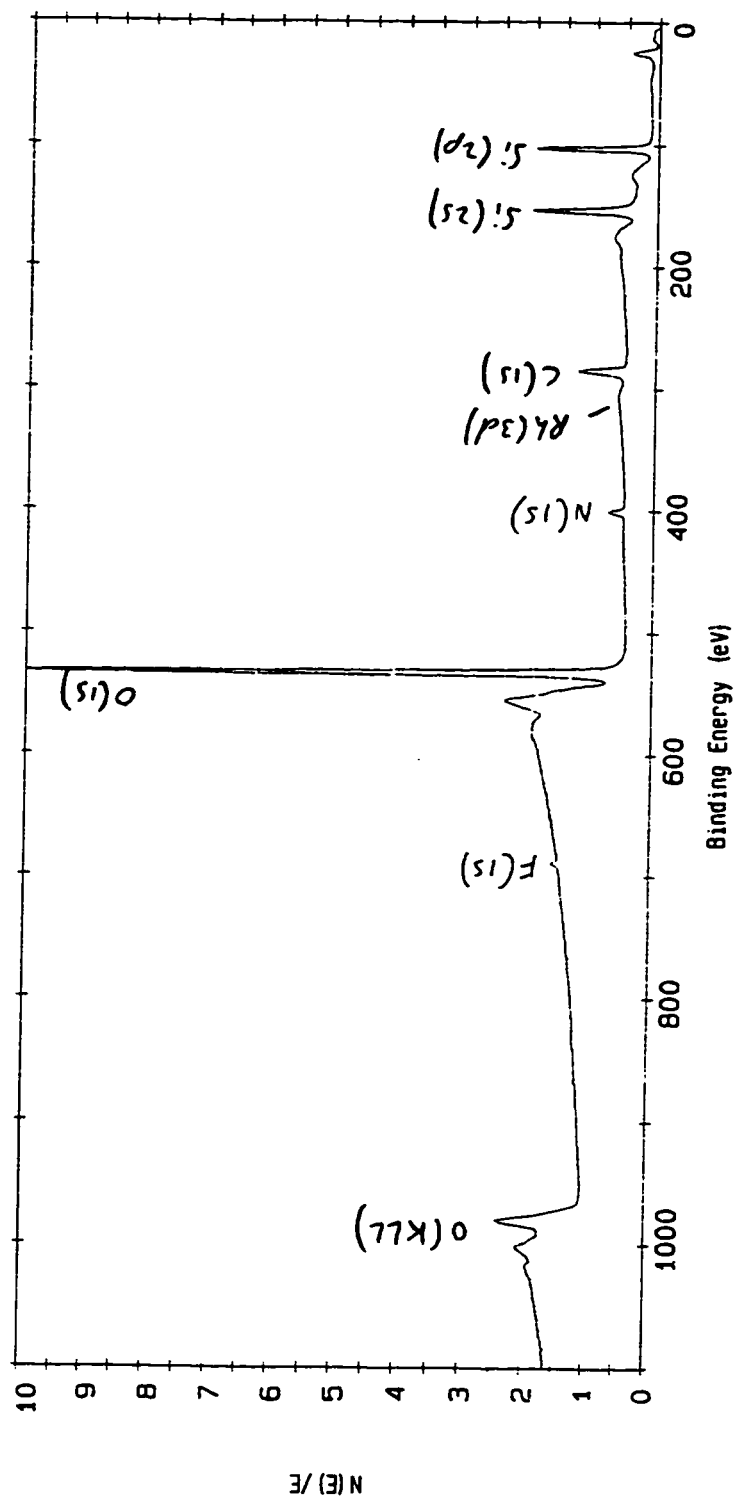
Figure 66: ESCA-Survey Spectrum of BKSIOO4

ESCA Survey 26 Nov 96 Area: 1 Angle: 70 degrees Acquisition Time: 29.34 min
File: ADM_1 2-METHYL-3-BUTENITRILE
Scale Factor: 7.603 kc/s Offset: 0.072 kc/s Pass Energy: 187.850 eV Aperture: 4 Al 350 W

Figure 67: ESCA-Survey Spectrum of 2-Methyl-3-Butenitrile

ESCA Survey 26 Nov 96 Area: 1 Angle: 70 degrees Acquisition Time: 29.34 min
File: AIDN_2 NC(CH2)4CN
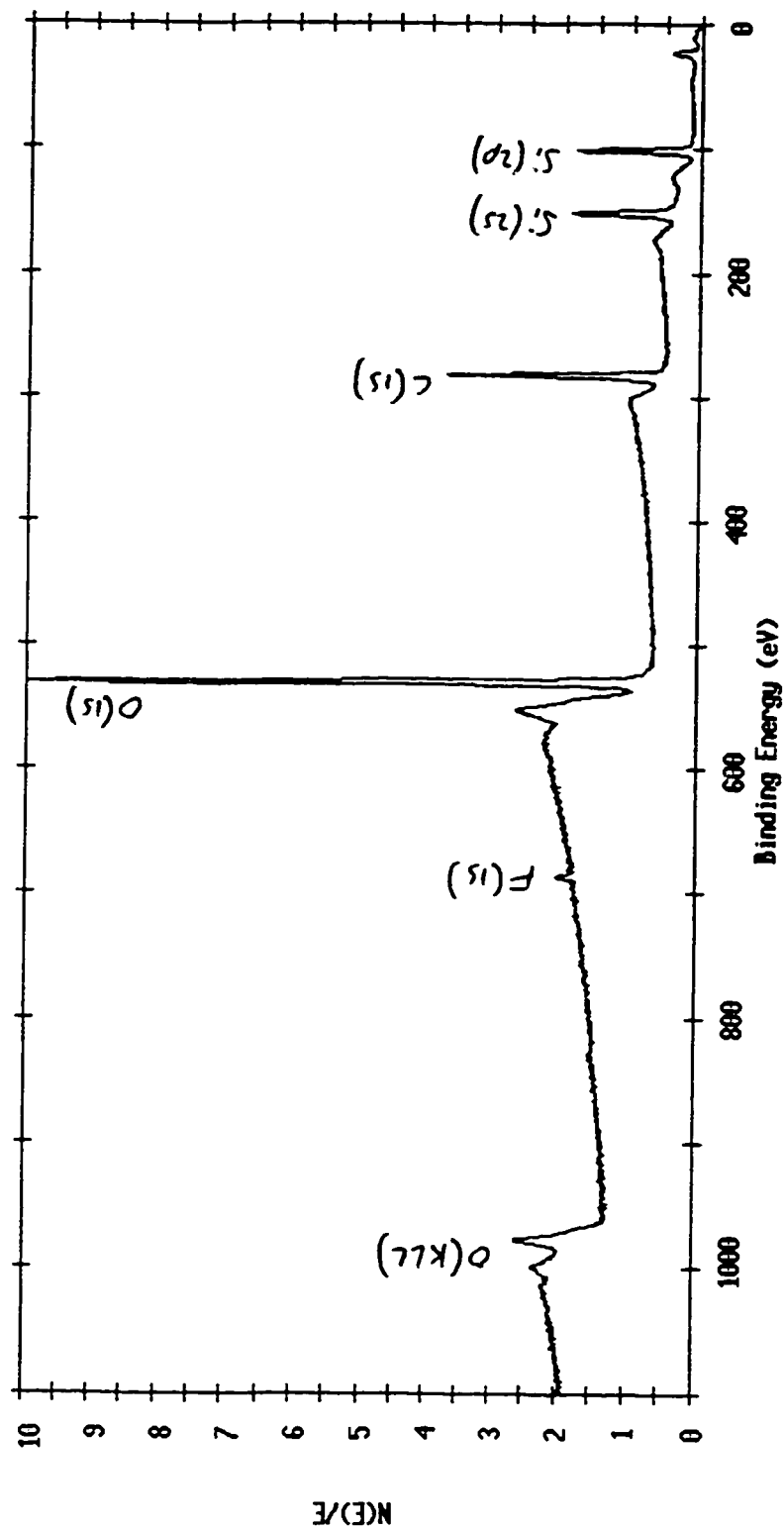Scale Factor: 6.933 kc/s   Offset: 0.061 kc/s   Pass Energy: 187.850 eV Aperture: 4 Al 350 W

S:(2p)

S:(2s)

C(1s)

O(1s)

F(1s)

O(KLL)

Binding Energy (eV)

N(E)/E

Figure 68: ESCA-Survey Spectrum of NC(CH₂)₄CN

ESCA Multiplex 26 Nov 96 Area: 1 Species: C1 Region: 1 Angle: 70 degrees Acquisition Time: 5.29 min
File: AIBN_9 2-METHYL-3-BUTENITRILE, HIGH SENS
Scale Factor: 1.520 kc/s Offset: 3.553 kc/s Pass Energy: 187.850 eV Aperture: 4 Al 350 W
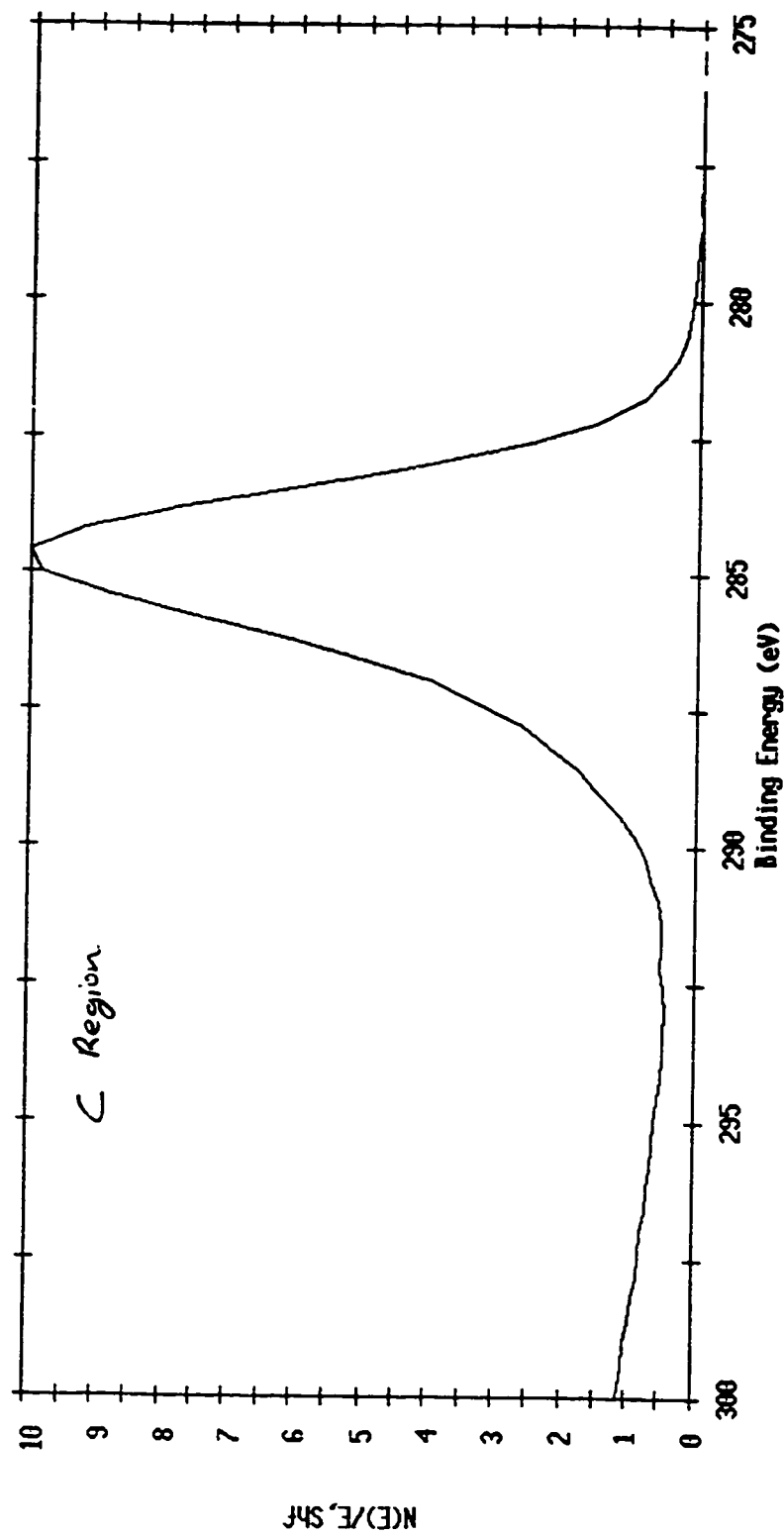
C Region

N(E)/E, Shf

Binding Energy (eV)

Figure 69: ESCA High-Sensitivity Spectrum for C (2-Methyl-3-Butenitrile)

ESCA Multiplex 26 Nov 96 Area: 1 Species: Pt1 Region: 2 Angle: 70 degrees Acquisition Time: 84.67 min
File: AIBN_9 2-METHYL-3-BUTENITRILE, HIGH SENS
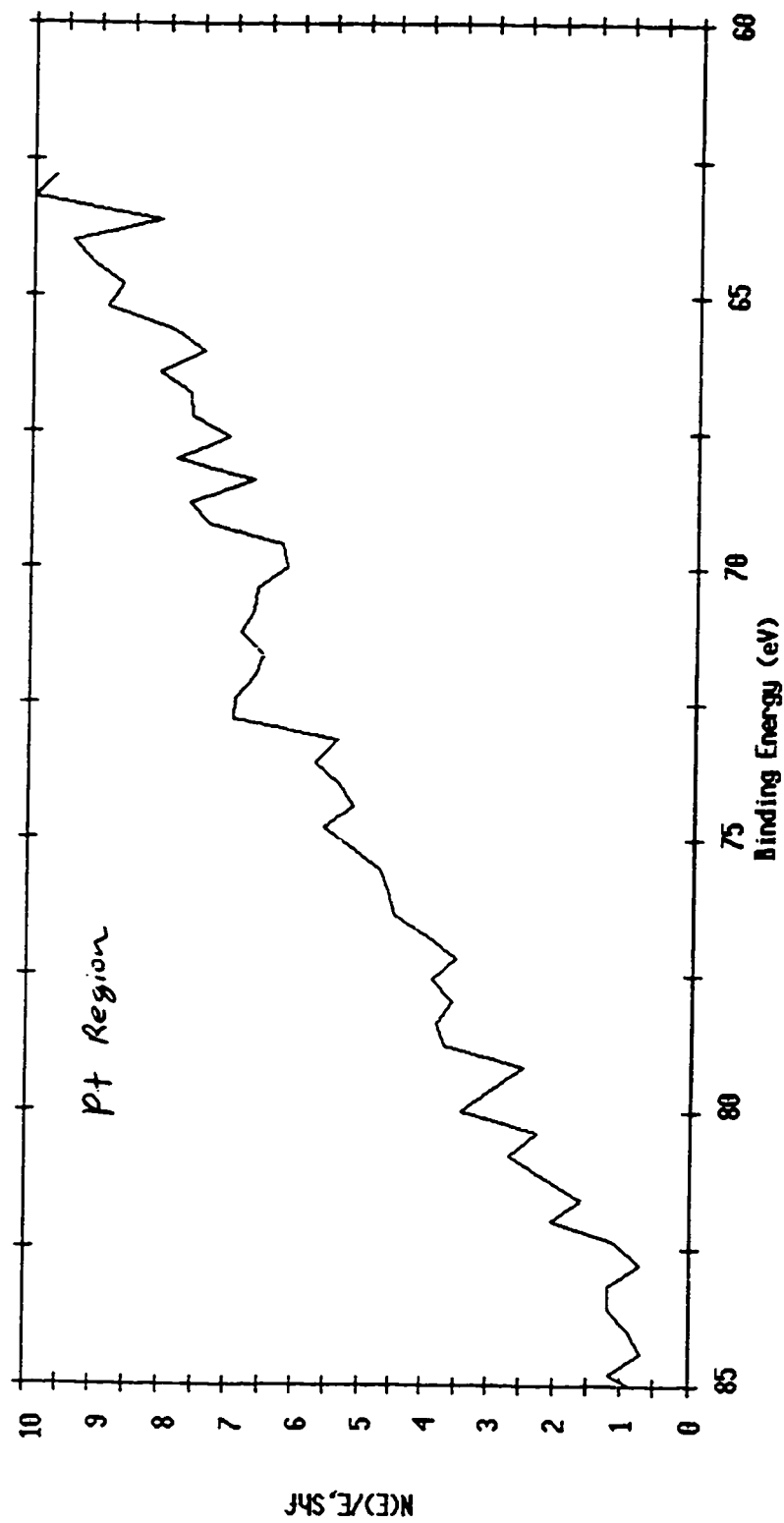Scale Factor: 0.007 kc/s Offset: 0.893 kc/s Pass Energy: 187.850 eV Aperture: 4 Al 350 W

Pt Region

N(E)/E,Shf

Binding Energy (eV)

Figure 70: ESCA High-Sensitivity Spectrum for Pt (2-Methyl-3-Butenitrile)

ESCA Multiplex   27 Nov 96   Area: 1   Species: C1   Region: 1   Angle: 70 degrees   Acquisition Time: 5.29 min
File: AIDN_10   NC(CH2)4CN, HIGH SENS
Scale Factor: 1.920 kc/s   Offset: 3.210 kc/s   Pass Energy: 187.850 eV   Aperture: 4   Al   350 W
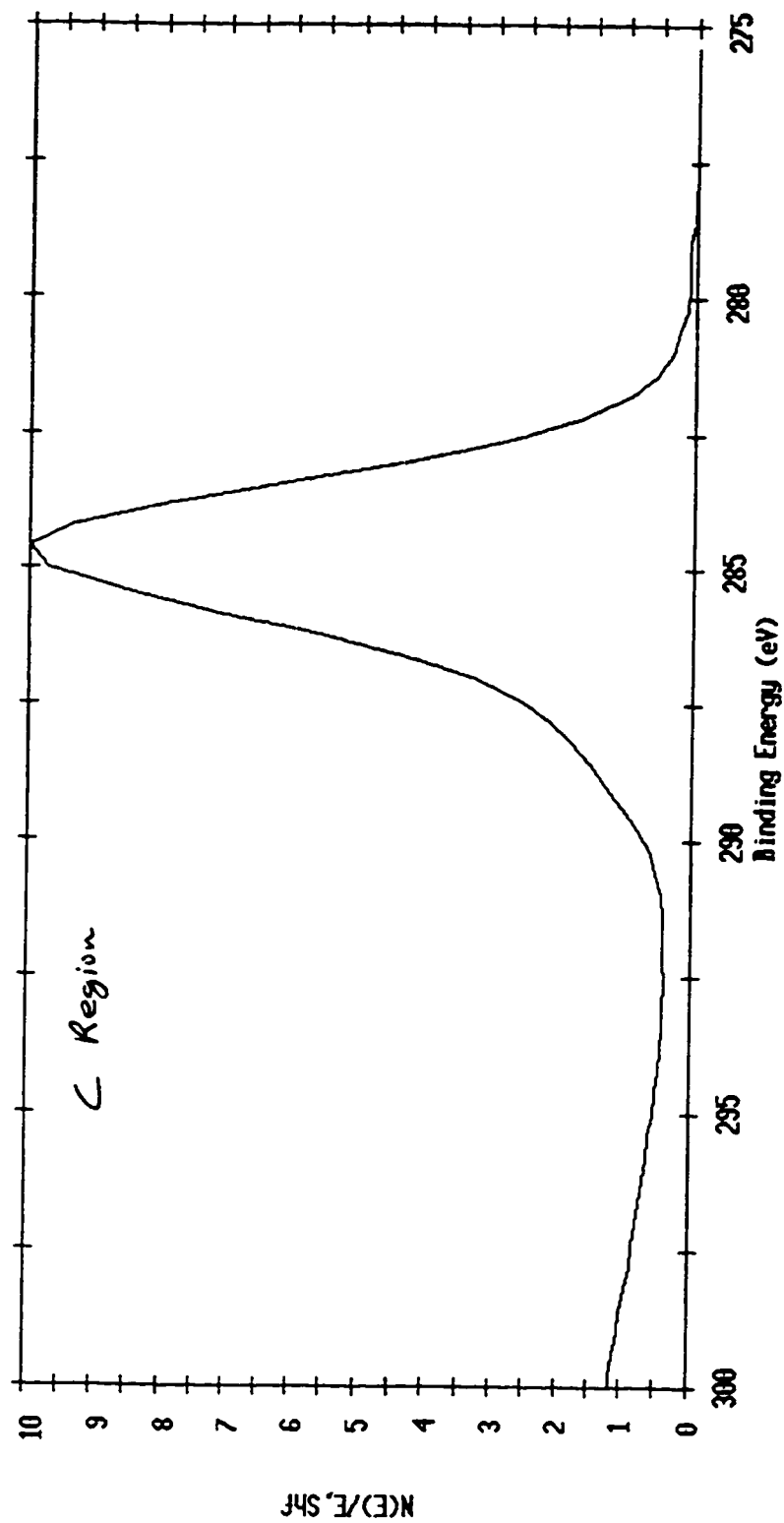
C Region

N(E)/E, SHF

Binding Energy (eV)

Figure 71: ESCA High-Sensitivity Spectrum for C (NC(CH$_2$)$_4$CN)

ESCA Multiplex 27 Nov 96 Area: 1 Species: Pt1 Region: 2 Angle: 70 degrees Acquisition Time: 84.67 min
File: AIBN_10 NC(CH2)4CN. HIGH SENS
Scale Factor: 0.006 kc/s   Offset: 0.810 kc/s   Pass Energy: 187.850 eV Aperture: 4 Al 350 H
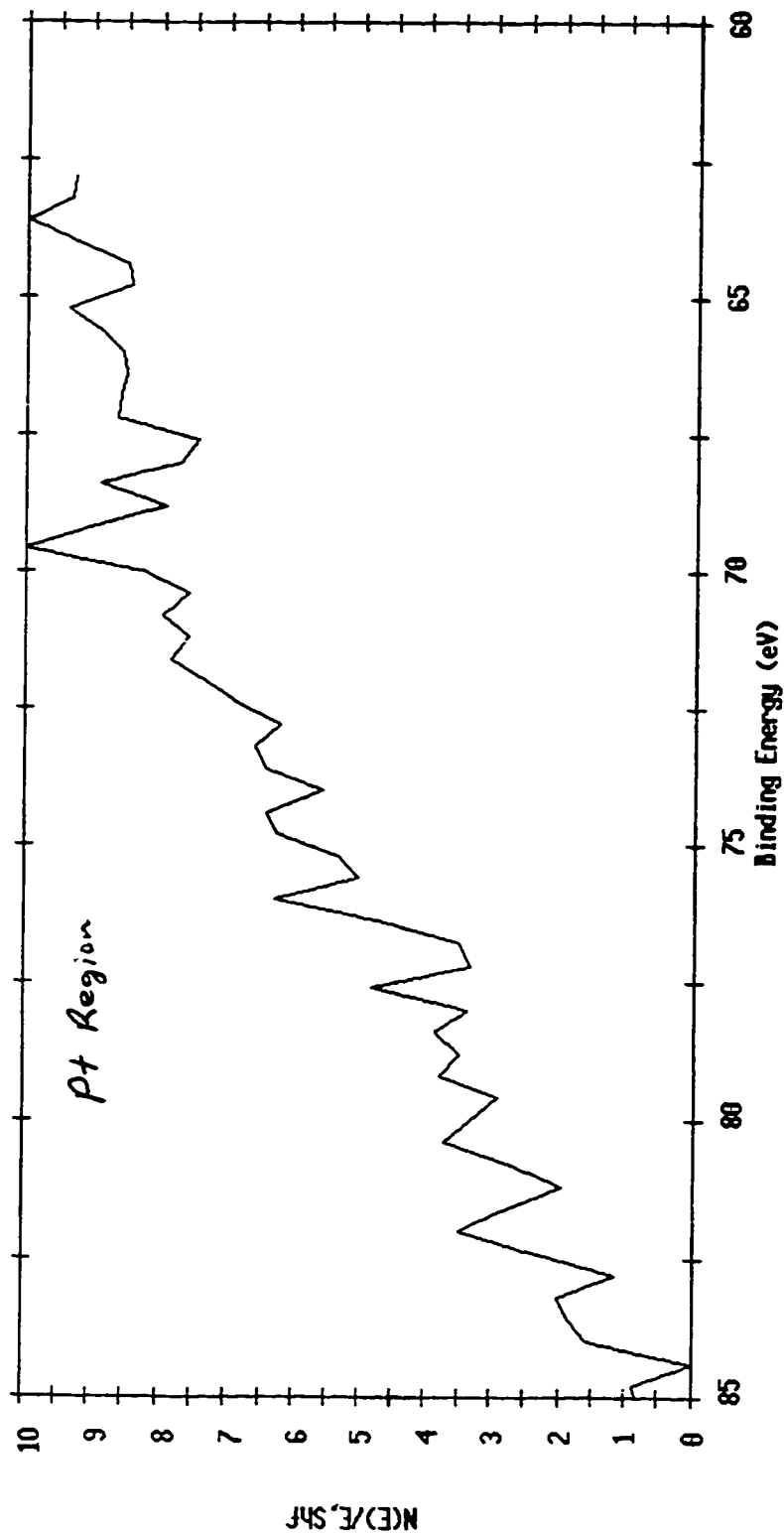
Pt Region

N(E)/E.Shf

Binding Energy (eV)

Figure 72: ESCA High-Sensitivity Spectrum for Pt (NC(CH₂)₄CN)

ESCA CURVE FIT 18 Mar 94 Angle: 70 degrees Acquisition Time: 19.32 min
File: Curve_Fit DAVISIL DIOL ALLYL GLYCIDYL ETHER (0.05M HCL) HRES 1
Scale Factor: 0.269 kc/s Offset: 4.095 kc/s Pass Energy: 58.700 eV Aperture: 4 Al 400 W

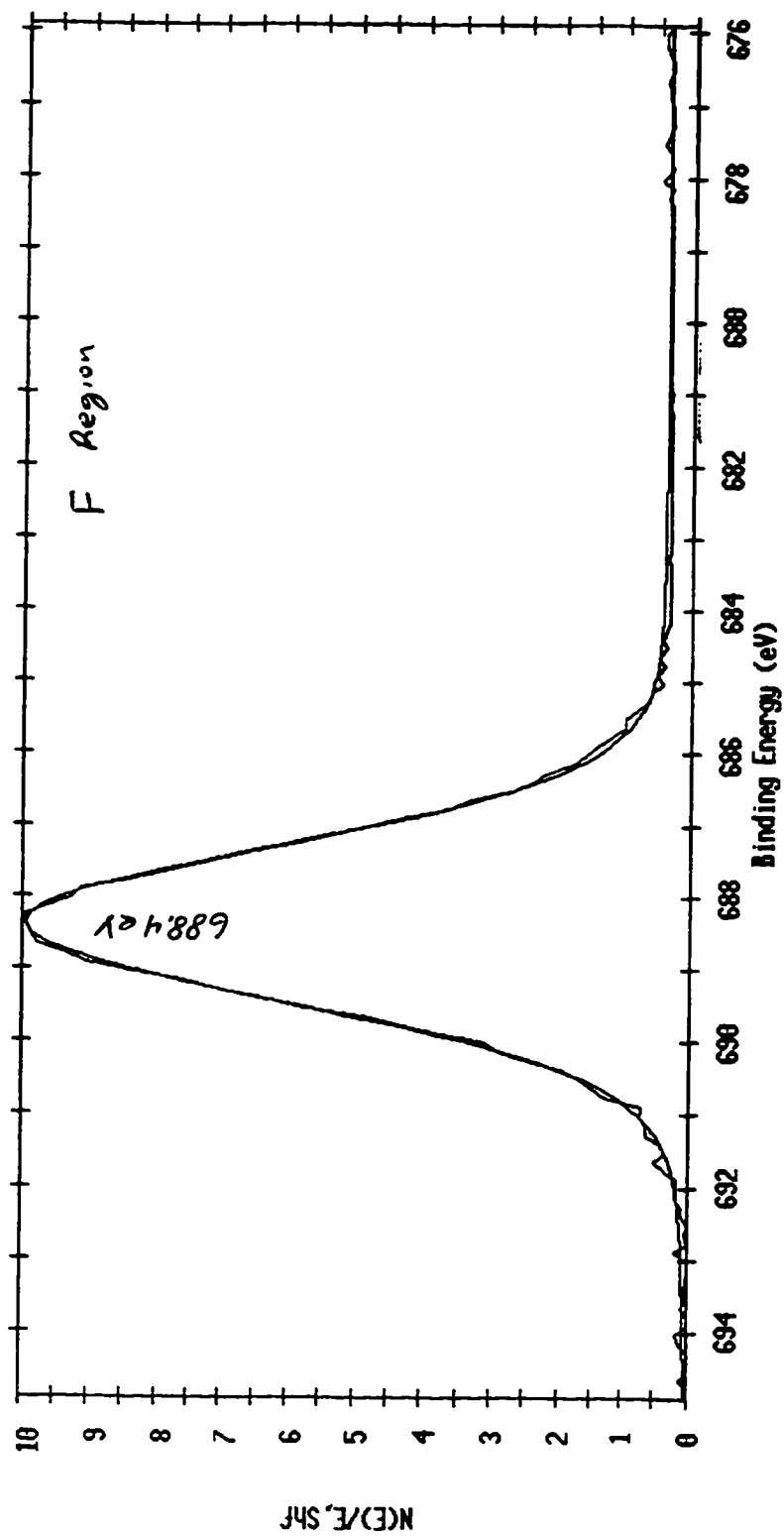F Region

688.4 eV

N(E)/E.SHf

Binding Energy (eV)

Figure 73: ESCA High-Resolution Spectrum for F (Davisil Diol Glycidyl Ether)

ESCA CURVE FIT   19 Mar 94   Angle: 70 degrees   Acquisition Time: 23.61 min
File: Curve_Fit   DAVISIL + 4-PHENYL-1-BUTENE UTIL RUN1
Scale Factor: 0.296 kc/s   Offset: 4.697 kc/s   Pass Energy: 58.700 eV   Aperture: 4   Al   400 W

F Region
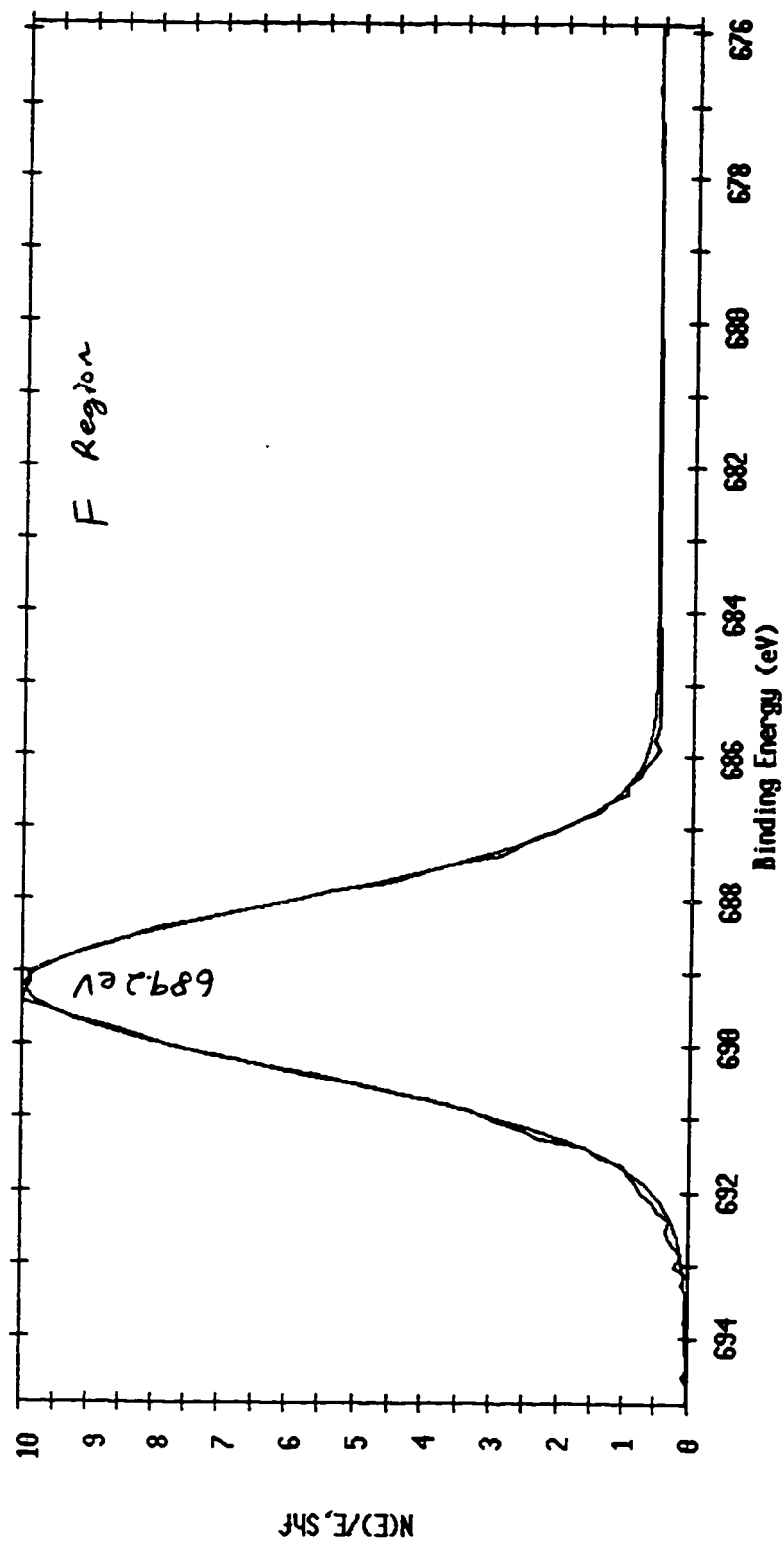
689.2 eV

Binding Energy (eV)

N(E)/E, SMF

Figure 74: ESCA High-Resolution Spectrum for F (Davisil + 4-Phenyl-1-Butene)

ESCA Survey 17 Jan 97 Area: 1 Angle: 70 degrees Acquisition Time: 29.34 min
File: VYDAC_34 VYDAC TPB5 (E950505-31) STIRRED 5 DAYS W/ TEFLON BARS
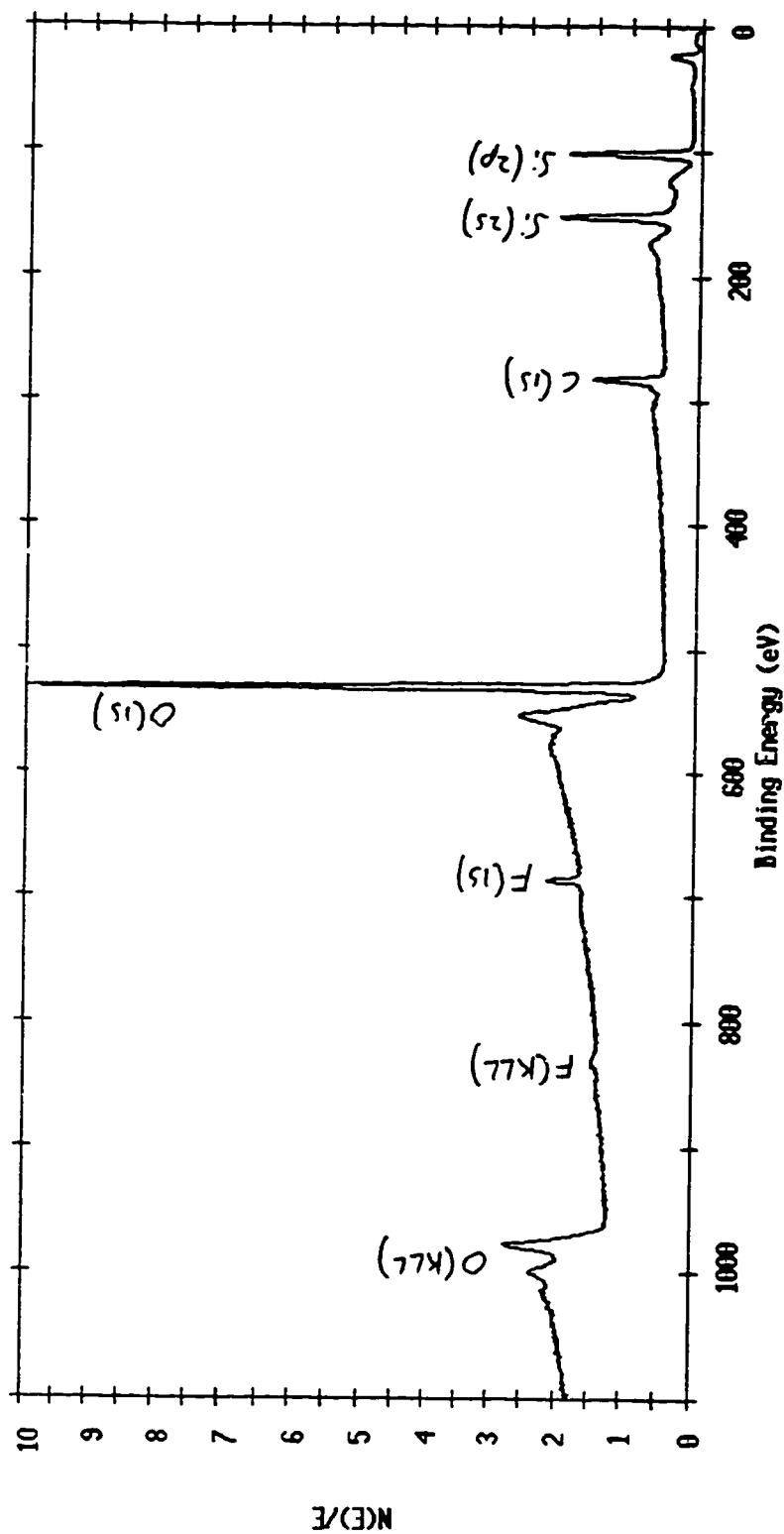Scale Factor: 10.049 kc/s Offset: 0.081 kc/s Pass Energy: 187.850 eV Aperture: 4 Al 350 W

Figure 75: ESCA-Survey Spectrum of Vydac TPB5 Stirred 5 Days with Teflon-Coated Bars

128

ESCA Survey 17 Jan 97 Area: 1 Angle: 70 degrees Acquisition Time: 29.34 min
File: VYDAC_33 VYDAC TPB5 (E950505-31) — CONTROL FOR F STIR-BAR TEST
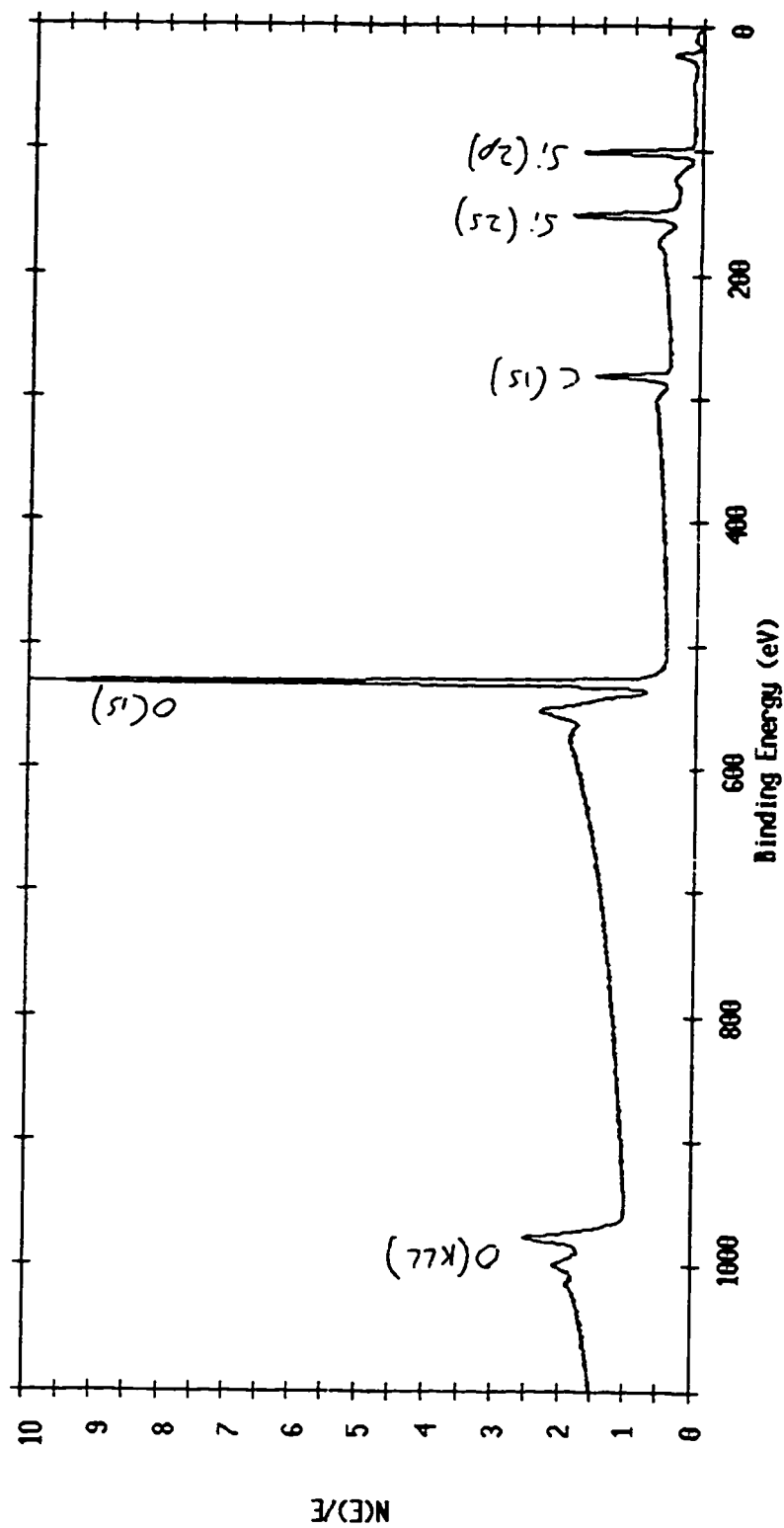Scale Factor: 17.233 kc/s Offset: 0.128 kc/s Pass Energy: 187.850 eV Aperture: 4 Al 350 W

Figure 76: ESCA-Survey Spectrum of Vydac TPB5 Control Sample